What controls the calving of glaciers? From observations to predictions

Hva kontrollerer kalving av breer? Fra observasjoner til prediksjoner

Philosophiae Doctor (PhD) Thesis

Anne Chapuis

Department of Mathematical Sciences and Technology

Norwegian University of Life Sciences

Ås 2011

Thesis number: 2011-60
ISSN-nr: 1503-1667
ISBN-nr: 978-82-575-1023-7

"Glaciers are delicate and individual things, like humans. Instability is built into them."

– Will Harrison

Summary

This thesis addresses the process of iceberg calving at the front of tidewater glaciers and tries to clarify what controls the calving of glaciers, from observations in the field to modeling and predictions. Iceberg calving is the detachment of ice from a parent glacier and it makes the glacier very sensitive to its local environment. In turn, calving at a glacier front has a strong impact on the glacier dynamics and can trigger and/or enhance glacier instabilities, acceleration and glacier retreat, making the calving process a crucial factor in glacier dynamics and hence in sea level rise.

This thesis is based on field observations, collected throughout 4 years at the front of Kronebreen, Svalbard. A special emphasis has been given to trying various observation techniques: ground-based RADAR, direct observations, seismic monitoring, terrestrial photogrammetry and remote sensing. Using ground-based RADAR we were able to automatically detect 92% of the largest calving events. The percentage detected by seismic monitoring is lower (about 10%) but the technique allows for finer distinction between different calving types and glacier-related seismic events. Seismic equipment also requires less maintenance, less technical expertise and less funding, and can be left in the field for several months. Terrestrial photogrammetry is a very useful tool that can provide glacier dimensions and a continuous monitoring of the general conditions at the front. Finally, direct observations are recommended for the study of calving because it can provide, when used together with terrestrial photogrammetry, both qualitative and quantitative data. The qualitative aspect provides key information for understanding the calving process but is especially hard to obtain with technical methods.

The question of seasonal calving variations is also addressed and we show that glacial seismic activity is highly variable throughout the year with recurrent increased activity in autumn, while velocity is low. However this thesis focuses on explaining very short-term variations: the individual calving events. Individual calving events have received so far very little attention in the field and no attention in modeling studies. This thesis was inspired by other studies of complex natural processes in which individual events are all equally considered, large and small, and which emphasize the value of understanding a process at the individual scale, for example the study of earthquakes or forest fires. We first show that general spatial patterns in calving activity can be explained by glacier characteristics like longitudinal stretching rate, which themselves are very linked to the glacier geometry. We then created a simple calving model with the object of understanding what controls the size and timing of calving events. Our simple model, focussing solely on the interplay between calving and its impact on the front stability, manages to reproduce the size and timing distribution of calving events as observed in the field. This result highlights the role of calving on front stability and on calving itself. Front stability is shown to be crucial in the control of calving. Implications of this new finding are that the size distribution of calving depends on the glacier stability: a glacier becoming unstable will produce a higher proportion of large calving events. Beyond a critical glacier stability, calving can become self-sustained and ongoing, leading to very rapid glacier retreat. We propose that the characteristics of the calving event sizes distribution indicate how close a glacier is to rapid retreat. One main point of this thesis is to show the importance of studying calving events at an individual scale to gain more understanding of the process.

Sammendrag

Denne avhandlingen omhandler kalvingsprosessen i fronten av en tidevannsbre og den forsøker å klargjøre hva som kontrollerer kalving av breer, ved hjelp av feltobservasjoner, modellering og prediksjon. Kalving av isfjell skjer når is brekker av fra en isbre, og kalving gjør breer svært sensitive til det lokale miljøet. Motsatt har også kalvingen ved brefronten en stor innflytelse på breens dynamikk, kalvingen kan initiere eller forsterke ustabilitet, akselerasjon eller tilbaketrekking av breen, hvilket gjør kalvingsprosessen til en sentral faktor for isdynamikken, og for havnivået.

Denne avhandlingen er basert på feltobservasjoner som er samlet gjennom fire år ved fronten av Kronebreen på Svalbard. Det er blitt lagt spesielt vekt på å prøve ut forskjellige observasjonsteknikker, bakkebasert RADAR, direkte observasjoner, seismisk monitorering, terrestrisk fotogrammetri, og fjernanalyse. Ved hjelp av bakkebasert RADAR kunne vi detektere 92% av de største kalvingsepisodene. Prosentandelen for seismisk monitorering er mye lavere, ca 10%, men denne monitoreringen tillater finere distinksjon av forskjellige kalvingsformer og brerelaterte seismiske episoder. Seismisk utstyr krever også mindre ettersyn, mindre teknisk ekspertise og lavere finansiering, og utstyret kan være utplassert i felt uten tilsyn i flere måneder. Terrestrisk fotogrammetri er et svært nyttig verktøy som kan fortelle om breens dimensjoner og som muliggjør en kontinuerlig monitorering av generelle forhold ved fronten. Tilsutt anbefales direkte observasjoner for å studere kalving, fordi disse i kombinasjon med terrestrisk fotogrammetri kan gi både kvalitative og kvantitative data. Det kvalitative aspektet gir essensiell informasjon for forståelsen av kalvingsprosessen, men er spesielt vanskelig å oppnå ved teknologiske metoder.

Spørsmålet om sesongbaserte kalvingsvariasjoner er også undersøkt og vi viser at kalvingsaktiviteten er svært variabel gjennom året, med gjentagende økning i aktivitet på høsten når også hastigheten er på sitt laveste. Allikevel fokuserer denne avhandlingen på å forklare de svært raske variasjonene, nemlig individuelle kalvingshendelser. Så langt har det blitt viet svært lite oppmerksomhet mot individuelle kalvingshendelser i felt, og ingen oppmerksomhet innen modelleringsstudier. Denne avhandlingen er inspirert av studier av komplekse prosesser hvor individuelle hendelser er vurdert likeverdige, store som små, og som vektlegger verdien av å forstå prosessen på en skala på individuelt nivå, for eksempel for studier av jordskjelv. Vi viser først at generelle romlige mønstre i kalvingsaktivitet kan forklares ved brekarakteristikker som longitudinell tøynings rate (stretching rate), som igjen er knyttet til breens geometri. Vi har laget en enkel kalvingsmodell hvor intensjonen er å forstå hva som kontrollerer størrelse og tidspunkt for kalvingshendelsen. Vår modell, som fokuserer kun på interaksjon mellom kalving og dennes innflytelse på frontstabiliteten, greier å reprodusere størrelses- og tidsfordeling av kalvingshendelser som observert i felt. Dette resultatet fremhever kalvingens rolle på frontstabiliteten og på kalvingen selv. Det viser seg at frontstabiliteten er en essensiell styringsmekanisme for kalvingen. Konsekvensene av dette nye funnet er at størrelsesfordelingen av kalvingshendelsene avhenger av breens stabilitet; en bre som blir ustabil produserer høyere proporsjon av større kalvingshendelser. Over en kritisk brestabilitet vil kalvingen bli selvopprettholdende og vedvarende, hvilket vil medføre en svært rask tilbaketrekning av brefronten. Vi fremsetter en påstand om at karakteristikken av fordelingen av størrelsene på kalvingshendelsene indikerer hvor nært forestående en rask tilbaketrekning er for breen. Et hovedpoeng ved denne avhandlingen er å vise hvor viktig det er å studere kalvingshendelser på en skala på individuelt nivå for å oppnå en bedre forståelse av prosessen.

Acknowledgments

My project was funded as a PhD stipend from UMB. I also received financial support from the international project GLACIODYN as part of the International Polar Year, and by a "Instituttbasert Strategisk Program" granted to the Department of Mathematical Sciences and Technology at UMB, both funded by the Norwegian Research Council. I benefited from arctic field grants though the Svalbard Science Forum in 2008-2011.

In addition to offering me this PhD project, I would like to thank my supervisor Cecilie Rolstad-Denby for allowing me as much freedom as I needed and for keeping a constant confidence in my work and my sometimes non conventional ideas.

I also received a lot of support from colleagues at UMB and at UiO. Ivar Maalen-Johansen has put me on the right tracks with terrestrial photogrammetry and has been of great support during several phases of my PhD. Trond Eiken should be thanked for a very special reason, it was him who made me realize that some things might never work, and that it is sometimes necessary to give up, thanks for showing me the obvious. ˚ystein Dick, thanks for helping me learn norwegian by regularly providing Tintin comics and other french-norwegian movies. Engineers from IMT gave me a great hand with my preparations for field work, thanks Andreas Flø and Tom Ringstad. Jon Glenn Omholt Gjevestad has been a great support during my entire stay at IMT, thanks for teaching me Matlab, for being always available and helpful. I would also like to thank Olav Mathisen, if nothing else, for being a great source of inspiration and motivation. Cecilia Futsæter has been a constant presence in my PhD, and gave me the right directions to follow. I have enjoyed a lot being around Bjørn-Ragnvald Petterson who told me about the world of research.

Fellow PhD students have been of great help during my entire PhD, thanks Kristian Breili for sharing your expertise on Matlab, for giving me a hand in the field, for teaching me about norwegian culture and for passing over your sound system when you finished your PhD. Dagny Lysaker has been an inspiring fellow PhD student, for she showed me that a woman can sometimes be the strongest man in the department and her expeditions filled me with endless inspiration for ski trips in Norway. Thanks John Hulth for being so clever with finding the most appropriate techniques for my field work, for coming in my office with new inventions that push further what can be done on a glacier, don t stop inventing. Thanks Katrin Bentel for coming with your big smile in the department, not to mention your expertise in Matlab, Latex and other computer-related mysteries. Thanks Michal Šprlak for keeping an eye on the calendar for me in the last months. A special thank goes to Tom Tetzlaff and the neuro-science group of IMT, for creating a "Self-Organized Critiality" seminar, gathering the most heterogeneous group I have never worked with before. Thanks for bringing a complete new perspective in my field, and it is the beauty of our unique department where we daily meet architects, pedagogues, glaciologists, neuroscientists, and renewable energy specialists. I am not sure what unites us but I know that exciting research can take place at the interface between these groups.

I also had the chance to receive help from abroad, Shad O Neel has been extremely helpful at a time when I really needed it. Two visits to Faezeh Nick in Copenhagen have been very

inspiring and have guided me. I must thank Etienne Berthier for allowing me to come visit him in Toulouse and work on satellite-related topics.

Thank you Jack Kohler for teaching me so much in the field and for sharing so much of your knowledge with me, great time in the helicopter over Kronebreen! Chris Nuth, you deserve special attention, you are always here to listen to me, my doubts, ideas, to give me advice, to encourage me to follow my ideas. On top of that you are a great person to be with in the field – cookies and tea are the key – and a lot of fun, rett og slett.

A very special thank should be dedicated to all my field assistants and other people who made field work both possible and unforgettable. Thanks Cédric, Neal, Allan (you even asked for coming back!), Karin, Mari, Damien (best cook!), Tobias (thanks for the ridge), Ian, Susie for organizing the great observations of Sveabreen with more than 40 youths, and Bas for your constant influx of ideas, your bridge-building ability, your strong second-degree humor, but not for burning my bench. I would also like to thank the Norwegian Polar Institute for being very helpful in the field, Wojtek, you are the best help I could hope for concerning logistics, calm and effective. Imiaq, without you Svalbard would not be quite the same, I completely fell for you on our first meeting, and since then you have been protecting me from the bears, pulling me when I am on my skis and a full member of our little expeditions in front of Kronebreen, you are my favorite polar dog.

Finally, life beyond work also kept me happy throughout the years in Norway. Thorben and Geir, you are excellent trip organizers and always willing to be outside, whatever the conditions are, thanks for showing me Norway! Marie, you are probably the most crazy outdoor girl I know, and I like it! Thanks for providing extra motivation when it was lacking and for helping me find the way forward. My family, through its constant support and huge confidence in my work, is a great source of motivation and comfort, merci! Massimo, you appeared quite late in the story, but you took the first place, thank you for remaining calm and for offering me a solid base where I can always forget everything about calving!

Ås, 12 September 2011
Anne Chapuis

Contents

Introduction

Chapter 1

Introduction

1.1 Climate change, glaciers, and sea level rise

1.1.1 Climate change

The Earth s climate has been changing through time as a result of changes in atmospheric composition of green house gases (GHG) and in solar luminosity. The atmosphere, mostly composed today of nitrogen and oxygen, was, at its formation, mainly composed of nitrogen and carbon dioxide CO_2, a powerful GHG. GHG are gases that absorb and emit radiation within the thermal infrared spectrum and therefore have the potential to impact the Earth s temperature. The solar luminosity received by the Earth is varying through time: first, because the solar luminosity itself is constantly increasing as the sun becomes older, and second because the energy received by the Earth varies cyclically as a function of the Earth s orbit in a phenomenon known as Milankovich cycles [65]. Even though the solar luminosity has been getting stronger and stronger, the temperature of the Earth has remained neither too cold nor too warm and suitable to sustain life. The reason for this rather constant temperature despite changes in sun luminosity is the capacity of CO_2 as a GHG to regulate the Earth s temperature.

Naturally-driven climate changes have been triggered by changes in the Earth s orbit and follow rather regular glacial/interglacial cycles every 26, 41, and 100-400 ky. In those cases, changes in the Earth s orbit initiated a slight cooling/warming, that is further fed by positive feedbacks, amongst which the most powerful impact is from the oceans that can either absorb or release GHG like CO_2. The current climate change, however, is primarily anthropogenically-driven owing to additional input of GHG to the atmosphere. The slight temperature increase caused by the addition of anthropogenic GHG is further amplified by the same positive feedbacks that enhance the initial warming during a naturally-driven climate change. The global average temperature increase for the year 1990-2005 is $+0.2^oC$/decade [44]. How will glaciers respond to this change? **What is the role of calving in the response of tidewater glaciers to climate change?** (*Paper 5*).

Figure 1.1: A: Dry calving on Deception Island, Antarctica, B: Calving in freshwater, Perito Moreno, Argentina, C: Tidewater calving at Kronebreen, Svalbard.

1.1.2 Impact of climate on glaciers and sea level rise

Glaciers are large persistent ice bodies that form where the snow deposited during the cold/wet season does not entirely melt during the warm/dry season. Glaciers are water storage bodies, and undergo seasonal mass variations due to an input of mass during the cold/wet season and a loss of mass during the warm/dry season. The resulting mass balance of the glacier over one year ($\delta M/\delta t$) can be expressed as [34]:

$$\delta M/\delta t = Qa - Qm - Qc - Qb \tag{1.1}$$

where Qa is the annual surface accumulation, Qm is the annual surface melting, Qc is the mass loss by iceberg production and Qb is the bottom melting under floating ice margins. In this thesis we consider Svalbard tidewater glaciers, which are grounded, so floating ice margins and the term Qb can be neglected. Annual surface accumulation Qa and melting Qm are directly dependent on climate and affect the glacier surface. Accumulation and melting processes are relatively well-understood, even if monitoring and modeling predictions of glacier surface mass-balance remain a challenge in glaciology. The calving component, Qc, on the other hand, is much more problematic, both to measure and to model [13]. Numerous questions remain unanswered, including: **How is most of the ice lost at a calving face?** (*Paper 4*). **What controls the calving process?** (*Paper 3, Paper 4, and Paper 5*).

Calving is the production of icebergs by detachment of ice from a parent glacier [13]. Calving glaciers can terminate on land (dry calving), in freshwater or in salty water (tidewater glaciers), see Fig. 5.4. In this thesis we consider only calving at tidewater glaciers.

Calving is a major component of the total ice loss by tidewater glaciers [30, 67, 56, 39]. Glacier assessments of glacier mass balance estimate that calving alone is responsible for 2400 Gt/y out of 3380 Dt/yr of ice lost annually, or 71% of the total ablation [108]. This percentage varies a lot depending on the amount of calving glaciers in the considered area. For example, Antarctica has the highest percentage with estimates lying between 75% and 87% [45], while estimates for Greenland are lower, around 56% [11] and from 16% to 40% for Svalbard [34].

The reaction of glacier to climate change is a complex chain of processes [79, 64], as illustrated in Fig. 1.2. Changes in atmospheric conditions (solar radiation, air temperature, precipitation, wind, cloudiness, etc.) trigger changes in the mass and energy balance at the

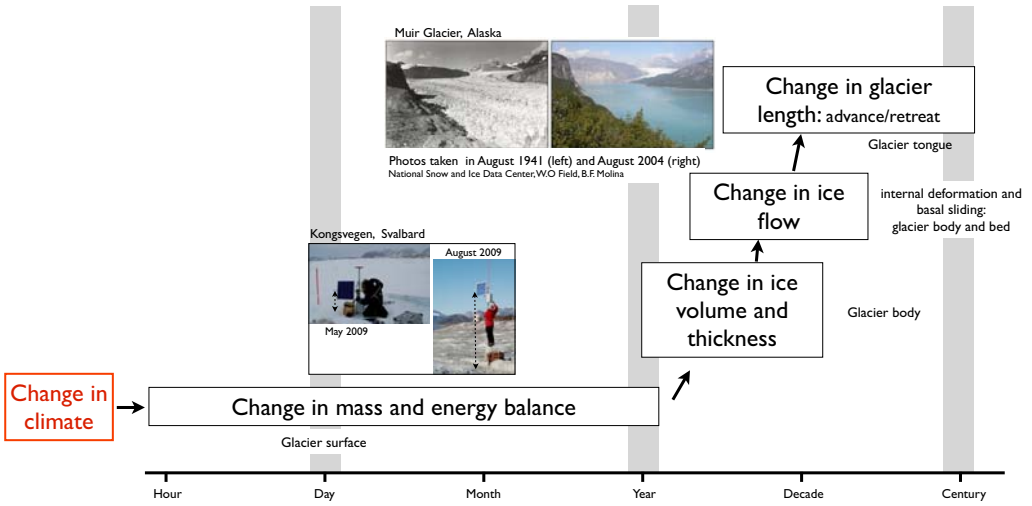

Figure 1.2: Response of glacier to a change in climate. Adapted from [120].

glacier surface [58, 80]. These are the "vertical" changes, that are the direct and undelayed effect of changes in atmospheric conditions [33]. Year after year, these "vertical" changes accumulate and can be measured in glaciers as changes in ice volume and thickness (e.g. [110, 77]). These changes in thickness and volume in turn alter the flow of ice via internal deformation and basal sliding. Changes in ice flow result in changes to the glacier length, corresponding to either advance or retreat of the glacier front. Thus, through this succession of steps, initial "vertical" changes are converted into "horizontal" changes. Changes in glacier length are therefore the indirect, delayed, filtered, enhanced and also easily observable signal of climate change [81].

The consequence of retreating and melting land ice bodies – glaciers, ice caps, and ice sheets – is a contribution to an increased sea level rise (SLR). Glaciers cover only 10 percent of the Earth s surface but contain about 3/4 of the fresh water [44]. If all land ice melted away, the sea level would rise by about 65 m. Tab. 1.1 lists the main contributors to SLR: thermal expansion alone is responsible for about half of the SLR, glaciers and ice caps, more than the large ice sheets, are responsible for the main glacier contribution, despite their small volume.

The current predictions of SLR are based on models using a simplified approach of glacier dynamics including only surface mass balance, considering a constant iceberg production at the front of tidewater glaciers and ignoring glacier geometric changes [44]. To arrive at better estimates of SLR, these simplifications must be taken into account. This thesis is part of

Table 1.1: Sea Level Rise estimates from [44] from 1961 to 2003 and from 1993 to 2003.

	Sea Level Rise (mm/y)	
Source	1961-2003	1993-2003
Thermal expansion	0.42 ± 0.12	1.6 ± 0.5
Glaciers and Ice Caps	0.50 ± 0.18	0.77 ± 0.22
Greenland Ice Sheet	0.05 ± 0.12	0.21 ± 0.07
Antarctic Ice Sheet	0.14 ± 0.41	0.21 ± 0.35
Sum	1.1 ± 0.5	2.8 ± 0.07
Observed	1.8 ± 0.5	3.1 ± 0.7
Difference (Observed-Sum)	0.7 ± 0.7	0.3 ± 1.0

a joint effort, the international project GLACIODYN that aims at improving observational techniques, assessing the detailed dynamics of a tidewater glacier, and providing simple calving models to make prediction of iceberg production. **How can iceberg production be incorporated into glacier models?** (*Paper 5*).

It is accepted that glaciers are generally good indicators of climate change, if they are not covered by debris, surging or calving. Indeed, debris reduces glacier melting, surging glaciers undergo cyclic instabilities with long periods of quiescence punctuated by rapid advances, and calving glaciers do not only change mass by surface melting but a large portion of the ice is lost through calving. **What can we learn in terms of climate by studying tidewater glaciers?** (*Paper 5*).

1.2 Tidewater glaciers and calving

1.2.1 Tidewater glaciers

Tidewater glaciers are calving glaciers terminating in salty water, they can be grounded or floating. Grounded tidewater glaciers are very unstable and they undergo cycles of slow advances and rapid retreats that can be asynchronous with climate change, e.g. [21, 90, 62, 91], see Fig. 1.3. While non-calving glaciers experience cycles mostly synchronized with climate, calving glaciers are affected by numerous other factors in and around the fjord that equally impact the cycles of tidewater glaciers, making them asynchronous with climate [62]. One important factor is the water depth at the glacier front. During a slow advance, the glacier is building a moraine shoal that supports the advance of the glacier into deep water. Without the building of this shoal, the glacier advance would be prohibited by a higher calving rate in deeper water (see Fig. 1.4). However, when the glacier starts loosing mass due to surface melt driven by unfavorable climatic conditions, the front is no longer stable in deep water and starts retreating very quickly until it reaches another stable position further back.

Rapid tidewater glacier retreats have been observed in many different parts of the world [88, 16, 68]: **how can they be interpreted in terms of climate change?** (*Paper 5*). Columbia Glacier, for example Fig. 1.5 has experienced a 16 km retreat since 1982 [88].

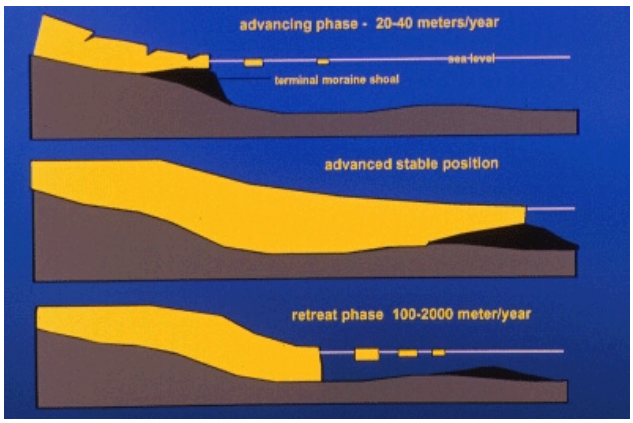

Figure 1.3: Tidewater glacier advance/retreat cycle [90]. In this thesis we focus on the rapid retreat phase.

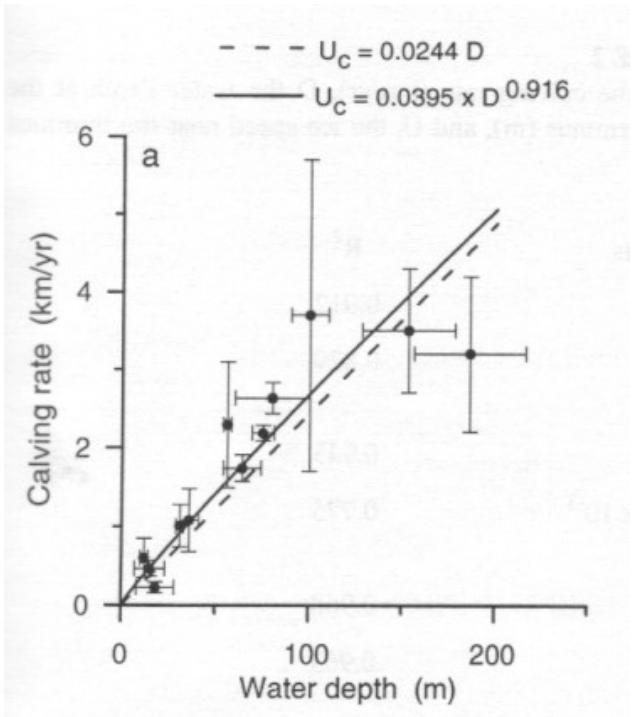

Figure 1.4: Best fit between calving rate and water depth for 12 Alaskan glaciers. From [17]

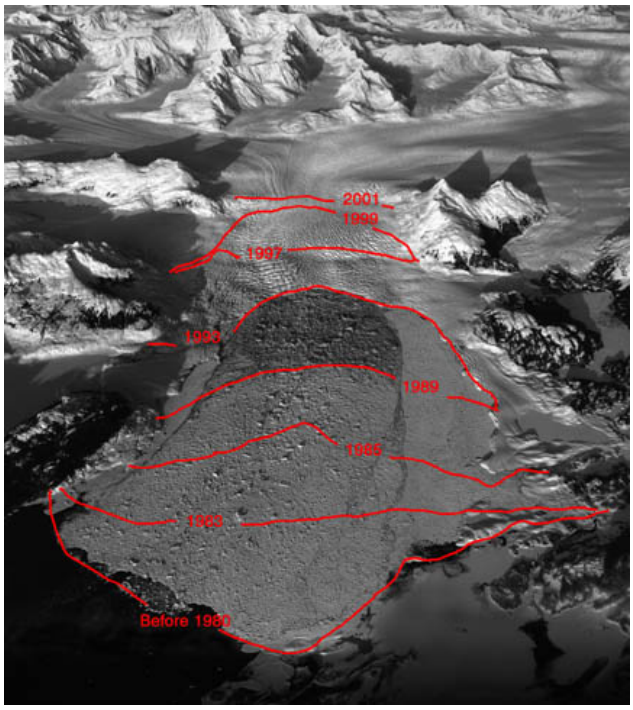

Figure 1.5: Successive positions of the front of Columbia Glacier, Alaska, showing the rapid retreat of the glacier during the last 20 years. Photo: R.M. Krimmel USGS.

In addition, large calving events have been observed in different parts of the world. A typical example is the recent massive calving event at Petermann Glacier [29] Fig. 1.6. The authors investigate several factors thought to influence calving, like the fjord geometry, tidal flexing, surface water ponding, surface temperatures, surface winds, without finding significant correlations. They propose that strong winds could drive sea ice out of the fjord and thus remove a possible inhibitor of calving. However the following questions remain unanswered: **Are these large calving events a sign of changes in the glacier's dynamics? Can they be characterized as part of the glacier's natural variability?** (*Paper 5*).

1.2.2 The calving process

The calving of icebergs is a very irregular process and with large variabilities in both the size and timing of events. In order to improve our understanding of the calving process, we must understand **what controls the size and intervals of calving-events?** (*Paper 5*). However, collecting data of individual calving events proves to be a challenge, both because of the dangers related to the collapse of columns of ice, and because calving events happen very fast (from seconds to several minutes) and are hard to observe continuously.

Several methods have been used to detect single calving-events. **What is the most effective and practical method to monitor individual calving events?** (*Paper 1, 2 and 3*).

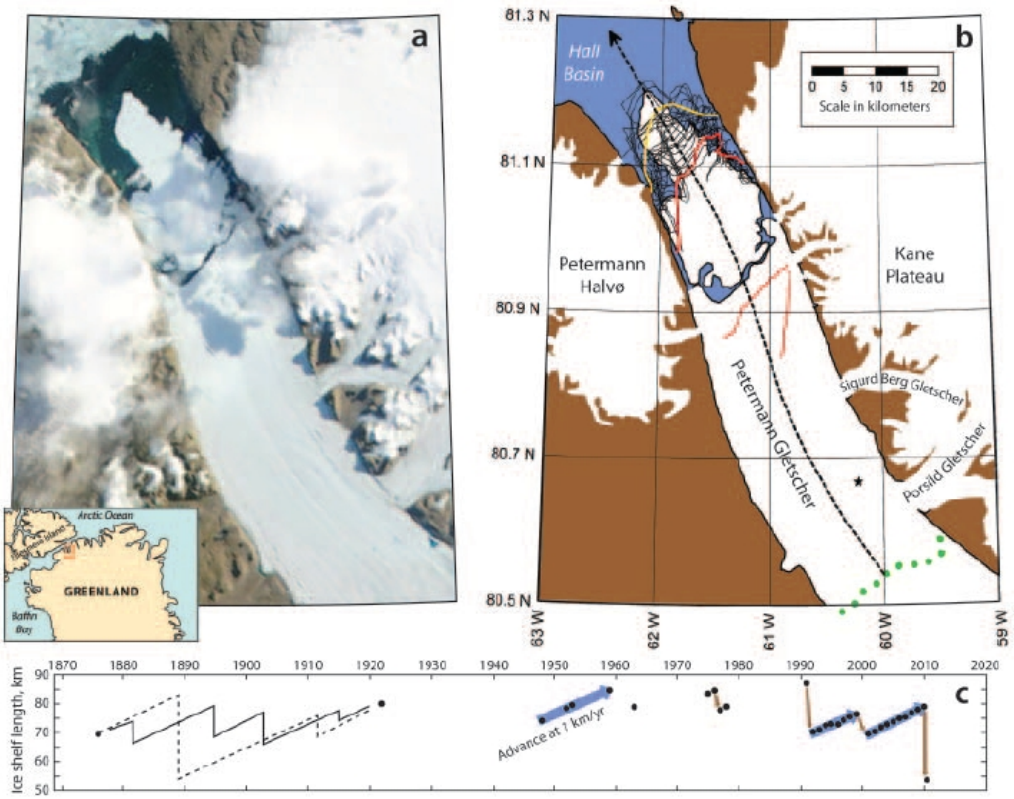

Figure 1.6: (a) Satellite image showing the calving event on August 5, 2010, (b) Map showing 31 known positions of the front, and (c) Time series of ice shelf length measured along the central axis from the grounding line. [29]

Passive seismic is a well-developed method that is extremely promising to detect individual events (e.g. [92, 84, 2]). Different processes can generate glacier seismic events: sliding at the base due to glacial flow [5, 103], opening of cracks or crevasses [15, 25], and calving [92, 86]. Most studies recorded local or regional events, however, moderate glacier earthquakes have also been observed globally at the outlet glaciers of Greenland and Antarctica [27, 70]. The previously cited studies suggest that single calving events can be detected automatically, and localized. The amplitude of the seismic signal also indicates the size of the events. One disadvantage of this method is that it does not provide qualitative description of the calving events and it might miss the smallest calving events.

Acoustic recording is another possible method since acoustic events due to calving are often well-correlated with seismic events [3]. Different types of audio signals correspond to different types of calving: sharp cracking sounds suggest ice fracturing while long low rumblings are caused by avalanche of ice debris. This method could potentially provide the location, size and timing of calving events. Once again it does not provide qualitative description of the events and the quality of the monitoring can be reduced by strong winds.

Tide gauge close to the glacier front can also be used to detect single calving events [3]. Calving events generate vertical oscillations up to more than 1 m, even as far as 3 km from the front. This method is promising for the detection of relatively large calving events although it might be difficult to distinguish between several small events and one big event.

Terrestrial photogrammetry has been used to follow the major changes of the front position (e.g. [84]) and large calving events, e.g. [2, 3] by using repeat photography, taken every few minutes. This technique is very useful, but does not allow for the detection of all calving events given the time lapse between pictures and the fact that some parts of the front might not be visible from the camera position.

Finally a very simple method for monitoring calving events is direct "human" observations, e.g. [118, 92, 117, 84, 86]. It does not necessitate very advance technical equipment since it relies only on the observers perception. This technique is very simple and presents obvious problems like the lack of attention from the observers or bad/cold weather conditions that can degrade the observation s quality, however it provides both qualitative and semi-quantitative data of single calving events. Methods involving more advanced technology provide more accurate data, but they are fragmented in space and time and place the researcher far from the object of research. So, despite the simplicity of this method, it should not be underrated. But, **can we learn anything of the physics of calving processes by simply observing at the glacier?** (*Paper 5*). Jensen [46] described painting and mathematics as different approaches to reality and "different but complementary ways of visualizing the concrete or abstract reality in which we are embedded". In the same way we see direct observations and sketching of the glacier as different but complementary methods for the study of calving. Additionally, the paleontologist Gould [31] argues that only "storytelling" can be used in many sciences because particular outcomes are contingent on many single and unpredictable events [6]. In this work we think that iceberg calving is part of those sciences in which events are not repeatable or predictable, but might be explainable. The goal of direct observations is then to get a narrative account, as accurate and quantitative as possible, of specific calving events. From this narrative we hope to explain in hindsight what has happened, even though it may not be possible to predict what will happen in the

future in details.

1.2.3 Known controls of calving

We have showed that tidewater glaciers are very sensitive to their immediate environment, both climatic (e.g. air temperature) and geometric (e.g. water depth), and are also linked to the glacier dynamics (e.g. velocity, creep rate). Despite their potential importance in terms of control, the relations between calving and these parameters are not completely understood [13]. A missing part of the study of calving is the study of individual calving events. Very few observational studies [118, 117, 92, 84, 86, 85] and no modeling studies report single calving events. However, in order to understand the physics of the calving processes, what initiates glacier retreat, and what processes are responsible for calving events, individual calving events must be explained [107].

Current knowledge about calving comes both from field observations (e.g. [67, 84, 86, 85, 92, 98, 117, 118]) and modeling (e.g. [4, 14, 17, 73, 82, 87, 106, 114, 115]).

Modeling attempts have mostly focused on predicting calving rates and front positions based on external variables like water depth [17, 82], height-above-buoyancy or buoyancy perturbation [106, 114, 115], the penetration of surface crevasses arising from the longitudinal strain rates near the calving front and enhanced by the presence of liquid water [14, 73, 87] and more general glacier characteristics like ice thickness, thickness gradient, strain rate, mass balance rate and backward melting of the terminus [4].

Observations studies have looked at the impact of several external processes on calving activity but it is still not very clear **what the effect of climate change is on iceberg calving** (*Paper 5*). The effect of rain has been observed in the field by [118] and [84, 86], as well as the effect of meltwater [85]. Those observations fit well with the controls on calving listed above. Tides have sometimes been reported as having an effect on the calving activity [117, 84, 86], but not for all studies [92, 85]. Submarine melting and seasonal changes in sea water temperature also impact the calving activity [67, 98].

Possible controls of calving have come from these studies, and are summarized by [13]

(i) first-order controls determine the position of the front. It is mainly the strain rate arising from variations in velocity at the front of the glacier causing the opening of crevasses. Meltwater and rain are two enhancing factors since their action can deepen the crevasses (hydro-facturing).

(ii) second-order controls are responsible for the calving of individual calving events, they are the force imbalance at the front due to the front geometry, undercutting at the terminus and buoyancy perturbations.

(iii) third-order controls are linked to the calving of submarine icebergs, a calving style that differs from subaerial calving.

1.3 Complex systems and tipping points

In this thesis we approach the study of calving from a single-event perspective, i.e. by looking at individual events and the relations between them. This approach is motivated by studies of complex systems. A complex system is a system composed of many heterogeneous parts that interact non linearly and can give rise to emergent behavior [99]. Individual events are believed to be all equally important in terms of dynamics of the system. The emphasis is on the relation between events – relative size and inter-event times – and interactions within the system. A tidewater glacier, composed of very heterogeneous parts such as the ice body, possible medial and lateral moraine, the bedrock, a frontal moraine, the water at the glacier face, the atmosphere interacting with the glacier surface, etc., can be seen as a complex system. In this view, calving is the response of the glacier system to perturbations, like earthquakes are the responses of the crust of the Earth to plate tectonics [7, 35], forest fires to the growth of trees and external perturbations [20], landslides to the landscape formation, erosion, soil properties, etc. [32], and sea ice fracturing to stress building in the ice due to winds, etc. [93].

The statistical analysis and the simple calving model of *Paper 5* are inspired by studies of complex systems. Additionally, much of the meaning and implications we extract from our calving data are inspired by other complex systems. **What can we learn by using this new approach and monitoring individual calving events? Is this approach valuable in terms of learning about glacier dynamics?** (*Paper 5*).

1.4 Kronebreen

Kronebreen, 78^o53 N, 12^o30 E, is a perfect candidate for observations of calving events Fig. 5.4 and Fig. 1.7. Its front is easily observable and access to the glacier is made relatively easy by the presence of the research station Ny-Ålesund, only 15 km away. Additionally this glacier has been observed for several decades, data about the glacier front position can be accessed since 1868 [61] and currently, several research groups are monitoring the weather, water depth, glacier front, glacier velocity, mass balance, etc., giving rise to a very complete dataset.

Kronebreen is a fast-flowing, grounded, polythermal tidewater glacier. Its front is joint to the one of Kongsvegen, its neighboring surging glacier. As a result of their proximity, Kongsvegen has been influencing the position of the front of Kronebreen. The map on Fig. 1.8 shows different positions of the front of Kronebreen since 1868. The last surge of Kongsvegen was in 1948 and since then the glacier has been retreating until it reached a more or less stable point in between Colletthøgda and Kongsvegen in a quiescent phase. It is still currently retreating and the velocity at the front varies between 2.5 and 3.5 m/d [100]. Calving represents 75% to 95% of the total mass loss of the glacier [78].

1.5 This thesis

The following questions have led to the work summarized in this thesis:

Figure 1.7: Artistic view of the front of Kronebreen by Kai Rune in 1998.

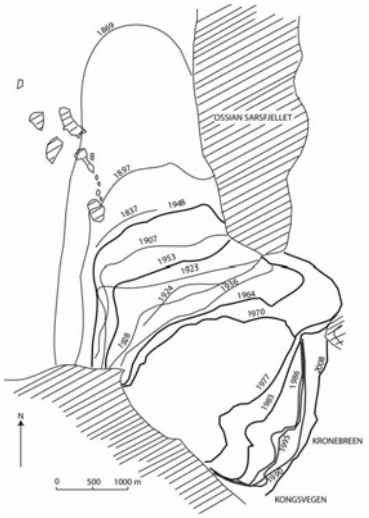

Figure 1.8: Position of the front of Kronebreen. Modified after [61].

- What is the most effective and practical method to monitor individual calving events?
- Can we learn anything of the physics of calving processes by simply observing at the glacier?
- Is the monitoring of individual calving events valuable in terms of learning about glacier dynamics?
- How is most of the ice lost at a calving face?
- What controls the size and interval of calving events?
- What is the effect of climate change on iceberg calving?
- What is the role of calving in the response of tidewater glaciers to climate change?
- How can rapid glacier retreats be interpreted in term of climate change?
- Are large calving events a sign of changes in the glacier s dynamics? Or can they be characterized as part of the glacier s natural variability?
- How to include iceberg production into glacier models?

The papers listed below are the result of the thesis work to answer those questions:

- **Paper 1** studies the destructive interference effect due to multipath scattering in combination with the geometry of radar, tidewater sea-level and glacier topography that can be observed by ground-based RADAR at the front of a tidewater glacier.
- **Paper 2** presents the results of two test seasons for automatically detecting calving events using a ground-based RADAR. The calibrating/validating dataset was obtained by visual observations and terrestrial photogrammetry.
- **Paper 3** explores the possibility for using simple seismic monitoring to detect calving events. We use two calibration/validation periods during which we have a seismic record, visual observations and terrestrial photogrammetry. Seismic activity, once calibrated, was extrapolated beyond the calibration periods to obtain seasonal variations in calving activity and look into the relationship between calving and glacier dynamics.
- **Paper 4** tests several calving criteria currently used in calving models and also investigates the role of preexisting crevasses by using visual observations for calving activity and satellite images for crevasse patterns and glacier speed and longitudinal stretching rates.

- **Paper 5** tests the impact of calving on the stability of the glacier front. We build a simple calving model which solely focuses on the interplay between calving and its impact on the front stability. We compare the resulting sizes and intervals distributions to the ones observed in the field for three different years and for two different glaciers. The aims of this paper are to determine the relationship between front destabilization and calving and if the glacier stability impacts the size of individual calving events.

1.6 Publications from this thesis

1.6.1 Peer reviewed journal publications

Rolstad, C., **Chapuis, A.**, Norland, R., 2009. Electromagnetic interference in ground-based interferometric radar data from Kronebreen (Svalbard) calving front due to multipath scattering and tidal cycles. Journal of Glaciology 55 (193), 943-945.

Chapuis, A., Rolstad, C., Norland, R., 2010. Terrestrial photogrammetry and visual observations for interpretation of ground-based interferometric radar data of the calving front of Kronebreen. Annals of Glaciology 55, 34-40.

Chapuis, A., Tetzlaff, T. (in prep.). What do the distributions of calving-event sizes and intervals say about the stability of tidewater glaciers? Prepared for submission to Journal of Glaciology.

Kohler, A., **Chapuis, A.**, Nuth, C., Weidle C., Kohler, J. (in prep.). Seasonal variations of glacier dynamics at Kronebreen, Svalbard, revealed by calving-related seismicity. Prepared for submission to Journal of Glaciology.

Chapuis, A., Berthier, E. (in prep.). Impact of geometric and dynamic constraints on the calving activity of Kronebreen, Svalbard. Prepared for submission to Journal of Glaciology.

1.6.2 Conferences contributions

Rolstad-Denby C., **Chapuis A.**, Norland R., 2010. Experiences with the use of ground-based radar near the calving front of Kronebreen, Svalbard. Invited talk at the American Geophysical Union Fall meeting, San Francisco, U.S.A.

Chapuis, A., Tetzlaff, T., 2010. Does iceberg calving reflect the dynamics of a system self-organized in a critical state? Talk at the Graduate Climate Conference, Seattle, U.S.A.

Chapuis A., Tetzlaff, T., 2010. On the nature of iceberg calving. Talk at the International Polar Year Oslo Science Conference, Oslo, Norway.

Chapuis A., Tetzlaff, T., 2010. On the nature of iceberg calving: a self-organized critical state? Talk at the European Geosciences Union conference in Vienna, Austria.

Chapuis A., Tetzlaff, T., 2010. On the nature of iceberg calving: a self-organized critical state? Talk at the International Arctic Science Committee- Glaciodyn meeting in Obergurgl, Austria.

Chapuis A., Berthier, E., Rolstad, C., 2009. Calving processes of Kronebreen, Svalbard: calving rate variations and their possible controls. Talk at the International Glaciological Society- Glaciology in the IPY meeting, Newcastle.

Chapuis, A., Rolstad, C., Norland, R., 2009. Terrestrial photogrammetry and visual observations for interpretation of ground-based interferometric radar data of the calving front of Kronebreen. Talk at the International Glaciological Society - Glaciology in the IPY meeting, Newcastle.

Chapuis, A., Berthier, E, Rolstad, C., 2009. Calving variations at Kronebreen, Svalbard. Talk at the International Arctic Science Committee - Glaciodyn meeting in Calgary, Canada.

Chapuis, A., Rolstad, C., 2008. Terrestrial photogrammetry for measurements of the calving rate of Kronebreen, Svalbard. Poster at the American Geophysical Union, San Francisco, USA.

Chapuis, A., Rolstad, C, Maalen-Johansen, I., 2008. Terrestrial photogrammetry for measurements of the calving rate of Kronebreen, Svalbard. Poster at the Workshop on the dynamics and mass budget of Arctic glaciers/GLACIODYN (IPY) meeting, Obergurgl, Austria, January 2008.

Chapuis, A., Rolstad, C., 2007. The dynamic response of Arctic glaciers to global warming. Poster at the Nordic Branch of the International Glaciological Society (NGIS) meeting, Uppsala. 25-27 October 2007.

1.6.3 Outreach activities and popularization

Christensen, A., 2011. Som hjernen, så breen. Vulgarization article in *Forskning.no*.

Chapuis A., 2010. Environment and Society circuit or short-circuit? Comments at the Spring Conference Environment at the Norwegian University of Sciences, Ås, Norway.

Chapuis, A., 2010. Exploring the dynamics of iceberg calving in Svalbard: implications for the future behavior of tidewater glaciers. Poster at the Jokkmokk Winter Conference Pathway to sustainable Northern Societies, Jokkmokk, Sweden.

Chapuis, A., 2009. Exploring the dynamics of iceberg calving in Svalbard, or how do the Arctic icemakers work. Talk at the WWF Arctic Tent for COP15, Copenhagen, Denmark.

Paper I

Chapter 2

Paper 1: Electromagnetic interference in ground-based interferometric radar data from Kronebreen (Svalbard) calving front due to multipath scattering and tidal cycles

Abstract In a recent paper, two of us [100] presented ground-based interferometric velocity measurements from 2007 of Kronebreen (Svalbard) calving front. It is of interest to determine whether the measured glacier velocities are influenced by tides. The intensity of the returned radar signal from the range 4100–4200 m (Fig. 2.1; Fig. 3 in [100]) has a sinusoidal pattern, correlated both in time and amplitude with the tidal signal (Fig. 2.1b). This pattern deserves an explanation. We show here that it is due to destructive interference (canceling the return signal) from multiple path reflections caused by the radar-target and sea-level geometry, and thus is not caused by variations in glacier movement. Radar signals are bounced by the sea surface, and ranges of the pathways between the radar antennas and the reflecting glacier vary according to the tides, and hence sea level heights. The sinusoidal pattern due to the destructive interference influences neither the measured velocity nor the accuracy of the measurements.

Published in Journal of Glaciology Vol. 55 (193), 2009, pages 943-945
Coauthored by C. Denby-Rolstad and R. Norland

The real-aperture antenna, frequency-modulated continuous-wave interferometric radar operates at 5.75 GHz at a high temporal rate (2 Hz). Velocities can be determined in the radar range direction by tracking natural permanent scatterers on the glacier ice in the radar data. We have not conducted any measurements to determine what surface features act as permanent scatterers, but related studies using ice cores and reflection horizons in firn and super- imposed ice measured by ground-penetrating radar at 5.3 GHz are presented by [59], and from glacier ice surfaces using satellite synthetic aperture radar European Remote-sensing Satellite (ERS-1) (5.3 Hz) data by [95]. Twenty-three hours of velocity measurements from the period of interest, 2930 August 2007, at the calving front and also ∼147 m further up-glacier are shown in Fig. 2.1c (Fig. 4 in [100]). These results show that the velocities are not clearly influenced by the changes in tidewater sea levels. The velocity ∼147m up-glacier from the front, at range 4189 m, is nearly stable during the period. The speed-up at range 4042 m from 0800 h to 1440 h local time (LT) is thought to be due to rotation of an ice block at the front in advance of calving, as discussed by [100]. The main argument for ice-block rotation is that the measured velocities yield surface strain rates, which implies stresses beyond the tensile stress for fracture of ice, and that large transverse surface crevasses are present near the front. However, the movement of the glacier clearly cannot explain the observed sinusoidal pattern in Fig. 2.1a.

Geometry of radar, sea-surface, glacier topography, and multipath reflections During the measurements, the radar antennas are placed ∼4 km from the calving front, emitting and receiving directly towards the calving front (Fig. 2.2a). The radar beam covers a width of ∼700 m of the calving front, with the center main beam (MB) position shown in Fig. 2.2b.

In interferometric radar we measure the phase of an electromagnetic wave scattered back from an object at some distance R (the range). The geometry of the reflection path from a target to the receiving radar antenna is shown in Fig. 2.2d. There are four possible paths between antenna and target (Fig. 2.2c); reflections following paths 1 and 3 go directly between the radar and the target, while reflections following paths 2 and 4 are bounced by the sea surface. Along paths 3 and 4 the beam from the transmitting radar antenna is bounced by the sea surface. Paths 2 and 3 yield the same path length, while the difference in path length d between paths 1 and 2 and between paths 3 and 4 can be expressed by a standard approximation [74] as:

$$d = \frac{2h_s h_T}{R} \tag{2.1}$$

where h_s is the height of the radar antenna and h_T is the height of the point target. A destructive interference pattern will occur when

$$d = (n + \frac{1}{2})\lambda \tag{2.2}$$

where n is an integer and λ is the electromagnetic wavelength. Both h_s and h_T will vary through the tidal cycle, thus yielding temporal variations in the horizontal distance R to the target giving rise to the destructive interference pattern seen in Fig. 2.1a. The above equations can be used to determine the distances R at which destructive interferometric patterns may

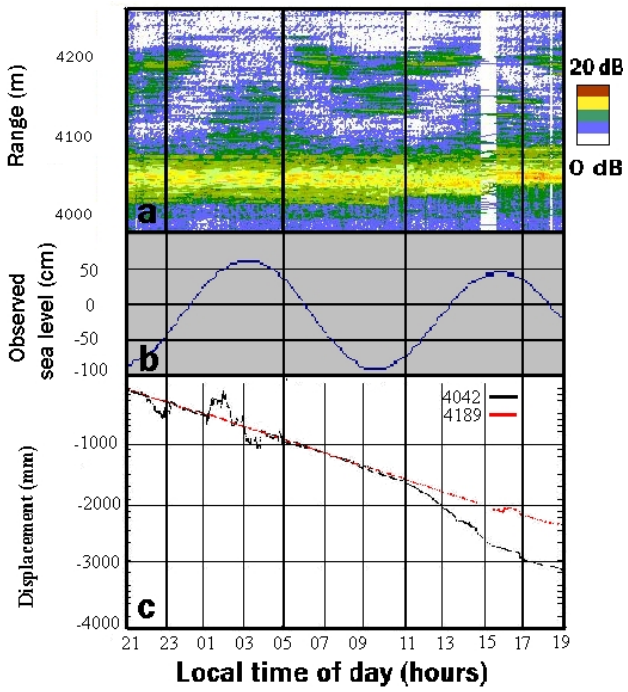

Figure 2.1: (a) Intensity of returned radar signal (dB), according to the color bar. Range ∼4020–4050 m is the vertical glacier front. Sinusoidal- shaped destructive interferometric pattern (white) occurs in range ∼4100–4200 m. Measurements from 2100 h LT on 29 August to 1900 h LT on 30 August 2007. (b) Observed sea level in Ny-Ålesund, Svalbard, during the same period, with mean sea level as reference level (Norwegian Hydrographic Service, Norwegian Mapping Authority). (c) Movement profiles in radar range direction at specific ranges, tracked from permanent scatters, 29–30 August 2007, range 4042 and 4189 m.

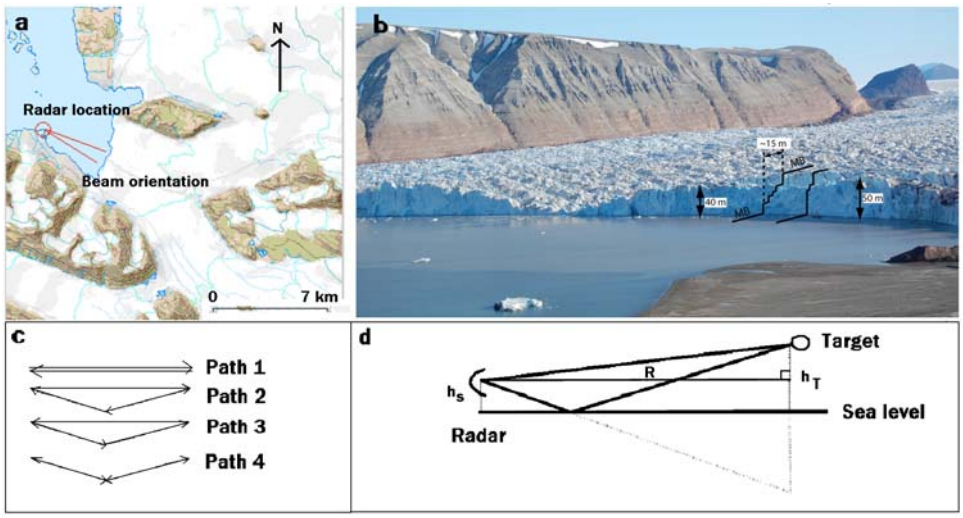

Figure 2.2: (a) Map showing location of radar and beam orientation during measurements. (b) Monophotogrammetry optical image of glacier calving-front measurement area. *MB* is main beam location, and black arrows show measured front elevations. The step-like topography near the front is also indicated by black lines. (c) Four possible paths of the radar beam. (d) Geometry of radar, sea surface and reflecting target geometry. R is the range to the scatterer, h_s is the height of the radar antenna and h_T is the height of the point target.

occur for a given target height for n = 0,1,2,3... when λ= 0.056 m. The height of the radar antenna, h_s =5.1 m a.s.l., was measured using a global positioning system (GPS). The GPS positions are referred to International Terrestrial Reference Frame (ITRF) 2000, and the elevations are ellipsoidal heights corrected with the geoid determined by the Norwegian Mapping Authority. From single-image terrestrial photographs we estimate an average target height near the ice front of $h_T \approx 57$ m (range 4100 m). Applying n = 0,1,2,3,4... we find that the destructive interference pattern may occur at corresponding distances from the radar antenna: $R_{n=0}$ = 20 764 m, $R_{n=1}$ = 6291 m, $R_{n=2}$ = 4152 m, $R_{n=3}$ = 2966 m and $R_{n=4}$ = 2307 m. As seen in Fig. 2.1, the range R $\approx$ 4150 m for $n = 2$ fits with our estimated geometry.

Table 2.1: Measured antenna heights h_s and ranges R from Fig. 2.1, and calculated target heights h_T for two cycles of tidewater, high and low, for n=2 and λ=0.056m

Time and sea-level height h	R m	h_s m	Estimated h_T m	Slope
29 July, 2110 h LT, h = 0.78 m	4100	5.88	49	0.18
30 Aug., 0330hLT; h=0.72m	4200	4.38	67	
30 Aug., 0940 h LT; h = 0.82 m	4100	5.92	48	0.2
30 Aug., 1550hLT; h=0.54m	4180	4.56	64	

The slope of the glacier determines the variations in range from $\sim$ 4100 to $\sim$ 4200m, to targets giving rise to the destructive interference pattern during the tidewater cycle. We now

evaluate whether the glacier, tidewater-sea-level geometry fits with the observed pattern in Fig. 2.1a. To estimate the height of the reflecting target h_T, (2.1) and (2.2) are solved for h_T using values of h_s corresponding to high and low tide during the cycle, and values of R scaled from Fig. 2.1 for that time. The results are listed in Tab. 2.1 for λ =0.056m and n=2. We find that the width of the destructive interferometric pattern requires a fairly steep glacier surface slope. This is consistent with Fig. 2.2b, which shows that the glacier surface topography is steep and step-like in the measurement area. We therefore conclude that the interference pattern in Fig. 2.1 is due to multipath scattering in combination with radar, tidewater-sea-level and glacier topography, and not a result of movement of the glacier.

Paper II

Chapter 3

Paper 2: Terrestrial photogrammetry and visual observations for interpretation of ground-based interferometric radar data of the calving front of Kronebreen, Svalbard

Abstract A ground-based radar has successfully been used for monitoring calving events and velocities at Kronebreen, Svalbard for two test seasons in 2007 and 2008. We here use daily terrestrial optical photogrammetry and continuous visual observation to validate the interpretation of a 116 hour ground-based radar amplitude of return signal data record from August 26 to August 30, 2008. The radar was placed 4 km from the glacier. It measured at high temporal rate (2 Hz), and the antenna lobe covered a width of 700 m of the front. The calving front geometry was extracted from the optical images, and its effect on radar backscatter, together with the movement of the glacier was identified in the plot of the amplitude of the radar return signal. Calving events were detected applying an automated change detection technique on the radar data set. This technique allowed us to detect 92% of the events that were observed during the same time. In this paper we focus on the method rather than on data interpretation. However, future use of this method, combined with meteorological data, tides and ocean temperature can be a valuable technique for calving process studies.

Published in Annals of Glaciology Vol. 51 (55), 2010, pages 34-40
Coauthored by C. Denby-Rolstad and R. Norland

3.1 Introduction

Calving is one of the most important sources of ice lost by tidewater glaciers, together with surface, basal and submarine melting. For all glaciers on Earth, surface accumulation adds about 3000 10^{12} kg water equivalent annually while surface ablation removes around 1000 10^{12} kg, and calving of icebergs around 2400 10^{12} kg [43]. Despite their importance, calving and associated dynamical changes are some of the least understood glacial processes and remain a key uncertainty in the future evolution of tidewater glaciers.

Data of temporal variation of calving events and velocities directly from the calving fronts are very valuable because they inform about calving processes. However, such data are rare, due to the dangers and difficulties connected with making the measurements. Studies like remote sensing can inform about the seasonality of calving, however, to learn about the details of calving processes, one must observe calving events in detail. Such detailed observations enable the understanding of what controls calving and what triggers individual calving events.

To capture the nature of the calving processes the following techniques have previously been used: direct visual observations [117, 84, 86], passive seismic [92, 84, 2] and ground-based interferometric radar [100]. Direct visual observations produce very detailed data about calving of icebergs, giving information about the timing, location and style of calving. However this method requires a permanent presence in the field and the results can be altered by bad visibility (darkness, fog), difficult conditions for observations (storm, rain, wind) or lack of attention from the observers. Passive seismic is a good technique to obtain calving event frequency and possibly location, independently of weather conditions. But uncertainty remains over the origin of icequakes and the fact that not all of them are caused by calving of icebergs but can also be caused by fractures in the glacier body or icebergs rolling in the fjord [2]. Recently, ground-based radar has proved to be valuable for measuring ice front velocity and identifying calving events of Kronebreen [100]. However, what was absent in that study was spatial information about the returned radar signal. They also showed that identification of calving events was possible on the backscatter amplitude plot, but made no attempt to extract calving event frequency automatically from the data set. The use of a ground-based radar is appealing because it can be conducted at a safe distance from the glacier front, and it produces both good spatial and temporal resolution. It can be operated automatically and does not require a constant presence in the field. This last characteristic offers a big advantage compared to direct visual observations, which also provide good spatial and temporal resolution but require a constant presence in the field. Finally, the topography in front of Kronebreen offers an ideal setting for radar studies, a lateral moraine providing a direct line of view to the glacier front (Fig. 3.1).

During the field campaign in August, 2008 we visually observed the calving front of Kronebreen during the same period as the radar campaign was conducted, and we collected photogrammetrical data. We wanted to investigate whether we could detect all calving events with the radar and if not, which calving events can be detected. In this paper we demonstrate spatial interpretation of a radar backscatter signal with the help of photogrammetry. We also present a new technique to automatically detect calving events using image processing change

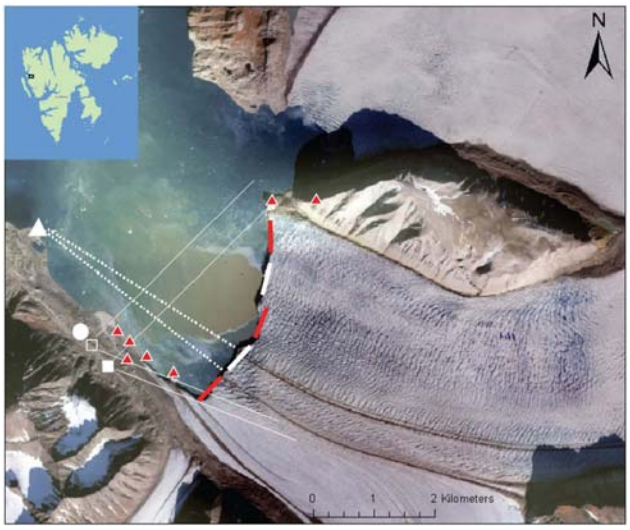

Figure 3.1: Orthorectified aerial photograph of Kronebreen in 1990 (Norwegian Polar Institute). The white triangle marks the position of the ground-based radar, the circle marks the position of the camp from where the direct visual observations were performed and the two squares mark the position of the cameras, the full square showing the position of the single-imaging camera. Red triangles mark the positions of control points. The white and red rectangles define the five different areas used for the direct observations.

detection, applied to radar backscatter data. We establish a time series of calving events using this algorithm, and compare the results with registered visual observation of calving events. Finally we look at the temporal geometrical evolution of the calving front.

3.2 Field area

Kronebreen is a grounded, polythermal tidewater glacier, located approximately 14 km southeast of Ny-Ålesund, western Spitsbergen. The glacier drains a glacial basin called Holtedahlfonna, which covers 700 km^2 and is approximately 30 km long. The lower 18 km of the glacier are heavily crevassed. The terminal ice cliff had an elevation ranging from 5 to 60 m above the fjord surface at the end of august 2008. The height of the front experiences numerous variations during the year. The lowest portion in August 2008 (around 500 m in length) reached only 5 m above the water, but had been standing at 40 m above the water in May 2008. This variation within 2 months indicates a very active glacier front.

3.3 Methods

To test this new technique of calving event detection on Kronebreen, we used a ground-based radar from August 26 to August 31, 2008. To validate the results, terrestrial photogrammetry and direct visual observations were performed during the same period. We chose to use a ground-based radar to collect data from the glacier front because it provides a continuous

dataset about the glacier front movement and the range to the front yielding the calving events.

Terrestrial photogrammetry gives good data about the front position and shape as well, but there is a trade off between spatial and temporal resolution which does not exist with the radar. In fact, terrestrial photogrammetry at Kronebreen does not provide a spatial accuracy better than 1 m. It is, however, a very good technique to image the front shape.

3.3.1 Ground-based radar

We used a 5.75 GHz, frequency modulated continuous-wave (FMCW) radar located about 4 km west of the glacier front (Fig. 3.1). The range resolution was 1 m and the measurement interval was 0.5 second. The antenna lobe had an opening of 9 degrees, which covered about 645 m out of the 3500 m of the entire ice front width. In this paper we define the dimensions as follows: width is the distance along the ice front, height is the vertical distance above the water line and depth is the up-glacier distance between the ice front and the calving fracture. A corner reflector was placed between the radar antenna and the glacier for calibration. The radar was running continuously for approximately 116 hours between August 26 and August 30, 2008. A technique used to obtain the range variation of natural scatterers on the glacier front for velocity measurements is described by [100]. In their paper, the relative velocities were determined interferometrically from the change in phase between two consecutive samples. In this paper we have used only the amplitude of the backscattered signal in conjunction with optical methods, to identify calving events and automate the process of this identification.

The radar can be left to run automatically. A similar permanent installation for mountain rock slide monitoring in the Norwegian fjord Tafjorden has run since 2006 [75]. The power consumption is similar to a PC (400-800 W) and the antenna output power is 0.001 W. The data storage capacity can be designed to fit the requirements for different monitoring duration. The system is very stable in our experience and, if installed correctly, there is no need to check the installation. Antennae may be protected with a radome and for permanent monitoring the radar may be placed in a house. This system can thus be used for future campaign that would cover a much longer time span.

3.3.2 Interpreting a radar backscatter amplitude plot of a glacier front

In order to interpret both spatial and temporal variations in the signal, it is necessary to understand what can affect the radar backscatter in theory. Five main factors can affect the radar backscatter signal: incidence angle, the frequency and polarization of the radar, surface roughness, and moisture.

The incidence angle plays the largest role in our study because it changes dramatically as the terminus geometry changes. The incidence angle is the angle between the normal to the object surface (calving front in our case) and the direction of the incident radiation. The smaller the incidence angle, the stronger the backscatter amplitude. In our case, the

incident angle is very large over the intervening water (incident angle being almost 90^o) and becomes close to 0^o when the radar beam intercepts the glacier front. This abrupt change in the incidence angle accounts for the overall patterns of spatial variations on the radar backscatter amplitude plot.

The frequency and polarization of the radar were kept constant during the week of investigation so the observed temporal changes in the backscatter values were mainly caused by temporal variations of the object surface properties and not the radar properties. Tests were conducted with different antenna configurations in 2007, yielding similar backscatter intensity for all polarizations [100].

Roughness influences the interaction of the radar signal with the ice surface and is a function of the incidence angle and the wavelength. The rougher the surface, the stronger the backscatter amplitude. In our case, the object surface is considered rough if the mean height of surface variations is larger than 0.02 μm, which is the case for the glacier surface. We can assume that the surface stays rough during the entire observation period.

Moisture has a strong impact on the surface reflectivity, which increases with the moisture content. So, changes in moisture, caused by rainfall or surface melting might induce some changes in the backscatter intensity. However, the overall intensity was relatively constant during the measurement campaign. Hence we conclude that moisture variations have little effect on our data set.

The propagation velocity of an electromagnetic wave in air varies with the refractive index, and the calculated range will vary accordingly. The refractive index varies with the meteorological parameters: temperature, pressure, and humidity. Variations in range due to this effect can be eliminated using measurements from a stable corner reflector [75] near the glacier, or by estimating the variations of the refractive index using local meteorological data [76]. However, experience shows that these variations in measured range are small and gradual. Variations in measured distance, mainly due to changes in the refractive index, over a distance of 2900 m was 30 cm during 2 winter months in Tafjorden [75]. We therefore assume that the ranges in the backscatter amplitude plot from Kronebreen vary by less than 10 cm due to refractive index uncertainties during the 116 hours of measurements in 2008.

Destructive interference due to multipath scattering of the electromagnetic wave and the tidal cycles may lead to a periodic pattern of zero intensity at specific ranges in the amplitude of the back scatter plot. This geometrical phenomena is described in [101], and it has no influence on the results described in this paper

Natural permanent scatterers on the glacier surface

A permanent scatterer on the glacier surface is moving towards the radar and reflects the signal back to it. On a backscatter amplitude plot, this is displayed as a permanent feature whose range decreases with time, as the permanent scatterer moves closer to the radar (Fig. 3.2).

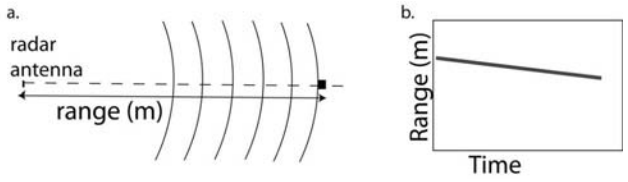

Figure 3.2: (a) Schematic aerial view of a natural permanent scattering reflector (black square) moving towards the radar antennae at constant speed. The distance between the radar and the reflector is called the range. (b) Resulting backscatter amplitude plot.

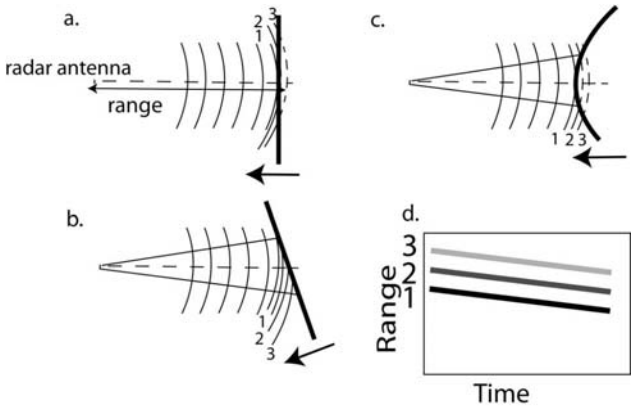

Figure 3.3: (a), (b) and (c) Glacier fronts (typical selected examples) moving towards the radar at constant speed and radar beams, one range-unit apart and (d) corresponding backscatter amplitude plots.

The spatial configuration of the glacier front

The shape of the front and its spatial arrangement with respect to the radar is important to correctly interpret the radar backscatter amplitude plot. Fig. 3.3 presents three different spatial configurations of a radar illuminating a glacier front. To simplify we only show radar beams, one range-unit apart. Each electromagnetic wave associated to a single range value can intersect the glacier front once or twice, depending upon the spatial configuration. Thus different configurations can produce similar amplitude plots, as shown in Fig. 3.3. In order to know how the radar beam interacts with the front and where the backscatter comes from, it is necessary to know the spatial configuration of the radar and the glacier front. In this study, we determined this configuration by the use of photogrammetry.

Geometry of vertical ice features acting as reflectors

Vertical ice features act as reflectors and form bands of high intensity in the amplitude backscatter plot (Fig. 3.3d). A glacier front which is a vertical cliff will produce a narrow band in the plot, whereas a front displaying a stepped shape will produce a wider band. This geometry is illustrated in Fig. 3.4. We can easily estimate s, the horizontal distance between the bottom and the top of the glacier front from how wide the high amplitude band is on the amplitude plot ($r_2 - r_1$).

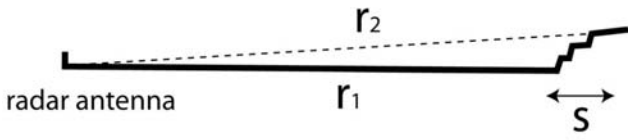

Figure 3.4: Geometry of the stepped shape of the front.

3.3.3 Terrestrial photogrammetry

Terrestrial photogrammetry is used here to obtain the shape of the glacier front at the time when the radar campaign was conducted. It is a method for measuring object sizes and shapes using photographs taken from the ground. In this study we have used mono-photogrammetry, analyzing single images to get two dimensional measurements, and stereo-photogrammetry using pairs of images to derive the three dimensions of the object. Photographs were taken with a Nikon D40 digital camera. Seven control points were placed on the shore and on nearby mountain peaks (Fig. 3.1). Because stereo-photogrammetry is a more complex procedure, we retrieved the three-dimensional measurements of the glacier front from one stereo-pair of clear and sharp images photographed in clear weather on August 29, 2008. Fluctuations in front position were documented from single images using mono-photogrammetry, which provides less accurate measurements, but can be performed faster and does not require very sharp images.

Mono-Photogrammetry

The camera position was about 1.5 km west of the front (Fig. 3.1). Images were taken on August 28, August 29 and August 31, 2008. The front position is seen as the intersection between the plane defined by the fjord surface and the glacier ice cliff. A mono-photogrammetric routine allowed the determination of the coordinates of this intersection line. This routine was developed by Truffer (UAF) based on [57], and further improved by O Neel in 2009. Several studies (e.g. [84, 67, 83]) have successfully applied this routine to document the fluctuations of glacier fronts. We measured the camera position, elevation and pointing angles, and used 2 ground control points. Tidal amplitude and timing in the fjord are required and were obtained from the Norwegian Mapping Authority. The spatial resolution of the mono-photogrammetry is about 3 m.

Stereo-photogrammetry

Stereo-photogrammetry uses 2 simultaneous images of the same object to reconstruct its 3 dimensions. We applied it here to get a precise map of the front topography: shape, height and width. The cameras were located about 1.5 km west of the front, on a side moraine (Fig. 3.1) and the distance between the two cameras was 309 m. The requirements for the stereo-photogrammetrical method are the known positions and elevations of the two cameras and the presence of at least 6 control points in the field of view of the camera (Fig. 3.1). Image analysis included camera calibration, relative and absolute orientation, stereo-resampling and measurements. The purpose of the calibration was to estimate the cameras optical properties: focal length, distortion parameters and the point of best symmetry. The horizontal accuracies

were obtained by comparing the position of known objects to their estimated position using stereo-photogrammetry. At the ice front, the accuracy varies from 5 to 45 m. The accuracy decreases as the object gets further from the cameras, it fluctuates from 0.5 to more than 200 m at 8 km from the camera. The vertical accuracy (around 1 m) was estimated by comparing the front heights obtained on three different stereo-pairs.

3.3.4 Visual observations

Direct visual observations consisted of identifying and registering calving events from a safe distance. Between August 26 and September 1, 2008, we continuously observed the front activity of Kronebreen at about 1.5 km west of the front on a lateral moraine (Fig. 3.1). Four people were involved with the observations. We recorded the timing, location, type and magnitude of the events. The timing was determined with an accuracy of 1 minute. To define the location, we divided the glacier front into 5 different areas (Fig. 3.1). Six different types of events were observed: avalanche of ice when the pieces were too small to be identified as blocks, block slumps when a block of ice was disintegrated from the front, column drop when a column of ice collapsed vertically or quasi-vertically, column rotation when a column of ice collapsed with a rotation movement, submarine when a block of ice was released from underwater, and internal when we could only hear a loud crack, assuming fracturing of ice not associated with calving of icebergs or any missed/out of view calving events. The magnitude was subjectively attributed for each event based on a combination of the volume of ice involved, the width of the glacier affected, and the duration of the event. We used a magnitude scale [86] which ranged from 1 to 20, 20 being the whole front collapsing. The subjectivity led to a discrepancy of ± 1 in the magnitude estimation from one person to another.

3.4 Results and Discussion

In this section we present the three main results obtained by analysing the radar signal in combination with photogrammetry and visual observations. This yields a more complete interpretation of the radar plot linked to the glacier front geometry, an automatic way to detect individual calving events through image-processing change-detection techniques, and a temporal interpretation of the variations of the front positions.

3.4.1 Glacier front topography

The stereo-photogrammetry shows that the front is about 50 m high at the place on the glacier where the beam centre intercepts the front (Fig. 3.5). For the rest of this study we call this location Beam Centre (BC). The front at this particular area of the glacier is not vertical but presents a stepped shape (Fig. 3.4, Fig. 3.5). At BC the front reaches its maximum height 15 to 20 m up-glacier from the actual terminus position.

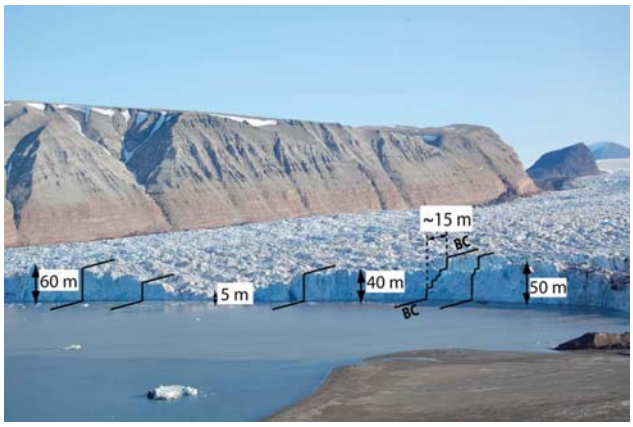

Figure 3.5: Photograph of the calving front on August 29, 2008. The black lines indicate the front topography. BC marks the intersection of the radar beam centre with the front.

3.4.2 Interpretation of the radar backscatter amplitude plot

Fig. 3.6 shows the radar backscatter intensity in the radar range (from 3900 to 4500 m) between August 26 12:00 and August 30 08:00 UMT. In general we see strong backscattered signals due to small incident angle and vertical ice walls. When these strong signals form continuous lines in the backscatter amplitude plot, with a trend representing a reasonable glacier velocity, we can assume that they are from vertical features of the moving glacier. We then used photogrammetry to determine one or several possible reflection points on the glacier corresponding to the measured range.

The range to the glacier front lies between 3950 and 4200 m. Beyond 4150 m, there is a periodical pattern of destructive interference resulting from multipath scattering due to radar-glacier geometry and tidal cycles [101]. The strongest and most permanent feature lies in the range 4100-4120 m. This is BC, the intersection of the centre beam of the radar with the calving front (Fig. 3.6b). Overall, this feature is advancing during the observation period with some sharp retreats corresponding to calving events (Fig. 3.6a) which are discussed in the following section. Results from the stereo-photogrammetry showed that the geometry of the front and the relative position of the radar are such that each transmitted electromagnetic wave front intercepts the glacier front only once. Any high reflecting features in the amplitude plot that appear closer than BC are parts of the glacier front located on the right-hand side of BC looking down-glacier, or an iceberg in front of the glacier, whereas any features that appear further away than BC on the amplitude plot are physically parts of the glacier front on the left-hand side of BC looking down-glacier. The topographical height of the ice feature of high-intensity backscatter at range 4120 m is about 20-25 m. Given the width of the high amplitude band at BC on the amplitude plot, we deduce that the front has a stepped shape. Photographs (Fig. 3.5) confirm this radar observation.

3.4.3 Detection of calving events

Black circles on the backscatter amplitude plot of figure 6a indicate sharp retreats at different places on the ice front at different times. Each of these is shown in more detail in Figure

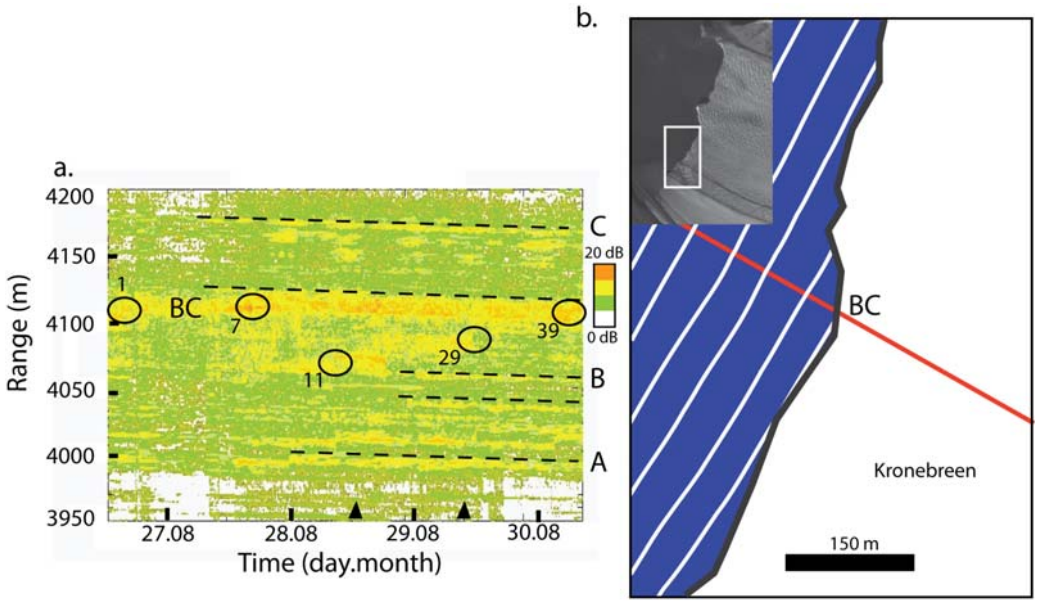

Figure 3.6: (a) Radar backscatter intensity (dB). The vertical glacier front ranges from 3950 to 4200 m. Measurements were conducted from local time 12:00 on August 26 to 08:00 on August 30, 2008. Black circles indicate sharp retreats of the front, representing the five calving events discussed in section 4.3. Dashed lines indicate strong permanent backscatter features. The two black triangles mark the time at which mono-photographs were taken (b) Calving front as imaged by SPOT on September 1, 2007. The red line marks the radar beam centre and the white arcs illustrate the radar waves hitting the glacier front.

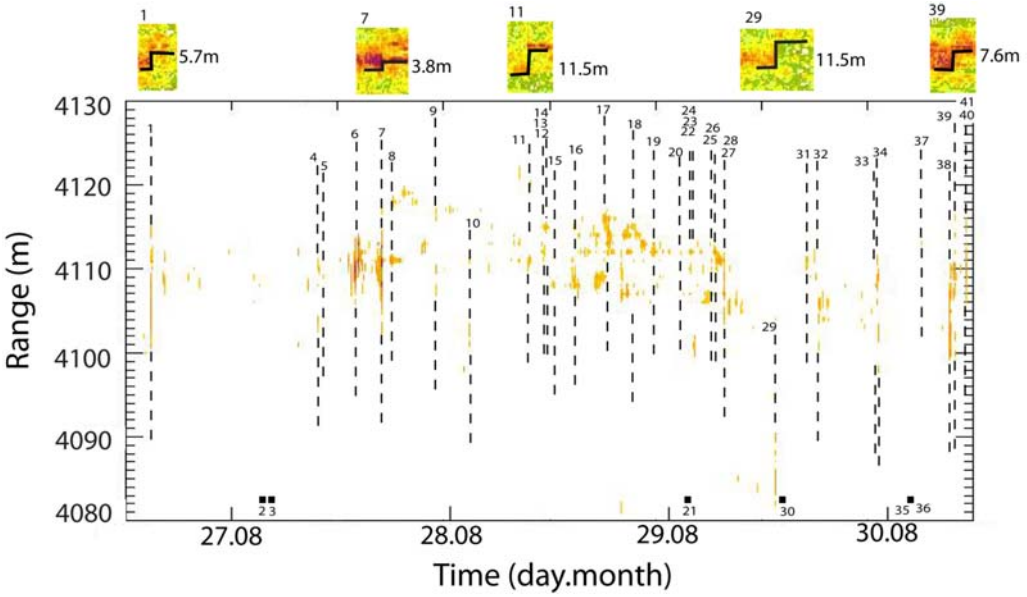

Figure 3.7: Change detection plot showing the time and place where column drops and column rotations were detected by the radar during 116 hours. Vertical dashed lines mark the visually observed events which were successfully identified automatically in the radar data by the change-detection routine. Dots below the plot mark observed events which were not detected. The upper part of the plot shows examples of five events (ID 1,7,11,29 and 39) identified in the raw backscatter radar data. The bold lines mark the corresponding interpreted retreat of the front.

7. We applied an automated change-detection algorithm on the backscatter data in order to build a calving event time series. The algorithm compared a 30 s averaged backscatter value at time $t = t_0$ with another at time $t = t_0 + 60s$, at the same range. We set a change threshold of 5 dB. If the change in the backscatter value was below this threshold, then we interpreted no change in the front geometry. However if the change in the backscatter value is larger than the threshold, we took this to indicate a change in the front geometry, and its intensity was indicated by the color scale ranging from green (small changes) to red (large changes). Fig. 3.7 shows the result of this change detection algorithm.

To validate the method, we compared the result of this radar backscatter change-detection with direct visual observations for the whole 116 h period. All column drops and rotations events that occurred within the radar beam (southern most side of the front) during the measurement period are plotted on the change detection plot (Fig. 3.7).

There is a good overall agreement between the observed calving events and the ones detected using the radar change-detection algorithm. Out of 41 events in total, 35 were identified with the radar (85%). Filtering out the events with a magnitude smaller than 2 (leaving 33 events), the percentage of identified calving events reached 92%. Almost all column drops and column rotations events with a magnitude larger than 2 that occurred within the radar beam were identified using the change-detection algorithm on the backscatter data.

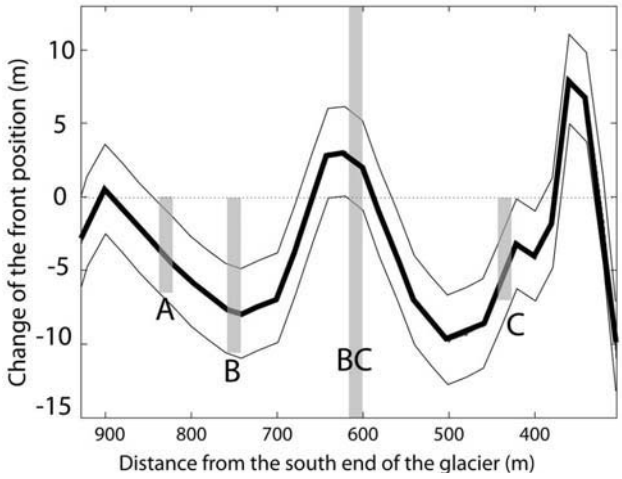

Figure 3.8: Variation of the front position along the glacier front (thick line) determined from mono-photogrammetry, looking up-glacier. Positive change in the front position is retreat. The two thinner lines indicate the estimated accuracy of the measurements. Grey bars mark the positions of the strong backscatters identified in Fig. 3.6a.

The observed calving events that were not identified using the algorithm, and thus not seen on the change detection plot (black squares below the plot), could possibly be out of the radar range because the area covered by visual observations was larger than the one covered by the radar. Conversely, changes automatically identified and displayed on the radar plot which do not appear in the visual observations list could have been missed by the observer for a number of reasons: lack of attention or bad visibility such as foggy conditions. Moreover, a block that rotates but does not calve within the time-window of 60 seconds during which the backscatter values are compared, may still modify its incident angle, thus leading to a changed backscatter value even though no calving happened. Icebergs floating in front of the glacier can also lead to changes in the backscatter value. This can be an issue in our case because icebergs can easily be in the way between the radar and the glacier front.

3.4.4 Temporal evolution of the calving front

Permanent strong backscatter features show the variations in front position at different places across the front.We followed several strong backscatter features on the radar plot (Fig. 3.6a) in order to obtain the change of the front position, or velocity during the observation period. Mono-photogrammetry was performed during the same period, with two images taken during the time the radar was operated (black triangles on Fig. 3.6).

Fig. 3.8 represents the variation of the front position dL between August 28 and August 29 for the area of the front covered by the radar. We observe an overall good agreement between the change in front position obtained by photogrammetry and by the ones from tracking different parts of the front on the radar signal. Although the front at BC shows a different behavior on the radar data and on the photogrammetry data. On the radar data the front shows constant velocity and hence an advancing front at BC whereas the

photographs suggest no net change or a slight retreat over the period. We cannot explain this discrepancy. The other locations (A, B and C) show a better agreement between the radar and photographs data. The fact the we observe almost no change in the front position at BC means that the calving events at this location have been neutralizing the general advance of the front, leading to a quasi non change in dL. On both sides of BC, the front has been advancing in average, as shown on Fig. 3.8, indicating that the calving activity was not large enough to counterbalance the advance caused by the glacier flow.

3.5 Conclusions

Ground-based radar is a powerful technique with great potential to investigate the behavior of a calving front. It presents the advantages of being conducted at a safe distance from the front and not requiring a permanent presence of personnel in the field. Moreover, coupled to terrestrial photogrammetry, it can provide very accurate data on the calving front behavior, both spatially and temporally. We have presented here the results of one week of radar data from the front of Kronebreen, coupled with terrestrial photogrammetry and direct observations. The main results are that:

- it is possible to determine the calving event frequency using a change detection algorithm on ground-based radar data.
- the majority (92%) of all column drops and column rotation events with an estimated magnitude larger than 2 ($\sim 1000m^3$) can be detected.
- terrestrial photogrammetry provides necessary information to spatially interpret the radar backscatter signal.

3.6 Acknowledgments

The work is part of the International Polar Year project GLACIODYN, funded by the Norwegian Research Council. The fieldwork was supported by Svalbard Science Forum. We wish to thank S. ONeel for his help with mono-photogrammetry analysis and A. Burras and N. Peters for their help in the field. Comments from reviewers J. Amundson, an anonymous reviewer and A. Smith greatly improved the manuscript.

Paper III

Chapter 4

Paper 3: Seasonal variations of glacier dynamics at Kronebreen, Svalbard, revealed by calving-related seismicity

Abstract We detect and cluster waveforms of seismic signals recorded close to the calving front of Kronebreen, Svalbard, to identify glacier-induced seismic events and to investigate their relation to calving processes. Single-channel geophone data recorded over several months in 2009 and 2010 and direct visual observations of the glacier front available for eleven days are used. We apply a processing scheme which combines classical seismic event detection using a sensitive trigger algorithm and unsupervised clustering of all detected signals based on their waveform characteristics by means of Self-Organizing Maps (SOMs). We are able to distinguish between false alarms, instrumental artifacts, and three classes of signals which are, with different degrees of uncertainty, emitted by calving activity. About 10% of the directly observed calving events close to the geophone (<1 km) can be correlated with seismic detections. By extrapolating the interpretation of seismic event classes beyond the time period of visual observations, the temporal distribution of glacier-related events shows an increase in event rate in autumn, particularly for the class which is clearly related to iceberg calving. Using the seismic event distribution in this class as a proxy for the calving rate and measurements of glacier velocity and glacier front position, we discuss the relationship between glacier dynamics and calving processes. On a seasonal time-scale, the well-marked glacier acceleration in spring is not followed by an increase in calving activity, and, in the opposite, a remarkable increase in calving activity during the autumn does not trigger higher glacier speed. On seasonal time-scales, calving rate seems to behave rather independently from the actual glacier speed, suggesting a complex and indirect dynamical link between the two quantities.

Prepared for submission to Journal of Glaciology
Coauthored by A. Köhler, C. Nuth, C. Weidle and J. Kohler

4.1 Introduction

Iceberg calving is a key process of glacier dynamics. It is responsible for 70% of the annual transfer of mass from glaciers to oceans [107], hence contributing to sea level rise [72]. With tidewater glaciers all around the world retreating, thinning, and accelerating, it is crucial to understand the relationship between glacier dynamics and calving processes. Is iceberg calving the cause or the consequence of glacier acceleration?

Iceberg calving is sporadic and therefore requires analysis of single-event data. A wide range of techniques has been used to obtain data of single-event iceberg calving, however none has proven totally optimal, i.e. reliable, not limited by darkness or bad weather conditions, providing the size, timing, type as well as location of iceberg calving events, and fully automatic. So far human-based perception has been used for different glaciers, e.g. [118, 117, 84, 86] and is recognized as the most practical method to acquire informations about the calving processes [107]. However, it has only been used for short observation periods due to the very intensive work in the field. It also presents some obvious problems linked to the lack of attention from the observers or limited visibility due to bad weather conditions that both reduce data quality. Other techniques include seismic recordings, terrestrial photogrammetry, ground-based radar [18], and remote sensing.

Seismic recordings have been used to monitor dynamic glacial activity for about 30 or 40 years [109, 121, 123]. Various studies have suggested different processes generating glacier-seismic events, such as sliding at the base due to the glacial flow [5, 103], opening of cracks or crevasses [15, 25], and calving [92, 86]. Calving events are described as emergent, low-frequency seismic signals, and impulsive, high-frequency acoustic arrivals when measured close to the glacier front [96]. The source mechanisms can be fracture processes before the calving [86] or the detachment itself, followed by overturning and scraping of icebergs [2]. Most studies recorded glacial, low-magnitude events in local or regional distances, however also moderate glacier earthquakes, which can be observed globally, have been identified within the last decade at the outlet glaciers on Greenland and in Antarctica [27, 70].

The use of seismic data supplementary to direct (visual) monitoring of calving activity bears therefore the potential to extend and complete observation time periods. Once the relation and scaling between calving events and their seismic signals is understood, seismic records can be employed to improve the understanding of that process and to reveal variations in iceberg calving activity over long time periods.

The objective of this study is to obtain a continuous record of calving activity over several months from seismic data recorded at Kronebreen, which is a grounded, polythermal tidewater glacier, located at 78°53 N, 12°30E , approximately 14 km south-east of Ny-Ålesund, western Spitsbergen (Fig. 4.1). Kronebreen is one of the fastest tidewater glaciers in Svalbard with an average front velocity ranging between 2.5 and 3.5 meters per day during the summer months [100] and with a terminal ice cliff having an elevation ranging from 5 to 60 m above the fjord surface at the end of August 2008 [18]. We installed a geophone in the vicinity of the calving front from spring to autumn in 2009 and 2010 and collected ground-truth data of iceberg calving for 16 days by visual observations with an overlap of dataset of 11 days. Seismic detections are calibrated against the direct observations to extrapolate seismic signals due to calving activity beyond the ground-truth period, giving us a proxy for the calving rate. In addition, we monitored the glacier velocity by using GPS measurements

close to the front, and recorded the changes in front position by tracking the glacier terminus using terrestrial photogrammetry. In combination with the estimated calving rate, this data set provides an insight into glacier dynamics at the front for several months.

4.2 Data

4.2.1 Seismic record

Several months of single-channel seismic data have been recorded on a PE-3 geophone from 29 June to 15 August 2009, 11 September to 11 November 2009, and 8 May to 6 November 2010 with a sampling rate of 50 Hz. The geophone was attached to a Campell CR1000 data logger with an Acumen memory module (compact flash memory). Power supply was provided by a 12V battery and a solar panel. The position of the geophone (see Fig. 4.1), and therefore also the coupling with the ice and the noise level, differ slightly between 2009 and 2010 since the instrument has been removed during the winter months. The geophone was initially buried 6 meters in the ice. The melting during summer decreased the thickness of the overlaying ice layer to about 3 meters. The seismic measurement has initially not been planned as a fully equipped seismic monitoring experiment. Therefore, the analysis of the seismic record in this paper will not include localization of events and the detailed investigation on their source mechanisms, what would require records of all three spatial wavefield components and more receivers.

4.2.2 Direct calving observations

We monitored the calving activity at Kronebreen based on human perception (viewing and hearing). Midnight sun in this region lasts from 18 April to 24 August, allowing to continuously monitor calving activity within this time period. Four persons observed the calving front of Kronebreen during a total of 16 days split into two periods: from 14 August 2009 00:00 to 26 August 2009 16:00 GMT and from 5 August 2010 23:30 to 15 August 2010 16:00. An overlap with seismic data of about one and a half day in 2009 (477 observations) and 10 days in 2010 (2438 observations) is therefore available for matching calving events and seismic detections. The camp from which we observed the glacier front was located approximately 1.5 km west of the front, which gave a good coverage of the front. We estimated that 90% of the front was visible for the observers (see Fig. 4.1).

For each calving event within the period of visual observation we registered the time, style, location and size. We gave time with a relative accuracy of 10 seconds. The style of iceberg characterizes the type of calving event. We follow here the classification into 6 classes suggested by [84]: avalanches, block slumps, column drops, column rotations, submarine and internal. Avalanches and block slumps affect only parts of the glacier front, block slumps being bigger than avalanches. Column drops affect the entire subaerial part of the ice front which collapses vertically. Column rotations collapse with a rotation movement and can affect the subaerial part of the ice front alone or the entire ice wall, submarine part included. Submarine events are icebergs being detached from the ice front below the water line. The last type of event is internal and refers to either very small calving events that we could not

visually observe or ice blocks falling into crevasses. In both cases they are related to glacial activity close to the front.

We also visually estimated a size for each event, which reflects the volume of ice detached from the front during a calving event. It allows a semi-quantitative approach as first introduced by [117]. The size scale repeats the one defined by [84] but we extended it from 1 to 20, 20 being the entire front width collapsing. We estimated the error on the size scale caused by the subjectivity of the observers to be $\pm$ 1 based on common observation periods where we compared the size each observer gave for a set of training events. This size scale is an indirect measure of iceberg volume [19].

Finally, we located each event by dividing the 3.5 km glacier front into 6 zones. Zone 6 comprises 700 m of the northernmost part of the glacier front, Zone 5 ranges from 700 to 1500 m, and Zone 1 to 4 are 500 m long each, where Zone 1 is the closest to the observation site.

4.2.3 Glacier velocity from GPS measurements

Additionally, GPS data is available to determine the velocity of the glacier. The GPS antenna is located approximately 5 km from the glacier front.

4.2.4 Front position from terrestrial photogrammetry

Repeat photographs were taken automatically every hour from the same location using Harbotronics time-lapse cameras, e.g. [18]. A star in Fig. 4.1 marks the camera position. We used weekly pictures to track the front position. The results are given in relative changes that allow us to determine whether the glacier front was retreating or advancing, which is the most relevant information for this study. We have photographs from 9 May 2009 until 29 September 2009 and from 16 April 2010 until 13 November 2010.

4.3 Method

Making use of machine learning techniques in seismology is becoming increasingly important and popular to handle the large amount of available data. Supervised classification algorithms can be employed to detect seismic events based on manually prepared training data sets, e.g. [47, 26]. On the other hand, unsupervised pattern recognition may be used to generate an initial understanding of the unknown data properties without utilizing existing class or event labels as done for supervised learning [10]. Here, we present and apply a processing scheme to detect and identify glacier-seismic signals which combines event detection based on a Short Time Average over Long Time Average (STA/LTA) trigger and (unsupervised) clustering. While the trigger algorithm will automatically detect all sorts of seismic events in the data, clustering all detections into groups of similar signals will help to distinguish between different kinds of seismic events and false alarms. This approach is suitable and reasonable for our purpose, since no detailed information about the character of potentially observable glacier-seismic signals was available a priori.

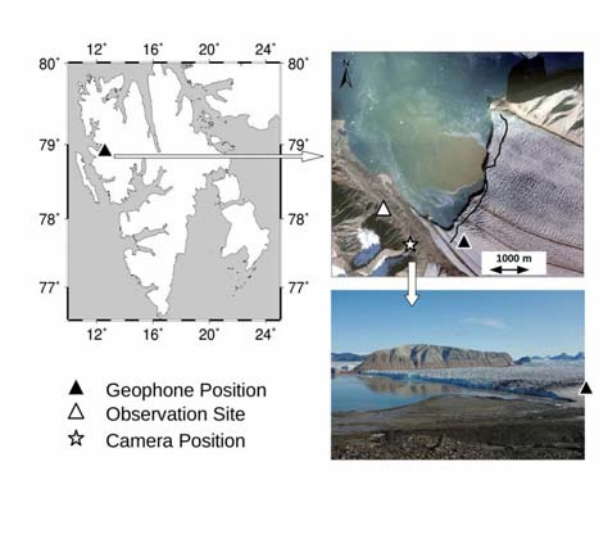

Figure 4.1: Location of Kronebreen on Svalbard and position of instrumentation and observation site close to the calving front. Lower photo shows view of glacier front as seen from the camera position close to the visual observation site.

4.3.1 Seismic event detection

We use a modified version of the STA/LTA trigger function introduced by [1] which is also giving an estimate for the end time of the event. Calibration of the algorithm parameters is done based on visual assessment of identified events in selected time windows. We use a STA window length of 0.4 seconds, a LTA window length of 3.5 seconds and a STA/LTA threshold of 3 (other parameters: C2=3, C8=3, D8=1 s, D5=0.6 s, see [1]). The parameters are chosen so that the detection algorithm is very sensitive to catch all kinds of events, including short and weak ones. A drawback of such a sensitive setting is that also many false alarm are generated. We deal with this problem in the second phase of our approach.

4.3.2 Seismic event clustering

Although clustering is considered as an unsupervised learning technique since grouping of data is done automatically, human interaction is an integral part of that approach. Choosing a meaningful number of clusters, validating and interpreting the results are crucial steps which remain to be done by the user. Most algorithms generate a cluster solution for a fixed number of clusters and have, therefore, to be tested using different values. Furthermore, cluster validation requires to assess if a clustering solution is in fact a good representation of the natural grouping of the data set. In order to select the most meaningful solution, quantitative approaches can be used to compute a measure for the cluster validity, e.g. the Davies Bouldin index (DB) [23]. However, there is often not only a single best solution and validity measures need not to lead necessarily to the actually most meaningful grouping. Visualization of an obtained clustering, which must be applicable also for multi-dimensional data, could be one way to solve this problem [112]. Finally, once a cluster solution has been found representing the natural grouping of the data, the meaning of clusters has to be

determined based on expert knowledge, e.g. by considering examples or a generalized pattern from each cluster. Within this process, it might become necessary to choose another cluster solution or split and merge individual clusters.

We apply the Self-Organizing Map (SOM) technique which is a sort of artificial, unsupervised neural network which can be used to intuitively visualize and cluster multi-dimensional data [54]. The main property of SOMs is that data can be mapped on a two-dimensional, regular grid of usually hexagonal SOM units. This mapping is ordered and topology-preserving, meaning that close or similar data vectors in the input space are also close on the SOM. In that way one can visualize the distribution of multi-dimensional data in two dimensions, so that location of data projected on the SOM reflects the natural data grouping in the input space. In a final step, the SOM units can be grouped automatically using common clustering methods. For more details about the SOM method see [54]. Examples and more detailed description of SOM clustering and visualization can be found e.g. in [52] and [53].

SOMs have been successfully applied for pattern recognition in seismology [63, 69, 104, 89, 28, 53]. In order to cluster a set of detected seismic events, a set of discriminative features is required for each detection which form the input data vector. We choose features that are potentially suitable to distinguish waveforms of different event types and false alarms. These features are based on statistics on the seismogram amplitudes, the frequency spectrum, and temporal characteristics of an event (Fig. 4.2):

- *Number of Runs* (Runs Tests [116] normalized with event duration)
- Spectral amplitude (*Spectrum*) from 12 to 20 Hz normalized with sum over amplitude between 0.5 to 25 Hz
- Signal to Noise ratio (*SNR*) computed as $10 \times \log_{10}$ of ratio of RMS of event amplitudes and RMS of time window before event (same length)
- *Length* of event in seconds obtained from STA/LTA trigger
- *Standard deviation* of signal envelope normalized with mean of envelope
- *Skewness* of envelope normalized with maximum of envelope

Amplitude-based features (Standard deviation and Skewness of envelope, Number of Runs) are computed using a seismogram time window beginning 20 seconds before the event onset and ending 20 seconds after the event stopped according to the estimate made by the trigger functions. The number of runs is based on a significance test for temporal randomness which evaluates whether all samples of a sequence are mutually independent [116, 52]. A run of a time series is a sequence of adjacent samples below or above the median, i.e. a white noise time series would have a high number of runs. The frequency spectrum is computed from the detected signal only.

4.4 SOM training and cluster definition

The STA/LTA trigger generates 24,278 detections for the entire seismic record, including an unknown amount of false alarms. We then use all detections to generate the SOM input data

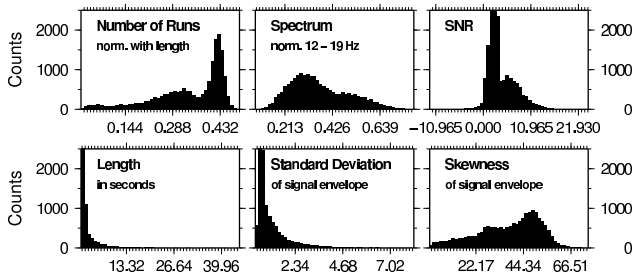

Figure 4.2: Distribution of features forming the input data vector for clustering computed for all detected seismic events. A mixture of at least two Normal distributions denotes existence of clusters.

set by computing the features introduced above from each signal. The frequency distribution of each feature in Fig. 4.2 reveals that at least two distinguishable classes are present in the data set, since some features show a clear mixture of at least two Normal distributions with different means.

After the SOM is trained, it is clustered using an average linkage hierarchical clustering algorithm [112]. Cluster solutions from 2 to 35 clusters are generated. The best solution is defined manually using the DB index as a guideline and evaluating the so-called unified distance matrix plot of the SOM (U-matrix, Fig. 4.3a) which illustrates the probability density distribution of data vectors [112]. Comparison of the clustered SOM (Fig. 4.3b) and the U-matrix allows for the validation of clusterings. For a perfect grouping, cluster borders should appear as more reddish (less-dense) areas in the U-matrix plot in comparison to the regions inside the clusters. In other words, a cluster is a bounded, blue area on the SOM. We correct the number of clusters obtained from one good solution (low DB index) by splitting individual clusters based on the hierarchical cluster solution (grey clusters in Fig. 4.3b), resulting in 25 clusters.

4.5 Results and Discussion

4.5.1 Classification based on direct observations

The cluster solution found in the previous section is well representing the grouping of seismic detections in the feature space. However, in order to identify the meaning of each cluster, we need ground-truth data to label some of the events and their corresponding clusters. Furthermore, we have to inspect detection examples from each cluster and decide what sort of signals is present based on seismological expertise. Due to the lack of man-made noise in the remote study area, we can assume that most detected seismic events are related to natural (e.g. glacial) activity.

First we identify all detected seismic signals that were recorded during the period of direct observations, where 98 (2009) and 238 (2010) detections are obtained (white symbols on the SOM in Fig. 4.3b). We then try to match these seismic detections with directly observed calving events at the glacier front. We choose a 40 seconds long time window (±20 seconds from start of a detection) to find calving events which could be related to the corresponding

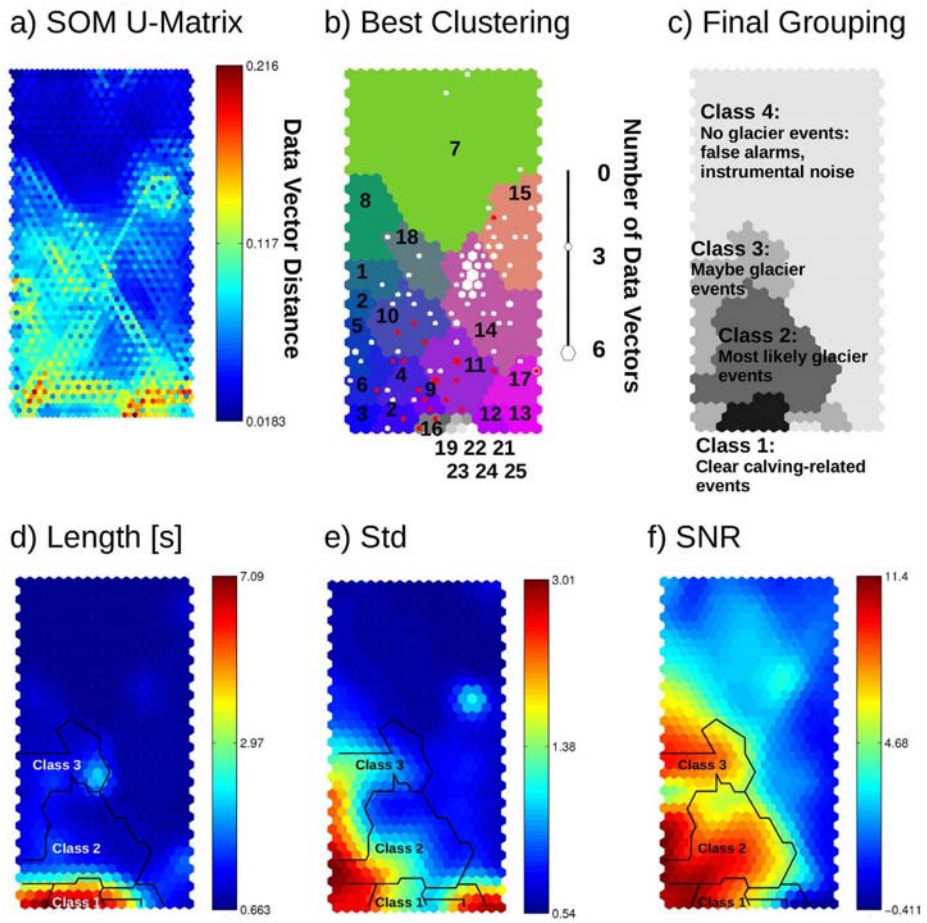

Figure 4.3: SOM and clustering of detected seismic events. a) Unified distance matrix (U-matrix) which reveals data density in input space. Each SOM unit is divided into seven sub-unit. Each sub-unit is colored according to distance between corresponding data vectors of neighbor units. Areas with low distances (blue) indicate high data density (i.e. clusters). b) Cluster solution chosen based on U-matrix and DB index (see text). Cluster membership of each SOM unit is indicated by color. Clusters with a grey scale fill are those which are obtained by splitting clusters from one solution with 18 clusters. Symbols show data projected on the SOM. Sizes of hexagons correspond to number of projected data vectors represented by a SOM unit. White symbols correspond to detections within 11 days long period where direct observations of glacier front are available (matched and unmatched). Red symbols are the detections matching with events observed in Zone 1. c) Final grouping of events based on matching rates and inspection of examples from each cluster. d) - f) Component planes for three selected features: Length of a detections, Standard deviation of signal envelope, and Signal to Noise Ratio. Each SOM unit is colored according to value of a particular data vector component. Red colors stand for high values of the corresponding feature. Outline of signal classes is indicated.

Table 4.1: Results of the matching between seismic detections and visually observed calving events for 11 days. "Matching Rate" is percentage of visual observations that can be related to seismic detections. "Random Matching Limit" refers to binomial test for statistical significance of matches. It is the upper limit of matches which can be produced by chance (1% significance level).

Calving Events	Visual Observations	Seismic Matches	Matching Rate	Random Matching Limit
All	2889	67	2.3%	41
Zone 1	222	20	9.0%	6
Zone 2	709	10	1.4%	14
Zone 3	488	6	1.2%	10
Zone 4	717	11	1.5%	14
Zone 5	469	13	2.8%	10
Zone 6	184	4	2.2%	5
Zone 1 avalanches	18	0	0%	2
Zone 1 block slumps	39	5	12.8%	2
Zone 1 column drops	17	2	11.8%	2
Zone 1 column rotations	6	1	16.7%	0
Zone 1 submarine	2	0	0%	0
Zone 1 internal	140	12	8.6%	5
Zone 1 Size 1	148	11	7.4%	5
Zone 1 Size 2	43	5	11.6%	2
Zone 1 Size 3	25	4	16%	2
Zone 1 Size>3	6	0	0%	0

seismic event. Table 4.1 presents a summary of the results for the different types, locations, and sizes of visually observed calving events.

In order to evaluate the resulting recognition rates and to exclude matches by coincidence, we apply a binomial test for statistical significance (Table 4.1). Assuming a significance level of 1%, results show that, except for the events observed in Zone 1 which is the closest to the geophone, the number of matches for all other zones are not significantly higher than those which can be obtained by chance. Zone 1 events are recognized with a rate of about 10%, which is clearly higher than for the other locations. The rates are even higher when we only consider block slumps and column drops in Zone 1. For column rotations and submarine events, too few observation are present to obtain a reliable statistic. However, it seems that avalanches do not emit clear seismic signals strong enough to be recorded by the geophone. The recognition rate is increasing with size of the observed calving event up to 16%. It is intuitively clear that we are only able to detect the closest and largest events, if the detection threshold is limited by the noise level in the seismic data. Even though we obviously do not monitor seismic emissions from the entire glacier front, we can proceed with investigating the subset which we are able to detect.

The matching rates in Table 4.1 have been computed using all detections and are not based on specific clusters. However, we are now able to identify individual event clusters

Table 4.2: Event classes obtained from clustering and defined based on matching seismic detections and visual observations. Class 1: clear glacier events related to calving, Class 2: most likely glacier events, Class 3: maybe glacier events, Class 4: no glacier events. "Detections*" is the number of seismic detections during the matching/ground-truth period. "Matches Zone 1" is number (and percentage) of seismic detections which can be related to a direct observation in Zone 1. "All detections" refers to seismic detection within entire time of seismic recording in 2009 and 2010. The last column states the clusters merged to define classes (see Fig. 4.3b and c).

Class label	Detections*	Matches Zone 1	All Detections	Clusters
1	9	5 (56.6%)	792	4,16,20
2	107	13 (12.2%)	3699	6,9,10,11
3	22	0	3359	1-3,5,12,18,19,21,22
4	200	2 (1%)	16428	7,8,13-15,17,23-25

considering the detections matching with Zone 1 events. The red symbols in Fig. Fig. 4.3b, which represent the matching detections in the SOM space, are clearly confined to the lower part of the map. Hence, clusters located within that area are most likely glacier-event classes (i.e. iceberg calving). Some clusters do not include matches with direct observations, but the corresponding detections are clear seismic events. Furthermore, there are transition clusters where it is not clear whether the corresponding detection are instrument artifacts or very short and weak seismic events. Those clusters are not labeled as event clusters. To simplify the following discussion, we reduce the obtained clusters to four classes based on the percentage of matched detections within a cluster (Table 4.2 and Fig. 4.3c). Those classes reflect the uncertainty of whether signals are related to the calving process as well as the character of its signal. The classes are:

- Class 1: Clear glacier-seismic events related to calving (>30% matched within cluster)
- Class 2: Most likely glacier-seismic events (>5% could be matched)
- Class 3: Maybe glacier-seismic events (no matches, but clearly no false alarms)
- Class 4: No glacier-seismic event (instrument artifacts and triggered background noise fluctuations)

Two matches with Zone 1 events (from 20 in total) are clearly identified as false alarms (Class 4) which matched by chance (see Fig.Fig. 4.3b and Table 4.2), in agreement with what is expected from the significance test (Table 4.1). For the other locations, the fraction of Class 4 events among all matches is significantly higher, what confirms our hypothesis that these matches are produced by coincidence (6 of 10 for Zone 2, 5 of 6 for Zone 3, 6 of 11 for Zone 4, 11 of 13 for Zone 5, 4 of 4 for Zone 6).

4.5.2 Seismic signal characteristics

In order to investigate the meaning of clusters, SOM component plane plots are useful for displaying the feature distribution or values of a particular data vector component which is

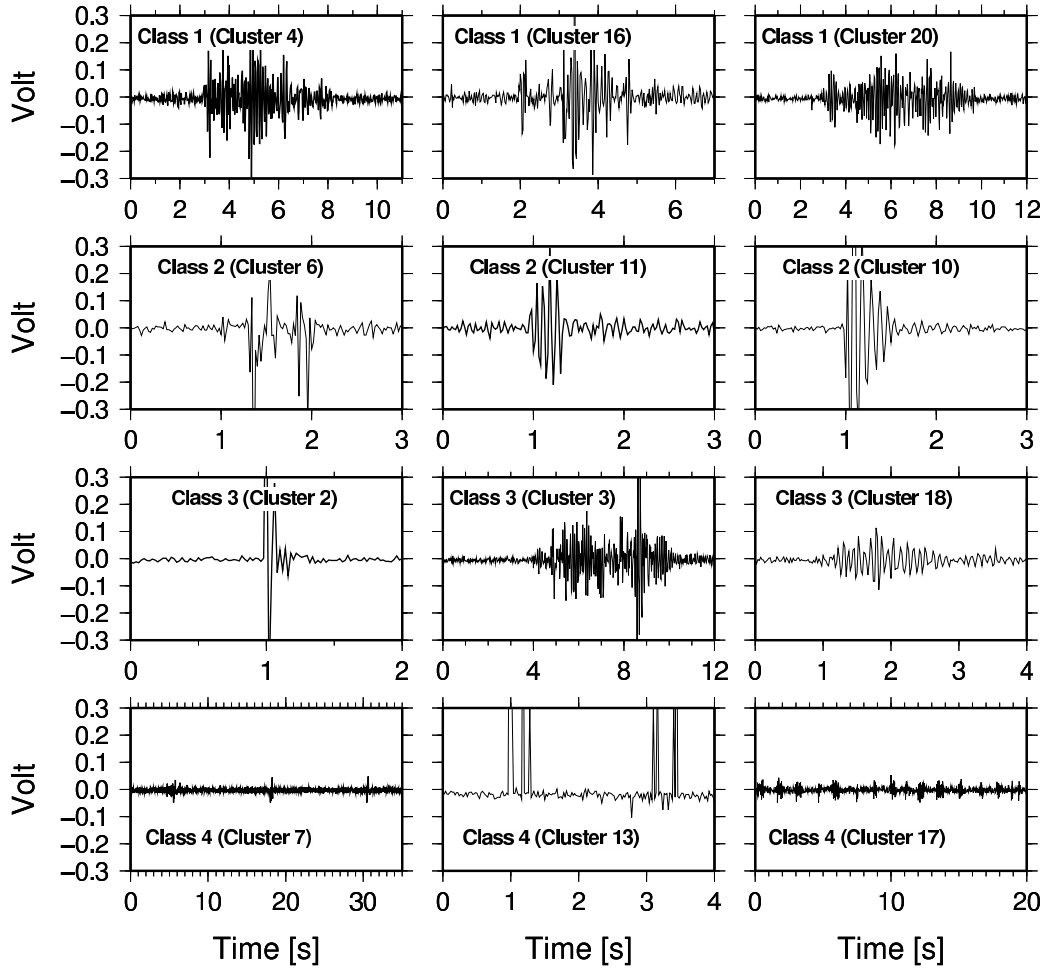

Figure 4.4: Randomly selected examples of from all event classes. Class 1: clear glacier events, Class 2: most likely glacier events, Class 3: maybe glacier events, Class 4: no glacier events. Same amplitude scale for all classes.

associated with any of the SOM units (Fig. 4.3d-f). Randomly selected examples of seismic waveforms (Fig. 4.4) and the SOM component planes show the different characteristics of each event class. As expected, all event clusters (Class 1 to 3) are characterized by high signal to noise ratios (SNR) compared to the rest of detections (Fig. 4.3f). Class 1, which is clearly related to iceberg calving, consists of rather long events, typically 4-10 seconds (see Fig. 4.3d), with several local maxima in their amplitude (Fig. 4.4). Very short signals seem to be characteristic of Class 2. Detections with high amplitude peaks (higher standard deviation, Fig. 4.3e) mainly belong to the event group which could not be correlated with calving events (Class 3).

We do not observe typical seismic signals with clearly separated P and S-Wave onsets. The complexity of waveforms, especially those of Class 1 (Fig. 4.4), could reflect the nature of a calving event, which is rather a sequence of events than a signal from a single, shortly acting source. It is also possible that we observe parts of the acoustic signal of an event coupled with the ice surface in addition to direct seismic waves [96].

4.5.3 Extrapolation of calving rate beyond calibration period

We obtain 138 detections belonging to Class 1, 2, and 3 which can be interpreted as glacier-seismic events within the period of direct observation. When we assume that seismic signals are generated by the same processes over the year, a number of 7850 events occurred within the entire time of seismic measurement, among which 792 are clearly related to iceberg calving (Class 1). These seismic events do no represent the total amount of calving events at the entire glacier front, but consist of signals emitted by the largest events close to the measurement site.

Considering Fig. 4.5, seismic activity seems to be generally higher in 2009 compared to 2010. However, the comparison between the absolute event rates in both years might be biased due to changing location and coupling of the instrument. In both years the event activity seems to be higher in autumn than in the spring and summer months.

The general seasonal trend is overlayed by short-term patterns of periods of 10 to 15 days in both years. For Class 1 events several peaks in the event rate in July 2009 can be observed. However, at least one minimum of activity in July coincides with increase background noise level in the seismic data (see Fig. 4.5a). Therefore, it is not totally clear whether simply less events are detected on the geophone or less signals are emitted by the glacier. In 2010 however the noise level is more stable besides one peak in the beginning of May. The noise level seems to increase slightly in summer 2010 which could be a result of decreasing burial depth of the geophone or continuous emitted noise of melt water. There are pronounced peaks in event rate in May and in beginning of August for Class 1 events (Fig. 4.5b).

4.5.4 Relationship between calving processes and glacier dynamics

Recent thinning, acceleration and retreat of tidewater in different parts of the world raises the question of the relationship between calving processes and glacier dynamics. Is iceberg calving the cause or the consequence of glacier acceleration? [13] reported that an equal number of studies bring evidence in favor for both views, calving causing glacier flow increase, e.g. [40, 66, 48, 72] and increased calving activity following glacier acceleration, e.g. [111, 55].

To investigate the relationship between glacier speed and seismic activity linked to calving on seasonal time-scales, we analyzed qualitatively the three dataset available for 2009 and 2010: indirect measurement of iceberg calving (counts from seismic monitoring), glacier velocity (GPS measurements) and front positions (photogrammetry). In Fig. 4.5 the front position is indicated by a relative position compared to the first day of observations. Furthermore, the change in front position is shown (first derivative). A positive front position indicates advance and negative retreat of the front with respect to the reference date. The solid green line represents the average position of the entire front while the dashed green line represents the front position only in Zone 1. We try to get a timeline of the processes described above to determine which happened first and triggered the other ones.

For the year 2009 (Fig. 4.5a), the glacier speed is rather constant during the spring and starts accelerating mid-June to reach several maxima during the summer and starts decreasing at the end of July. It then remains more or less constant during the entire autumn apart from a peak at the end of August. The seismic activity, amongst which the seismic Class 1 events are likely to be calving events, remains rather low during the summer with three

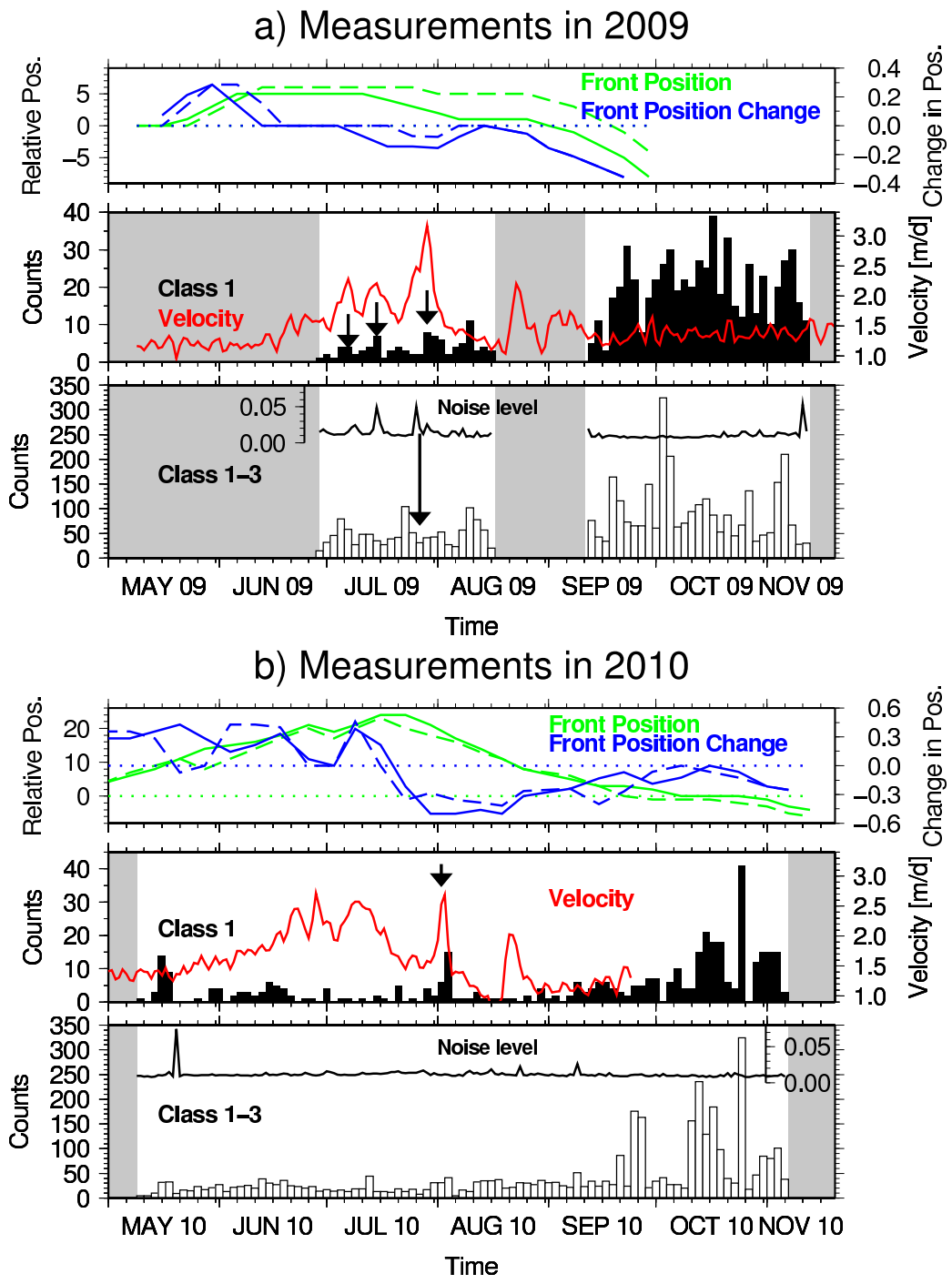

Figure 4.5: Temporal distribution of seismic detections belonging to event classes 1 to 3 and Class 1 only. Class 1 are seismic events clearly related to iceberg calving. Noise level in seismic data is shown using same scale for amplitude as in Fig. 4.4. Grey areas represent data gaps. Red curve shows velocity of Kronebreen measured close to the calving front. Arrows indicate short-term correlations between GPS velocity, noise level, and event rate. Green curve represents average, relative position and blue curve change in front position of the entire front. Dashed lines indicate front position and change only in Zone 1. Horizontal, green-dotted curve shows position at first day of measurement (zero) and blue-dotted curve no change in front position. Positive values correspond to advance and negative to retreat of front.

peaks that are more or less synchronous with the glacier speed peaks. During the autumn, the seismic activity is about three times larger than during he summer. Finally, the glacier front is slowly advancing during the spring to reach a plateau at the beginning of July where the front advance is at its maximum. The front remains rather constant all summer and starts retreating at the mid or end of July until the end of our photographs dataset, end of September. The change in front position is positive only during spring, it then becomes zero until the beginning of July and then negative until the end of September.

For the year 2010 (Fig. 4.5b), the glacier speed starts to increase mid-May until it reaches a maximum around the end of June, starts decreasing, reaches another maximum at the end of July and then decreases drastically until mid-August where it reaches another smaller maximum and finally decreases until the end of September. The seismic activity remains rather low during the spring and the summer apart for two maxima, one mid-May and one at the beginning of August which correlates well with a speed peak. At the end of August the seismic activity starts increasing to reach a maximum at the end of October. Finally the glacier position behaves differently than in 2009 with a fast and constant advance from mid-April until mid or the end of July, immediately followed by a rather fast and constant retreat until the beginning of October when it starts to plateau while continuing to retreat. The change in front position is mostly positive until mid-July, is zero for a few weeks and then becomes negative until mid-November.

From those two timelines we can identify some patterns in the timing of the glacier dynamics events. Seismic activity remains relatively low from May until mid-September while both velocity and front position undergo large fluctuations. For both years, seismic activity increases drastically in the autumn, when velocity is lowest and rather constant and the front retreating. Changes in velocity do not affect the seasonal fluctuations observed in seismic activity, namely low activity during spring and summer and increased activity from September on. Changes in velocity might affect small, weekly variations observed in seismic activity, with an increase of events when velocity increases, in case the front position is constant, as it is the case in spring 2009. On seasonal time-scales, seismic activity seems to be an independent dynamical process, not following the variation in velocity. This suggests that calving – assumed to be correlated to seismic activity – behaves rather independently from velocity. Seismic activity – and therefore calving – show a marked increase in the autumn, which is visually translated by a continuous retreat of the glacier front. The velocity is then at its lowest and rather constant. In this case, the high seismic activity, most probably linked to high release of ice at the front cannot be explained by a larger ice flux, since velocity is at its lowest. This shows that calving rate is controlled by other dynamical variables and that calving activity is independent from the absolute value of glacier velocity at the front. Velocity and calving rate are obviously linked, but through intermediate processes like stretching rate that favors the opening of crevasses [111]. basal velocity that influences the basal conditions, velocity linked to stretching of the ice and potentially thinning, etc., all those processes leading to a more unstable glacier front more prone to calving.

4.6 Conclusions

We have analyzed seismic data and direct visual observations of calving events at the terminus of Kronebreen, Svalbard. We have applied a traditional STA/LTA trigger algorithm with a very sensitive setting to detect seismic signals emitted by glacial activity. The signals of all detections have been clustered to distinguish between different types of events and false alarms. For clustering and identification of event clusters Self-Organizing Maps have been used which simplifies work with multi-dimensional data. By comparing ground-truth data from the calving front with the obtained seismic detections, we are able to match about 10% of close calving events (<1km from the geophone) with seismic signals. This allows us to define three seismic event classes which are, with different degrees of uncertainty, related to glacier activity.

By extrapolating our results beyond the time of direct observations, about 5100 seismic events are detected overall during several months in 2009 and 2010, including signals due to calving and probably also signals emitted by other sources in the glacier. The class of seismic events clearly related to calving activity suggests about 790 larger calving events in the vicinity of the seismic instrument. We have found that we are not able to monitor the entire calving front and to detect smaller events due to the noise level in the seismic data. Nevertheless, using this subset of events as a proxy for activity at the glacier front, temporal patterns in the event rate are found that reveal seasonal changes.

We have analyzed the relationship between glacier velocity, front position and seismic activity, a possible indicator for calving activity. Higher seismic activity is found in autumn compared to the summer. Considering short-term variations, the event rate is at least partially correlated with patterns in the ice flow velocity measured close to the glacier front with peaks in velocity corresponding to small peaks in calving activity. However, on a seasonal time-scale, velocity and seismic activity behave rather independently: in the autumn we observe a large increase in seismic activity while velocity is constant and at its lowest values for the year. We conclude that, on seasonal time-scales, seismic activity, and therefore iceberg calving, might be controlled by other glacier dynamical processes like stretching rate, basal sliding, crevasse deepening due to melt water at the glacier surface, buoyancy perturbations, front destabilization due to changes in the front geometry or to calving activity itself [19].

Our results showed the capability of monitoring glacier activity with seismic receivers to extend observational data sets and to obtain new insights about glacier dynamics. Even though more instruments would allow for the location and a more detailed investigation of glacier-seismic signals, a single-channel geophone can deliver useful information. More investigations on glacier-seismic signals and measurements over a longer time period are required to improve our understanding of the relation between glacial processes and seismicity.

4.7 Acknowledgements

The calving observation project was supported by the IPY-GLACIODYN project (176076) and a "Institutt Basert strategisk Program" granted to the Department of Mathematical Sciences and Technology at the Norwegian University of Life Sciences, both funded by the Research Council of Norway (NFR). Fieldwork was made possible thanks to the Svalbard

Science Forum funding (NFR). We would also like to thank Allan Buras, Bas Altena, Karin Amby, Damien Isambert and Mari Svanem for their great work observing the glacier in the field. Special thanks go to Tobias Baumann for the implementation of the STA/LTA trigger algorithm. Figures have been generated using the SOM toolbox [113] and the Generic Mapping Tools [122].

Paper IV

Chapter 5

Paper 4: Impact of geometric and dynamic constraints on the calving activity of Kronebreen, Svalbard

Abstract What is the impact of geometric and dynamic constraints of the calving activity of Kronebreen, Svalbard? What is the most frequent type of iceberg? How most of the ice is lost at a calving front? What happens in the submarine part of the front? We bring answers to those questions by analyzing single calving event data in relation to preexisting fractures field, water depth, velocity and longitudinal stretching rate. We obtain single calving event data by direct observations, fracture fields by analyzing Formosat-2 images, velocity and stretching rate by performing feature-tracking on Formosat-2 images, and water depth by echo-sounding in the fjord. We show that the most frequent type of calving event is very small, often hard to see, while the type of calving event that bring most ice in the fjord is column drop event, where a column of ice the height of the front, and of various width and depth, slides down without rotation. The submarine part of the front remains complicated to observed, but based on our observations, submarine calving events account for only 13% of the total ice loss at the front through calving, which suggests that submarine melting represents about 80% of the total ice loss at the front. Finally, amongst the geometric and dynamic constraints we tested (water depth, velocity, and longitudinal stretching rate), longitudinal stretching rates explain most of the variability observed in calving event numbers and calving volumes. This relation between stretching rates and calving materializes through the crevasses fields visible on the glacier surface.

Prepared for submission to Journal of Glaciology.
Coauthored by E. Berthier

5.1 Introduction

Calving of icebergs alone is responsible for 70% of the annual transfer of mass from glaciers to oceans [107]. However, despite its obvious importance in term of glacier dynamics and sea level rise, the process of iceberg calving remains a large problem in glaciology. Recently, the knowledge around iceberg calving has increased thanks to studies based on observations and modeling. Numerous studies have tried to parameterize calving processes by using various factors in an attempt to establish a "calving criterion". Some of the main factors widely used are water depth [17, 82], height-above buoyancy [106, 114, 115], the penetration of surface and basal crevasses generated by the longitudinal strain rates near the calving front and enhanced by surface melt and therefore linked to climate [14, 73, 87] and more general glacier characteristics like ice thickness, thickness gradient, strain rate, mass balance rate, and backward melting at the terminus [4].

Studies based on observations have been very useful too in term of finding main controls of the calving processes [118, 92, 117, 67, 84, 86, 85, 98]. Most of them report observations confirming the theoretical controls previously cited.

Possible controls of the calving processes emerge from those studies and were summarized by [13] into three orders:

(i) first-order controls are the controls that determine the position of the glacier front by imposing the main limiting factors to the advance of the glacier. It is mainly the strain rate arising from the velocity gradient and causing the formation of crevasses. Meltwater and rain can also be included in this control because the presence of liquid water allows surface crevasses to propagate deeper.

(ii) second-order controls are responsible for the calving of individual icebergs, they are the force imbalance at the terminus due to changes in geometry, undercutting at the terminus, and buoyancy perturbation.

(iii) third-order controls are linked with the calving of submarine icebergs.

However, one main issue remains to understand the processes of calving at an individual scale [107] because most studies focus on average calving rate. To bring more light into this question we report continuous observations of iceberg calving events, as well as basic geometry – bathymetry and crevasse patterns – and glacier dynamics – velocity and strain rate – at Kronebreen, Svalbard for a total of 16 days in the summers 2008 and 2009. Those observations provide a very detailed dataset, both spatially and temporally, allowing us to answer the following questions:

- What is the most frequent type of iceberg calving?
- What is the role of preexisting fractures on both the types and amount of icebergs?
- What is the influence of water depth, which is still the number 1 control of calving used in models

5.2 Methods

5.2.1 Calving observations

We have continuously observed the front of Kronebreen, Svalbard (Fig. 5.1) during 16 days, using direct observations, based on hearing and seeing. This type of direct visual observations is described in [18] and is said to be the most practical method to monitor the activity at a calving front in details [107]. Four persons observed the front from August 26, 2008 to September 1, 2008 and from August 14, 2009 to August 26, 2009. We reported the time of the event, the type or style, the size, and the location on the glacier front.

The time of the event is given with an accuracy of $\pm$ 10 seconds. The type characterizes the style of the calving, we follow here the classification initiated by [84] which suggests 6 different types: avalanches that corresponds to relatively small pieces of ice avalanching from the front of the glacier, block slumps that describes the case when larger blocks of ice collapse from the ice front, column drops when entire subaerial columns the height of the front slide down vertically, column rotations when entire subaerial columns the height of the front collapse with a rotation, submarine events when a submerged part of the glacier foot shoots up from under water, and "internal" events which are based on hearing and which are in reality very small events very hard to see or internal calving happening up-glacier.

The size estimation allows a semi-quantitative approach to calving events monitoring, first introduced by [117]. When out in the field we give an estimation of the iceberg size that corresponds to an estimation of the iceberg volume (see e.g. [19]). The size of the "internal" events is based on the duration of the acoustic signal, we associate short acoustic signals to small volumes and vice versa. This approach has been validated for some events that we later identified on the time-lapse images, but of course presents limitations.

5.2.2 Crevasse pattern

Crevasses are the physical manifestation of strain, so, by determining their types and orientations, one learns about the main strain in various parts of the glacier. Transverse crevasses are manifestation of longitudinal extension and very often of acceleration towards the terminus. Longitudinal crevasses, at the opposite, are a sign of resistance due to the presence of a pinacle or dead ice. Marginal crevasses are a manifestation of shear strain, generally on the lateral margins of the glacier.

We use a Formosat-2 image from August 29, 2008, to identify the main geometric features around the glacier front and the preexisting crevasse fields. It has a spatial resolution of 2m and has been orthorectified prior to the crevasse analysis.

5.2.3 Bathymetry

Echosounding was performed in Kongsforden, close to the front of Kronebreen, from August 1 to August 11, 2009.

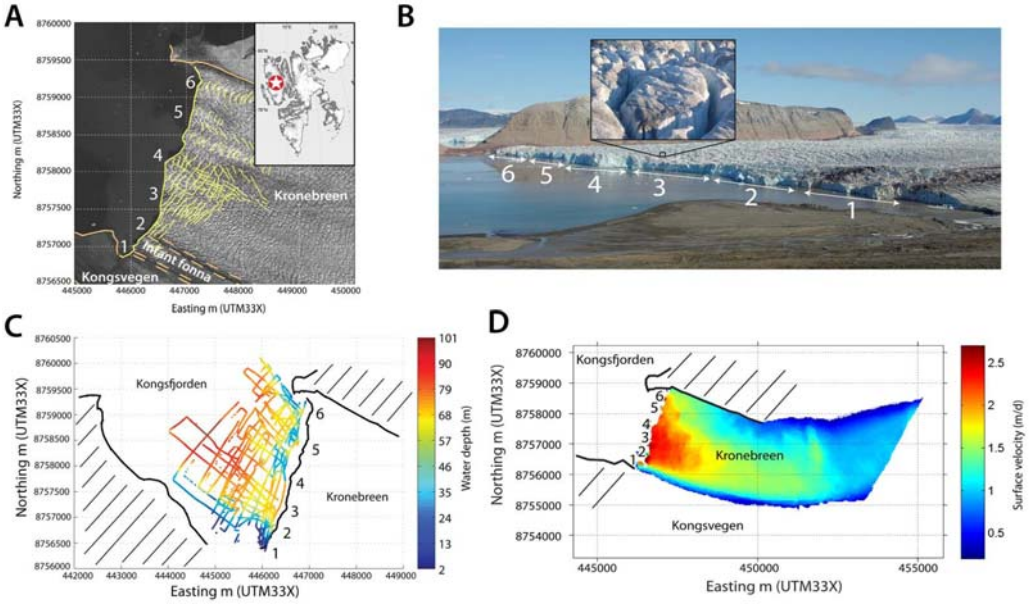

Figure 5.1: A; Formosat-2 image on August 29, 2008, with the main crevasse fields highlighted in yellow. The inset shows the position of Kronebreen in Svalbard. B: Terrestrial picture of Kronebreen on August 17, 2009, showing the glacier front. The inlet shows an aerial picture of the glacier surface in zone 4. C: Kongsfjorden bathymetry [51]. D: Glacier velocity from Formost-2 images between July 13, 2008 and Aug 29, 2008.

5.2.4 Glacier velocity and longitudinal stretching rate

Formosat-2 images were first orthorectified using SPOT5-HRS as a reference, and then velocity fields were derived from 2D correlation. Velocity fields are obtained for the period July 31, 2008 to August 29, 2008. In this paper we focus on spatial heterogeneities rather than absolute values so we assume that the spatial velocity pattern remains similar in 2008 and 2009.

We calculate longitudinal strain rate along 6 profiles corresponding to the 6 glacier zones at the front with a spatial interval of about 1500 m. The resulting accuracy is 4. 10^{-4} d^{-1}.

5.3 Results and Discussion

We collected a very detailed dataset of calving events, both temporally as we report here events on individual scale, and spatially, since we divided the calving front into 6 different zones of about 500m wide each. This allows a detailed analysis of the possible controls of calving since we also report here crevasse patterns, water depth, glacier velocity close to the front, and longitudinal stretching rates. How do those parameters influence the calving activity?

Fig. 5.2 synthesizes the results of this analysis.

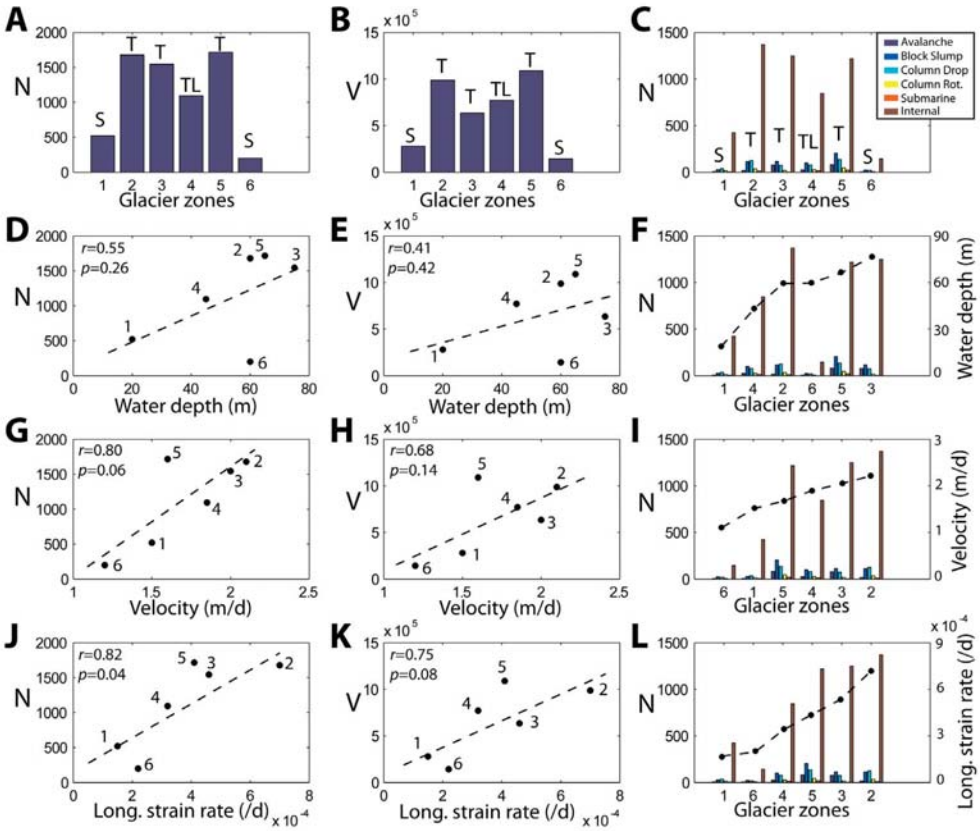

Figure 5.2: Total amount(A, D, G, J), volume (B, E, H, K) and amount by types (C, F, I, L) of iceberg calving events sorted by glacier zones according to four potential controls of iceberg calving often used as calving criteria in models: preexisting crevasse pattern (A-C), water depth (D-F), glacier velocity (G-I), and longitudinal stretching rate (J-L).

5.3.1 Impact of local environment

Preexisting crevasses and local geometry

There are two stable points on either side of the glacier front: on the north side the mountain Colletthøgda and on the south side a surging glacier in a quiescent phase Kongsvegen (Fig. 5.1A). Another characteristic of the glacier geometry is the presence of a recurring pinacle in zone 4. Two medial moraines are visible on the front surface, they mark the border between, from north to south, Kronebreen, Infantfonna, and Kongsvegen.

This geometry gives rise to a highly heterogeneous crevasse field at the front of Kronebreen (Fig. 5.1 A and B) but overall the lower part of the glacier is characterized by strong, well-marked transverse crevasses. Zone 1 is characterized by marginal crevasses reflecting the shear zone with the neighboring glacier Kongsvegen. Zone 1 is also placed in between the two medial moraines and displays a rather clean vertical wall. Zone 2 has mostly transverse crevasses, and a step-like glacier front rather than a clear vertical wall. Zone 3 has mostly transverse crevasses and clean vertical wall. Zone 4 corresponds to where the pinacle is. It has multiple fracture directions, resulting in the division of the glacier body into multiple individual "islands" that stand in between deep crevasses (see inset in Fig. 5.1 B). There are both transverse and longitudinal crevasses, a sign that there must be some resistance at this place of the front. The glacier front at this place is high and rather vertical. Zone 5 is characterized by transverse crevasses and a clean vertical wall. Zone 6 has rounded marginal crevasses that reflect the shear zone with the mountain wall.

Crevasse fields are the physical result of stress in the glacier. Longitudinal stretching rates thus impact the shape and directions of crevasses. Since stretching rate have the best correlation with calving activity, we can expect the different crevasses fields to be related to various calving activity.

Existing crevasse patterns give clear trends to the calving activity (Fig. 5.2 A-C). The two shear zones (1 and 6) are the area with least number of icebergs and least volume of ice calved. Zones with mainly transverse crevasses (2, 3 and 5) have the most calving events. Finally, area 4, with both transverse and longitudinal crevasses, and the presence of a pinacle, has the least number of calving events apart from the two shear zones. The main type of iceberg calving in areas 1 and 2 is column drops, while it is block slumps in all other areas, internal excluded. Areas 1 and 2 are also the only two zones with the presence of medial moraine which might favor the development of laminated ice, more prone to calve as column drops. We show here the possible influence of moraine on the type of iceberg.

5.3.2 Water depth

The water depth at the glacier front is highly heterogeneous with values from 2 to 80 m (Fig. 5.1 C). There are two deeper bays in zone 2-3 and 5 and a shallower area in zone 4. This geometry probably reflects the past glacial history of the bay, the deeper bays reflecting the advance of both Kongsvegen and Kronebreen in 1948, at the time when Kongsvegen was

in an active surge phase, and the shallower area in zone 4 being where the medial moraine was at that time [61].

Water depth explains some of the variations observed in the amount and volume of iceberg calving events (Fig. 5.2 D-F) but the linear regressions are not statistically significant ($p \geq 0.05$), however it does capture the general pattern of increased calving activity in the deeper areas. Calving in area 6 is particularly poorly explained: given its depth the calving activity is expected to be much higher. The three deepest areas are characterized by a majority of block slumps events, if internal events are neglected, while column drops is most common for the other areas.

Water depth gives a general idea about the calving pattern but does not explain all the spatial variability observed in calving activity.

5.3.3 Velocity

The velocity field is asymmetric due to the bend in flow direction happening further up glacier: the highest velocities are 2.7 m/d and are centered around zones 3 and 4, while the velocity is quasi null at the margins (Fig. 5.1 D).

Glacier velocity close to the front gives much better correlation coefficients than water depth (Fig. 5.2 G-I). Both relations are more statistically significant than with water depth and the general pattern of calving activity is well described. This time, the low activity in area 6 is well explained by very low velocity. However the very high activity in area 5 cannot be explained by glacier velocity. Iceberg volume is less correlated with velocity than iceberg amount.

5.3.4 Longitudinal stretching rate

The local geometry of the glacier generate local field stress and strain, including longitudinal extension rates. In turn, those are manifested physically on the glacier surface as crevasses. We have seen above that crevasse pattern is well related to calving activity, so longitudinal strain rates should be well correlated with calving activity. This relation indeed gives the best statistically significant correlations, especially in term of iceberg number (Fig. 5.2 J-L).

5.3.5 Spatial characteristics of calving

Iceberg calving events are unevenly distributed along the glacier front (Fig. 5.3 A) with most events in zones 2 and 5.

5.3.6 Style characteristics of calving

We classified the calving events observed into 6 classes that can be grouped into two main categories according to their type of failure [117] (Fig. 5.4). Column drops, block slumps and avalanches are characterized by shear failure with blocks of ice sliding down the ice wall without rotation. Such shear failure is characteristic of extension zones can assimilated to a

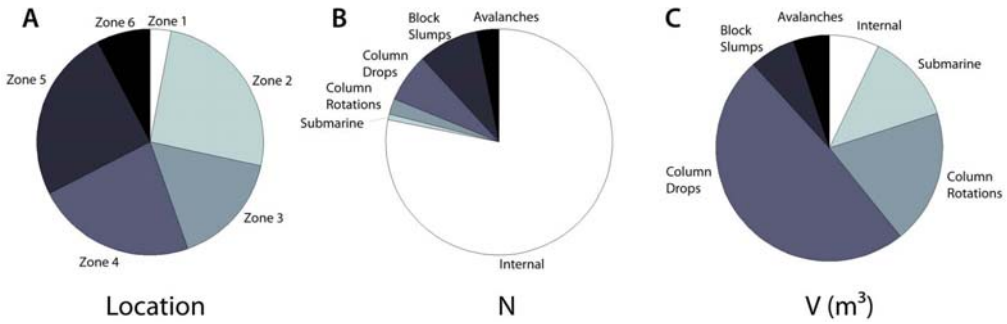

Figure 5.3: Proportions of the number of iceberg calving events by (A) locations and (B) types. (C) shows the proportions by types in term of iceberg volume.

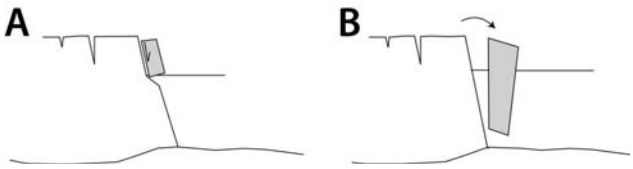

Figure 5.4: A comparison between (A) shear failure, characteristic of column drops, block slumps and avalanche, and (B) tensile failure characteristics of column rotations.

"normal fault", typical of extension zones. Column rotations belong to the second category and are characterized by tensile failure, where blocks are rotating about an axis near its base.

As shown on Fig. 5.3 B, most events are reported here as "internal", they are the very small events and possible internal calving, i.e. ice collapsing inside crevasses, and possibly glacier cracks. The next most frequent events are block slumps and column drops. Avalanches, column rotations and submarine events are very rare.

In term of iceberg volume the picture is completely different (Fig. 5.3 C) with column drops responsible for half of the calved ice, while it is only 7% of the amount of observed events. Oppositely, "internal" calving events, which represent close to 80% of the numbers of iceberg calving event, are responsible for only 7% of the total ice calved. However, none of the calving event should be neglected, even if they do not contribute much in term of volume, because they are as important as the large events in term of glacier dynamics [19].

5.3.7 Submarine calving and melting

An interesting point, already discussed previously, e.g. [117, 67], concerns the very few submarine calving events, even though about two third of the calving front is submerged. In our observations, submarine events account for 1% of the total number of iceberg calving events and contribute to 13% of the ice volume. It means that submarine events are typically very large, and in average larger than subaerial calving events. This observation agrees with both theoretical work [41, 42] and observations [117] . However, there is a large discrepancy between the volume of glacier ice submerged and the volume of ice calved by submarine

events. This suggests that the submarine melting rates are probably very large and that submarine melting is responsible for a large part of the loss at the terminus, and thus of front retreat. Motyka [67] found that 57% of the total ice loss at the terminus of LeConte Glacier, Alaska, is due to submarine melting. In our case, this would suggest an even greater submarine melting rate close to 80% of the total ice loss at the glacier terminus. But this number should be corrected because the period of observation was relatively short and we might have systematically underestimated the volume of the submarine events.

5.4 Conclusions

We have showed that the most frequent type of calving event is very small and often not seen. However it does not contribute to the majority of calved ice in the fjord since such calving events represent only 7% of the total ice loss at the calving front. Most of the ice is lost through column drop and column rotation events, which are columns of ice the height of the calving front, and of various width and depth, either sliding down (column drop) or collapsing in the fjord with a rotation (column rotation). They are generally very big calving events. This means that the main changes at the calving front happen due to those large calving events, although they are rare. Submarine melting rates must be very high at the front of Kronebreen since the submarine calving events represent only 13% of the total ice loss at the front, while the submarine part of the front is about 2/3 of the entire glacier face. Finally, we showed that the local geometry and water depth around the glacier are controlling the strain rates, crevasse patterns and ultimately the calving activity.

5.5 Acknowledgements

We wish to acknowledge support by the Research Council of Norway (IPY-GLACIODYN [project 176076] and a "Institutt Basert strategisk Program" granted to the Department of Mathematical Sciences and Technology at the Norwegian University of Life Sciences) and the Svalbard Science Forum. We thank Cecilie Rolstad-Denby, Nial Peters, Allan Buras, Bas Altena and Karin Amby for their precious work observing the glacier front for long hours.

Paper V

Chapter 6

Paper 5: What do the distributions of calving-event sizes and intervals say about the stability of tidewater glaciers?

Abstract Calving activity at the front of tidewater glaciers is characterized by a large variability in iceberg sizes and inter-event intervals. Does this variability carry valuable information about glacier stability? We present calving-event data obtained from continuous observations of the fronts of two tidewater glaciers on Svalbard, and show that the distributions of event-sizes and inter-event intervals can be reproduced by a simple calving model focussing on the mutual interplay between calving and the destabilization of the glacier front. The event-size distributions of both the field and the model data extend over several orders of magnitude and resemble power laws. In the model, the width of the size distribution increases with a parameter reflecting the calving susceptibility of the glacier front. Inter-event interval distributions, in contrast, are insensitive to this calving susceptibility parameter. Above a critical susceptibility parameter, small perturbations of the glacier result in ongoing self-sustained calving activity. We suggest that the distributions of calving-event sizes and inter-event intervals reflect the stability of the glacier front and how close it is to a critical transition point. Observations of rapid glacier retreats can be explained by supercritical self-sustained calving.

Prepared for submission to Journal of Glaciology
Coauthored by T. Tetzlaff

6.1 Introduction

Iceberg calving plays a key role in glacier dynamics and, hence, in how tidewater glaciers and ice sheets respond to climate change and how they will impact sea level rise in the future [107, 84, 13, 72]. However the process of iceberg calving is poorly understood, and most studies address this complex process from a time-average calving rate perspective rather than looking at individual calving events. We ask here whether the distributions of calving-event sizes and inter-event intervals (time between two consecutive events) can inform about the stability of the glaciers fronts or, in other words, how close a glacier is to rapid retreat. Several questions need to be addressed: What is the impact of climate on calving activity? Which characteristics of iceberg calving are informative: the occurrence of single events, long-term averages (average calving rate), the distributions of event sizes or event times? Is iceberg calving predictable?

To summarize the different possible controls of iceberg calving, [13] proposed the following classification: first-order control that determines the position of the glacier front, second-order controls that are responsible for the calving of individual iceberg calving events and third-order controls that are related to the calving of submarine icebergs. The first-order control on calving is the strain rate due to spatial variations in velocity, responsible for the opening of crevasses. This first-order control can be reinforced by the presence of liquid water, either from surface melt or rain events, that fills crevasses and enables them to propagate deeper. The second-order controls on calving contain all processes that can weaken the glacier front and favor fractures, like the presence of force imbalances at the front due to the margin geometry, undercutting of ice at the front and torque due to buoyancy. The third-order controls are processes like basal crevasses and tide/buoyancy that can trigger submarine icebergs. Fig. 6.1 illustrates the relations between the different controls and their effects on calving. Tab. 6.1 presents those theoretical controls on calving, together with observations from the literature. In the table, most field observations support those controls, showing especially the importance of the presence of liquid water on the glacier surface on calving activity. The loss of tipping points due to changes in front geometry is also susceptible to have a strong effect on iceberg calving, however it has not been observed in the field so far. In this study we focus on this particular control and more precisely on the effect of calving on the glacier front stability and calving itself.

Previous modeling attempts have mostly focused on predicting calving rates based on external variables like water depth [17, 82], height-above-buoyancy [106, 114, 115], the penetration of surface and basal crevasses arising from the longitudinal strain rates near the calving front and enhanced by surface melt and therefore climate [14, 73, 87] and more general glacier characteristics like ice thickness, thickness gradient, strain rate, mass balance rate, and backward melting of the terminus [4].

In this paper we use a simple physical calving model that focuses on the front only and the interplay between calving and the front destabilization. Rather than modeling calving rate like in the studies previously cited, we model single events, their size and temporal occurrence.

In our paper we aim at finding what determines the distributions of calving-event sizes and inter-event intervals, and whether those distributions can inform about the stability of

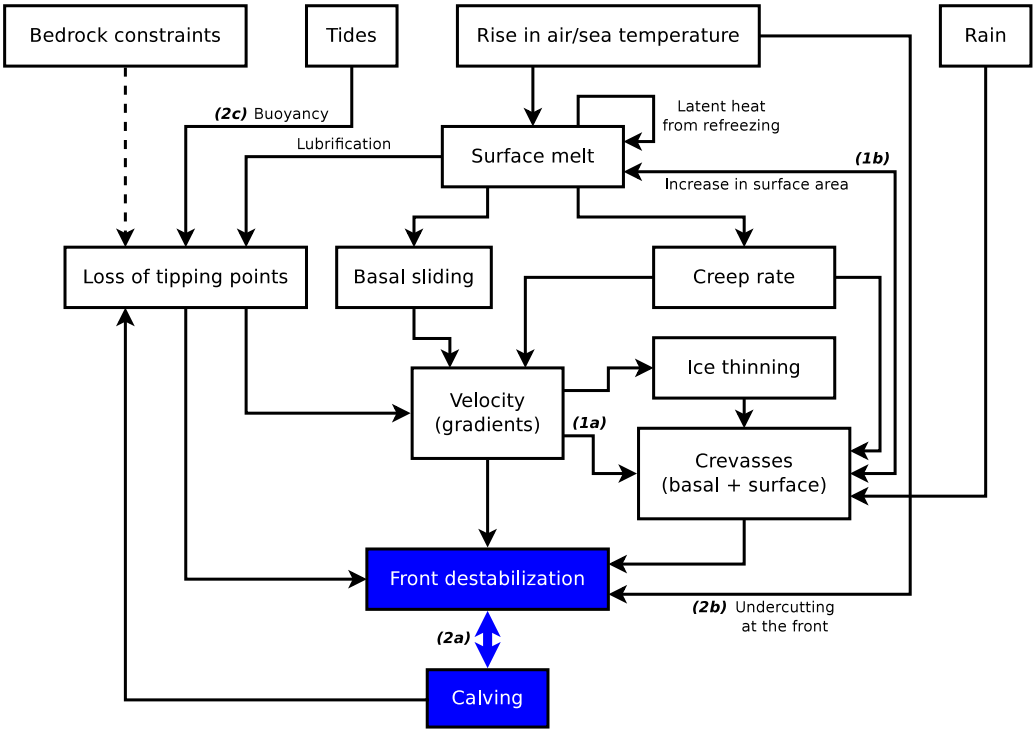

Figure 6.1: Sketch of known mechanisms controlling iceberg calving (see text and Tab. 6.1 for details). The numbers in parentheses indicate the controls of calving also listed in Tab. 6.1. "Tides" also includes "water depth". Solid/dashed arrows indicate positive/negative interactions. Adapted from [40]. The simple calving model in this article solely focusses on the interplay between "front destabilization" and "calving" (blue part). The remaining controls are treated as constant external parameters.

the observed glaciers.

We analyze three datasets of continuous observations of individual calving events, gathering more than 7000 events, containing both time and size of each event. For some events we even got detailed photographs of the different stages of the iceberg break-off allowing us to investigate the detailed dynamics of individual calving event. For example, Fig. 6.2 shows a typical succession of iceberg calving events. This figure illustrates the unstable dynamics at a calving front and underlines that small events can cascade to any size event.

We describe the iceberg calving events by size and inter-event intervals and find long-tailed distributions, characteristics of complex dynamical systems. We also create a simple calving model that focuses on the dynamics of the glacier front. The motivation behind this simple model is to set up a "calving" system under stationary conditions to examine whether the variability of calving sizes and inter-event intervals can be explained by the internal dynamics alone without changes in external conditions.

The distributions of event-sizes and inter-event intervals can be reproduced by a simple calving model focussing on the mutual interplay between calving and the destabilization of

Control order	Mechanism	Observations	Location	References
First order	**(1a)** Stretching due to variations in velocity	Influence of rain on velocity and possibly on average calving activity	South Crillon, Alaska	[118]
	(1b) Presence of water in crevasses and deepening	Effect of rainfall on individual calving events	LeConte and Columbia Glacier, Alaska	[84, 86]
		Impact of daily melt cycle	Saint Elias Mountains, Alaska	[85]
Second order	**(2a)** Force imbalance at the front (margin geometry)	Modeling of stress field near the calving face	–	[94, 36]
	(2b) Undercutting at the front: tides, water temperature, density and circulation	No correlation between calving and tides	Columbia Glacier, Alaska	[92]
		Impact of submarine melting on terminus position	LeConte Glacier, Alaska	[67]
		Influence of sea water temperature and of subglacial freshwater discharge on seasonal calving variations	Hubbard Glacier, Alaska	[98]
	(2c) Torque: tides	Potential effect of tidal stage on timing of large submarine calving	Glaciar San Rafael, Chile	[117]
		Impact of buoyancy perturbations on calving	LeConte and Columbia Glacier, Alaska	[84, 86]
		No tidal forcing on individual calving events	Saint Elias Mountains, Alaska	[85]

Table 6.1: Classification of mechanisms driving iceberg calving (see also Fig. 6.1). Adapted from [13]

Figure 6.2: Typical iceberg calving events succession observed on August 16, 2009 at 21:46 GMT. Each image is 3 seconds apart. The black arrow and circles indicate where the calving event is happening. It starts with very small ice blocks (Fig. 6.2b) where only parts of the glacier front detach and fall, followed by larger column drop (Fig. 6.2d) where the entire height of the glacier front collapses vertically, to finally reach large column rotations calving events (Fig. 6.2h and Fig. 6.2i) where the blocks of ice rotate during their fall.

the glacier front. The event-size distributions of both the field and the model data extend over several orders of magnitude and resemble power laws.

The calving control we investigate in this study is a second-order control, and more precisely it concerns the front geometry and the effect of calving on the glacier front. This parameter has barely been investigated so far. We conclude that the shape of the size distribution is a prominent characteristics of iceberg calving, it may reflect the glacier state more than the occurrence of large, catastrophic iceberg calving events, that reflect the internal variability of the system.

6.2 Methods

In this section, we describe the acquisition of the field data, derive a simple mathematical calving model and outline the analysis to obtain the distributions of both the field and the model data.

6.2.1 Quantitative monitoring of calving events

Monitoring the size and inter-event interval of individual calving event on a continuous time scale is very difficult because of both the dangers related to blocks of ice collapsing from glacier fronts and the sporadic nature of the process that makes it very hard to capture. Most studies reported in Tab. 6.1 are based on human perception, also referred to as visual observations. This non instrumental technique is problematic, most calving events are short and require a lot of attention to be captured. The observers rely on both hearing and seeing to identify calving events, and anything that perturbs either visibility or hearing has a negative impact on the observation quality. Visibility can be altered by periods of darkness or fog, low clouds, or sun at an unfavorable angle – darkness being the main limiting factor in all studies reported here. Hearing is mostly perturbed by strong winds. Despite those problems, direct visual observations is said to be the most practical method to acquire information about the calving process [107]. Terrestrial photogrammetry, for example, is limited by the iceberg size, visibility and illumination of the glacier. Iceberg size and type also limit the use of ground-based radar. [18] showed that radar could only detect events larger than 150 m^3. Remote sensing (optical and radar imagery) has the same limitations as terrestrial photogrammetry with in addition a low temporal resolution that does not allow to solve for individual calving event. Finally, seismic monitoring is a very promising technique where both calving events and their associate size could be detected [85].

We monitored the calving activity at two glaciers: Kronebreen and Sveabreen, Svalbard. Midnight sun in this region lasts from April 18 to August 24, allowing us to continuously monitor calving activity.

Kronebreen is a grounded, polythermal tidewater glacier, located at 78^o53N, 12^o30E, approximately 14 km south-east of Ny-Ålesund, western Spitsbergen (Fig. 6.3A). Kronebreen is one of the fastest tidewater glaciers in Svalbard with an average front velocity ranging between 2.5 and 3.5 m/d during the summer months [100] . At the end of August 2008 the

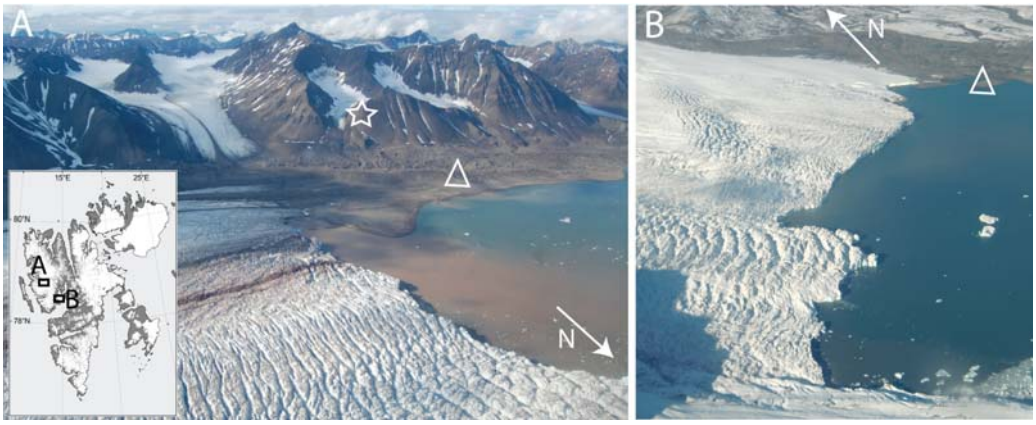

Figure 6.3: Aerial pictures of Kronebreen taken in August 2009 (a) and Sveabreen taken in August 2010 (b). Location of camp and time-lapse camera are marked by a triangle and a star, respectively. Inset: map of Svalbard showing the location of the two glaciers.

terminal ice cliff had an elevation ranging from 5 to 60 m above the fjord surface [18] . Four persons observed the calving front of Kronebreen during a total of 16 days split into two periods: from August 26th, 2008 19:00 to September 1st, 2008 05:11 and from August 14th, 2009 00:00 to August 26th, 2009 16:00 (GMT). The camp from which we observed the glacier front was located approximately 1.5 km west of the front (Fig. 6.3, open white triangle). So we estimated that around ∼90% of the front was visible for the observers.

The second observed glacier, Sveabreen, is a 30 km long, grounded tidewater glacier located at 78^o33N, 14^o20E, flowing in the northern part of Isfjorden (Fig. 6.3B). The observation of Sveabreen was part of a Youth Expedition program. About 45 persons observed the front of Sveabreen during 4 days from July 17, 2010 14:40 until July 21, 2010 15:00 (GMT). The camp was located approximately 500-700 m from the glacier front and offered a good and open view of the front.

For each calving event, we registered the time, style, location and size. We gave time with a relative accuracy of 10 seconds. The absolute precision is ± 1 minute. This error comes from the delay between the actual event and the hearing and delay to register the time. The style of iceberg characterizes the type of calving event, we follow here the classification suggested by [84]. In our analysis we consider all types of calving events because they characterize the same mechanism. We visually estimated the size for each event, which reflects the volume of ice detached from the front during a calving event. It allows a semi-quantitative approach as first introduced by [117]. The scale of perceived sizes repeats the one defined by [84] but we extended it from 1 to 20, 20 being the entire front width collapsing. We estimated the error on the size scale caused by the subjectivity of the observers to be ± 1 based on common observation periods where we compared the sizes different observers assigned to a set of training events. To relate the perceived iceberg event size to the iceberg volume, we used photogrammetry. Photogrammetry provides the glacier dimensions we use to estimate the real size of icebergs. Once we estimate the glacier dimensions, we identify and measure the dimensions of calving events on repeat photographs that were taken automatically every 3 seconds from the same location using Harbotronics time-lapse cameras, e.g. [18]. A star in

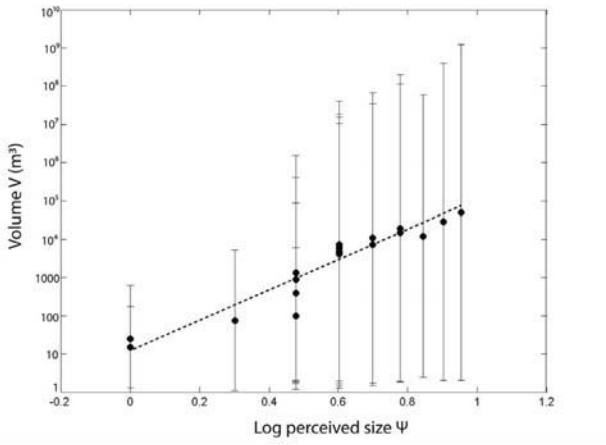

Figure 6.4: Measured iceberg volume V versus perceived size ψ (log-log scale) for the 18 calving events shown in Table 1. The dots represent the 18 calving events with their error bar and the dotted line the best linear fit in log-log representation.

Figure 1 marks the camera position. We chose 18 calving events of various sizes to calibrate the size scale.

The relation between the volume V and the perceived size ψ of calving events is well fit by a power law (see Fig. 6.4):

$$V = 12.6.\psi^{3.87} \tag{6.1}$$

The correlation coefficient between the volume and the perceived size is, in logarithmic representation, $c = 0.68$. The power law model (Equation 6.1) is consistent with psychological findings (Stevens power law) [102]. Using Equation 6.1, we convert the perceived iceberg size (scale 1 to 20 in the dataset) to estimated volume V in m^3 for all calving events.

6.2.2 Simple calving model

Breaking of ice, formation of fractures (crevasses) and, in turn, calving are a consequence of internal ice stress [13]. Several mechanisms contribute to the build-up of stress at the glacier front (see Fig. 6.1), e.g. glacier-velocity gradients, buoyancy, tides, and changes in the glacier-front geometry due to calving itself. In this study, we focus mainly on the latter: the mutual interplay between calving and the destabilization of the front. We show that this interaction loop alone is sufficient to explain the large variability of iceberg sizes and inter-event intervals observed in the field data. In our model, all other stress contributors are treated as external stress or described by parameters. Keeping the parameters constant allows us to study the glacier dynamics under ideal external conditions.

Model parameters

Model parameters are summarized in Tab. 6.2.

Table 6.2: Model parameters. Curly brackets $\{\ldots\}$ represent parameter ranges.

Name	Description	Value
W	width of glacier front	$\{200, 400\}$
H	height of glacier front	$\{50, 100\}$
z_{crit}	critical stress (yield stress)	1
w	calving susceptibility	$\{0.5, \ldots, 1.5\}$
J_{ext}	perturbation amplitude	0.1
M	number of trials	10000

Model geometry

The simple calving model focuses on the calving dynamics at the glacier front. For simplicity, the front is described as a two-dimensional rectangular plane of width W and height H. The front is discretized, i.e. subdivided into WH cells with coordinates $\{x, y | x = 1, \ldots, W;\ y = 1, \ldots, H\}$ (see Fig. 6.5C). Each cell represents a unit volume of ice.

Stress dynamics and calving

The internal ice stress in a cell $\{xy\}$ at time t is described by a scalar variable $z_{xy}(t)$. The cell "calves" at time t^i_{xy} if its internal stress exceeds a critical value of $z_{\text{crit}} = 1$ (yield stress see e.g.[13] and references therein), i.e. if $z_{xy}(t^i_{kl}) > 1$. The cell s calving activity can be described mathematically as a sequence of calving times $\{t^i_{xy} | i = 1, 2, \ldots\}$, or, more conveniently, as a sum of delta pulses, $s_{xy}(t) = \sum_i \delta(t - t^i_{xy})$. After the cell has calved, its internal ice stress is instantaneously reset to zero. We assume that the dynamics of the internal ice stress $z_{xy}(t)$ represents a jump process which is driven by calving of neighboring cells and external perturbations. Mathematically, the (subthreshold, for $z_{xy} \leq 1$) stress dynamics can be described by

$$\frac{dz_{xy}}{dt} = \sum_{k=1}^{W} \sum_{l=1}^{H} J^{xy}_{kl} s_{kl}(t) + J_{\text{ext}} s^{xy}_{\text{ext}}(t) - s_{xy}(t)\,. \tag{6.2}$$

Here, the left-hand side denotes the temporal derivative of the stress variable. The term on the right-hand side (rhs) of (6.2) describes different types of inputs to the target cell $\{xy\}$. In the absence of these inputs (i.e. if the rhs is zero), the stress level z_{xy} remains constant. The first term on the rhs corresponds to stress build-up due to calving in neighboring cells: calving of cell $\{kl\}$ at time t leads to a instantaneous jump in z_{xy} with amplitude J^{xy}_{kl}. The second term represents stress increments as a result of external perturbations $s^{xy}_{\text{ext}}(t)$ with amplitude J_{ext}. For simplicity, we assume that these external perturbations are punctual events in time (see below), i.e. $s^{xy}_{\text{ext}}(t) = \sum_i \delta(t - t^i_{\text{ext},xy})$. The last term on the rhs of (6.2) captures the stress reset after calving (as described above). See Fig. 6.5A for an illustration of the single-cell stress dynamics described here. Note that the single-cell calving model described here is identical to the perfect integrate-and-fire model which is widely used in many other fields to describe systems of pulse-coupled threshold elements, for example, networks of nerve cells [60, 105], sand piles [8, 9], or to study the dynamics of earthquakes [37].

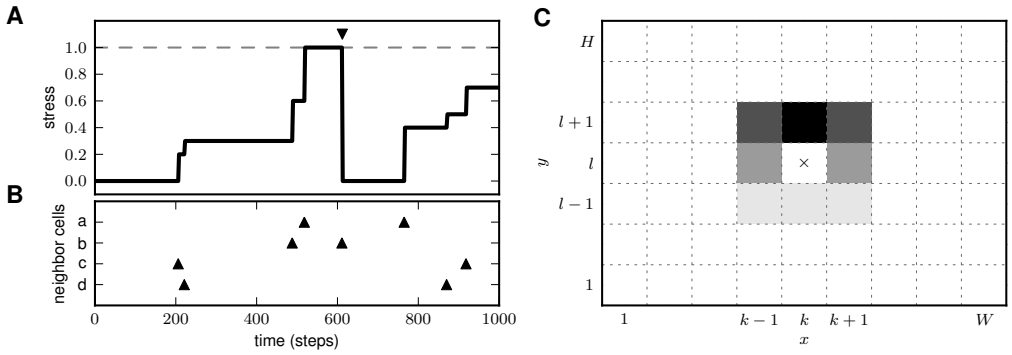

Figure 6.5: Sketch of the calving model. A: Time evolution of internal ice stress z in an individual cell. Calving of neighboring cells or external perturbations (triangles shown in B) cause jumps in ice stress z. Crossing of critical stress $z = 1$ (dashed horizontal line) leads to calving (triangle-down marker) and reset of stress level to $z = 0$. C: Glacier front (width W, height H) subdivided into WH cells. Calving of cell $\{kl\}$ (cross) leads to stress increments (gray coded) in neighboring cells (depending on relative cell position).

Intra-glacial interactions

Calving of a cell at position $\{kl\}$ leads to a destabilization of its local neighborhood, mainly caused by a loss of buttress. In consequence, the stress level in neighboring cells $\{xy\}$ is increased (first term on rhs of (6.2)). For simplicity, we assume that the interactions $J_{kl}^{xy} = J(x-k, y-l)$ depend only on the horizontal and vertical distances $p = x - k$ and $q = y - l$ between the cells $\{kl\}$ and $\{xy\}$. Further, we restrict the model to excitatory (positive) nearest-neighbor interactions without self-coupling, i.e.

$$J(p,q) = \begin{cases} 0 & \text{if } p = 0 \text{ and } q = 0 \\ 0 & \text{if } |p| > 1 \text{ or } |q| > 1 \\ > 0 & \text{else}\,. \end{cases} \tag{6.3}$$

An asymmetric kernel like the one described in Equation 6.4 provides more realistic intra-glacial interactions

$$J(p,q) = C \begin{cases} 4 & \text{if } p = 0 \text{ and } q = 1 \\ 3 & \text{if } |p| = 1 \text{ and } q = 1 \\ 2 & \text{if } |p| = 1 \text{ and } q = 0 \\ 1 & \text{if } |p| \leq 1 \text{ and } q = -1 \\ 0 & \text{else}\,. \end{cases} \tag{6.4}$$

Here, C is a normalization constant. The asymmetry in the vertical direction reflects that cells above the calving cell will likely experience a larger stress increment than those below the calving cell due to gravity. To test whether the dynamics of the model critically depends

on the specific choice of the interaction-kernel shape we also consider symmetric kernels like

$$J(p,q) = C \begin{cases} 1 & \text{if } p = 0 \text{ and } |q| = 1 \\ 1 & \text{if } |p| = 1 \text{ and } q = 0 \\ 0 & \text{else}\,. \end{cases} \tag{6.5}$$

Qualitatively, the results for symmetric and asymmetric interaction kernels are the same (not shown here). Note that with the symmetric kernel (6.5), our calving model is (almost[1]) identical to the sandpile model used in [8, 9].

To study the dependence of the calving dynamics on the coupling between cells, we consider the *total calving susceptibility* $w = \sum_p \sum_q J(p,q)$ as a main parameter of the model. The total calving susceptibility w characterizes the susceptibility of the ice, i.e. the change in internal ice stress in response to perturbations. In our terminology, an increase in this susceptibility parameter w corresponds to a *destabilization* of the glacier front. Further, note that w is measured in units of the critical stress z_{crit}; an increase in w can therefore also be interpreted as a decrease in z_{crit}. To study the effect of ice susceptibility and/or yield stress, it is therefore sufficient to vary w and keep $z_{\text{crit}} = 1$ constant. Both ice susceptibility and yield stress are determined by external factors like temperature, glacier velocity, buoyancy, glacier thickness, etc. An increase in temperature, for example, lowers the yield stress [13] and, thus, leads to an increase in the calving susceptibility w.

Experimental paradigm

Due to intra-glacial interactions, calving of individual cells may trigger calving in neighboring cells, thereby causing calving avalanches. At the beginning of each experiment, the internal ice stress of each cell is initialized by a random number drawn from a uniform distribution between 0 and 1.1. On average, 10% of the cells are therefore above the critical stress $z_{\text{crit}} = 1$ and start calving immediately. In general, this initial calving seizes after some time. After this warmup period, we perform a sequence of perturbation experiments: In each trial $m = 1, \ldots, M$, a single cell $\{kl\}$ is randomly chosen and perturbed by a weak delta pulse $s^{kl}_{\text{ext}}(t) = \delta(t)$ of amplitude $J_{\text{ext}} = 0.1$ (at the beginning of each trial, time is reset to $t = 0$). The trial is finished when the calving activity in response to the perturbation has stopped. We define the number of cells calving in a single trial as the *event size* μ. The distance $u - v$ between two subsequent successful trials v and $u > v$, i.e. trials with $\mu > 0$, defines the *inter-event interval* τ.

Simulation details

The model dynamics is evaluated numerically using the neural-network simulator NEST (see www.nest-initiative.org). Simulations are performed in discrete time $t = 0, 1, 2, \ldots$. Cell states are updated synchronously, i.e. calving activity at time t will increment the stress in neighboring cells at time $t + 1$.

[1] In [8, 9], the "stress" z is reset *by* a fixed amount after "calving", whereas we consider a reset *to* a fixed value $z = 0$.

6.2.3 Statistical analysis

Distributions of event-size and interval

We describe here how we obtain distributions of sizes and inter-event intervals for both the field data and the model data of iceberg calving. Size refers to the iceberg volume while the inter-event interval is the time between two consecutive calving events. For graphical illustration we count the number of observations in size and inter-event logarithmic bins (e.g. in [50]). This method provides a graphical illustration of the size and inter-event interval distributions but such representations are biased. They can produce inaccurate estimates of distributions parameters and, more importantly, they do not indicate what kind of distribution the data obey [22].

For a proper statistical characterization of the distributions we apply the following technique:

(i) Estimation of the mean, standard deviation (SD) and coefficient of variation (CV) which is the standard deviation divided by the mean. The CV measures the degree of regularity of a process. A CV of zero indicates a perfectly regular process (clock). If the CV is one, the process is as irregular as a Poisson process while a CV larger than one indicates a clustering in the data (bursts).

(ii) Fitting of model distributions (decay exponents). Contrary to regular graphical representation and least-square fitting, fitting of model distributions is not biased by binning. To fit model distributions we use a maximum likelihood fitting of power-law and exponential distributions, the two most likely distributions. We use an additional tool called the log likelihood ratio R that describes which hypothesis is better. Maximum likelihood fitting consists on three main steps [22]. First, we estimate the parameters of the model distribution (decay exponents). Second we calculate the goodness-of-fit p^* between the data and the model distribution. If p^* is greater than 0.1 the model distribution is a plausible hypothesis for the data, otherwise it is rejected. Finally we compare the two model distributions – power law and exponential – via the log likelihood ratio R. If R is significantly different from zero, its sign indicates which of the two model distributions is favored.

Auto-correlation

We computed the auto-correlation of sizes and inter-event intervals which is the correlation between the event n and the event $n-i$ for the i^{th} order correlation. The inter-event intervals auto-correlation indicates the predictability of the system: the higher the auto-correlation the more predictable the system is.

Table 6.3: Overview of the three field-data sets.

	Kronebreen		Sveabreen
	2008	2009	2010
Total number of events	1041	5868	386
Observation period (days)	4	12	4
Start date	26 Aug.	14 Aug.	17 July
End date	1 Sept.	26 Aug.	21 July
Size (V, m^3)			
Mean	88	53	96
Standard deviation	15	13	44
Minimum	13	13	13
Maximum	93405	135070	135070
Inter-event interval (τ, min)			
Mean	7.56	3.11	15
Standard deviation SD	11.12	5.12	23
Minimum	0	0	0
Maximum	122.8	98.4	237
Coefficient of Variation CV	1.47	1.65	1.53

6.3 Results

6.3.1 Variability of event-sizes and inter-event intervals

Tab. 6.3 gives basic statistics of the iceberg calving data collected during the three different observation periods: number of events, mean, SD, CV, minimum, and maximum. The longest observation period is in 2009 with 12 continuous days and 5969 events, while the observation period is 4 days in 2008 and 2010. The size of calving events ranges over several orders of magnitude: from 10 to more than 130000 m^3. The mean inter-event interval varies between 3 and 15 minutes. During the three observation periods the CV is larger than 1, indicating a clustering in events times and showing that iceberg calving happens by bursts of activity.

6.3.2 Impact of external parameters

Fig. 6.6 illustrates the temporal evolution of sizes (Fig. 6.6A), inter-event intervals (Fig. 6.6B), air temperature measured in Ny-Ålesund (Fig. 6.6C), air temperature gradients or time derivative of air temperature (Fig. 6.6D), and tidal amplitude (Fig. 6.6E) during the 12 days of observation in 2009.

The resulting calving events from the model are shown on Fig. 6.7. The model is run with an asymmetric kernel corresponding to Equation 6.4. We chose a calving susceptibility $w = 1.3$ because it enables the model to generate a wide range of calving events sizes.

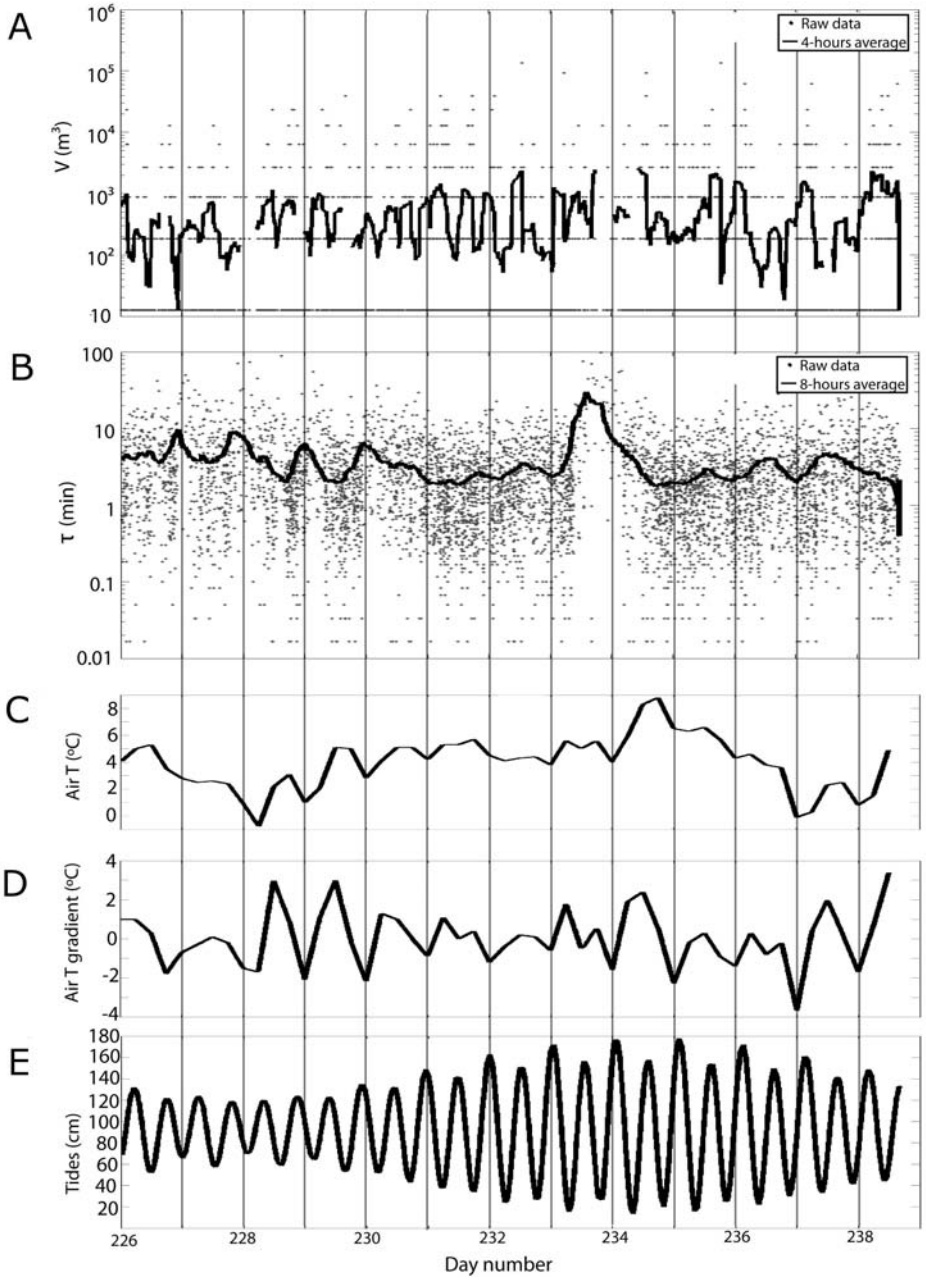

Figure 6.6: All panels show data from the 2009 observation period. A: volume of each calving event. Blanks in the graph correspond to periods where we could not estimate the size due to bad visibility. B: inter-event interval between each calving event. The dots are the raw data for each calving event while the solid black line is a 4-hours average of the size in A and a 8-hours average of the inter-event interval in B. Both the size and inter-event interval are plotted on a logarithmic scale for better visualization. C,D and E: external parameters fluctuations. C: air temperature (Norwegian Meteorological Institute), D: air temperature gradient and E: tidal amplitude (Norwegian Mapping Authorities).

Fig. 6.7A shows the glacier responses to 1000 consecutive random perturbations. Most of the perturbations do not trigger any response at the glacier front, or in most cases they are limited to a few cells, as it is the case for the calving event reported on Fig. 6.7 B, D and F where μ=15. Only a few perturbations trigger large responses like the event on Fig. 6.7C, E and G where μ=27903.

Fig. 6.8A shows the temporal succession of calving events happening at Kronebreen during 12 days of observation in 2009, showing very similar patterns to the ones observed in the model data Fig. 6.7A: the range of the events size is very large in both cases, trains of events are followed by long quiescent periods and the events are short-lived.

Based on the data from the field and from the model we computed the size and inter-event interval distribution shown in Fig. 6.8 (B-G) and Fig. 6.9 (A, B, D, and E). In all cases the distributions are broad and long-tailed. For the model data the size of calving event can get close or even exceed the system size (Fig. 6.9 A and B).

In both the field and model data, size distributions are well fit by power laws, and since the log likelihood ratio R is significantly positive (Fig. 6.8 B-D, Fig. 6.9 A and B), power law model is better than exponential.

Inter-event interval distributions are rather exponential for both the field and the model data (Fig. 6.8 E-G and Fig. 6.9 D and E), but this time the log likelihood ration R is not significantly different from zero, making definitive conclusions impossible to draw.

In the case of the model data, the width of size distributions is dependent on the calving susceptibility w. The power law exponent decays with w and approaches 1 (Fig. 6.9 B and C). At the opposite the width of inter-event interval distributions is rather independent of calving susceptibility with the exponent constant (Fig. 6.9 E and F). This means that the stability of the glacier, reflected by the calving susceptibility w, does impact the distribution of iceberg size, but not of inter-event intervals. By knowing the distribution of iceberg size, one can learn about the dynamic stability of the glacier. Oppositely, distributions of inter-event intervals do not vary under different glacier stabilities, inter-event intervals are not informative in terms of glacier dynamics.

Both field and model data show wide and long-tailed distributions of event-sizes and inter-event intervals with the size distributions well fit by power law while inter-event interval distributions are better described by exponential. What causes those wide distributions?

Do external parameters change the overall shape of distributions? For example, is the mean inter-event time influenced by changes in external parameters such as air temperature (Fig. 6.6 B)? On long time scale, the correlation with external parameters is not significant (Fig. 6.6). To test the impact of external conditions on the overall shape of distributions we group the data into high/low temperature/tide intervals (Fig. 6.10) and compute the distribution for each group where external conditions are similar. The low/high temperature ranges are from -0.8 to $+4.2\,^{\circ}$C and $+4.2$ to $+8.8\,^{\circ}$C, respectively, and the low/high tide-level ranges are from 14 to 92 cm and 92 to 178 cm, respectively. This grouping does not affect the shape of the distributions (Fig. 6.10), indicating that the overall shape of size and inter-event interval distributions is not dependent on the external conditions such as air temperature and tidal amplitude. This means that the wide range of event-sizes and inter-event intervals can be present even under stationary conditions.

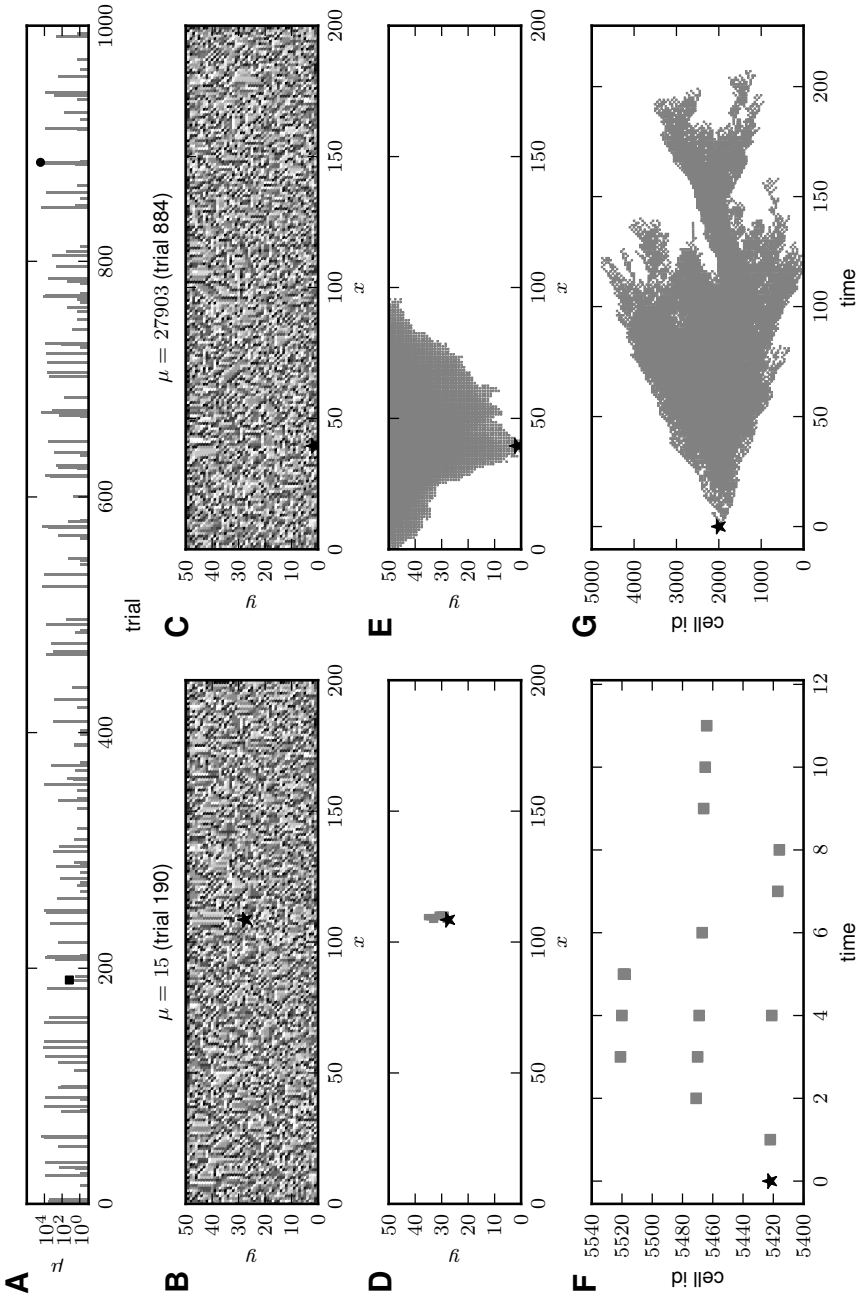

Figure 6.7: Size and duration variability of calving events in response to random external perturbations (model results). A: Glacier responses (event size μ; log scale) to 1000 consecutive random perturbations. Black square (trial 190) and circle (trial 884) mark events shown in B,D,F and C,E,G, respectively. B–G: Moderate-size (B,D,F; $\mu = 15$) and large calving event (C,E,G: $\mu = 27903$) in response to punctual random perturbations (perturbation sites indicated by black stars) in trials 190 and 884, respectively. B,C: Distribution of stress z_{xy} (gray coded) across the the model-glacier front after calving response. D,E: Spatial spread of single-trial calving activity across the model glacier front. Gray dots mark cells which have calved. F,G: Spatio-temporal spread of the events shown in D,E (id of cell at position (x, y) $= Hx + y$; discrete time). Note different scales in F and G. Glacier width $W = 200$, glacier height $H = 50$, calving susceptibility $w = 1.3$.

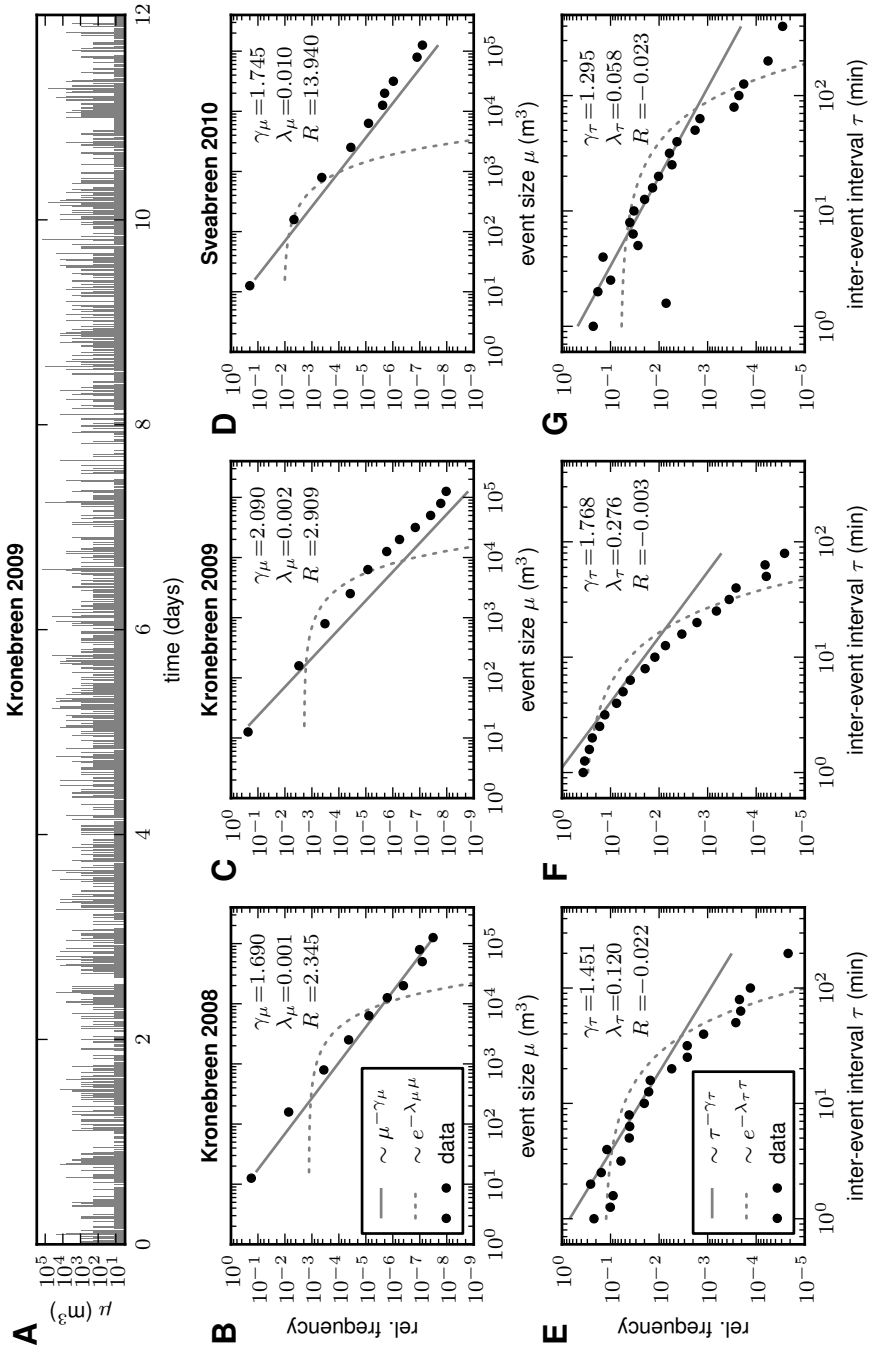

Figure 6.8: Field data. A: Example time series for 12 observation days at Kronebreen (2009). Each bar represents a calving event of size μ (log scale). B–G: Distributions (log-log scale) of iceberg sizes μ (B–D) and inter-event intervals τ (E–G) for Kronebreen 2008 (B,E), 2009 (C,F) and Sveabreen 2010 (D,G). Field data (symbols), best-fit power-law (solid lines; decay exponents γ_μ, γ_τ) and exponential distributions (dashed curves; decay exponents λ_μ, λ_τ). R represents corresponding log-likelihood ratio.

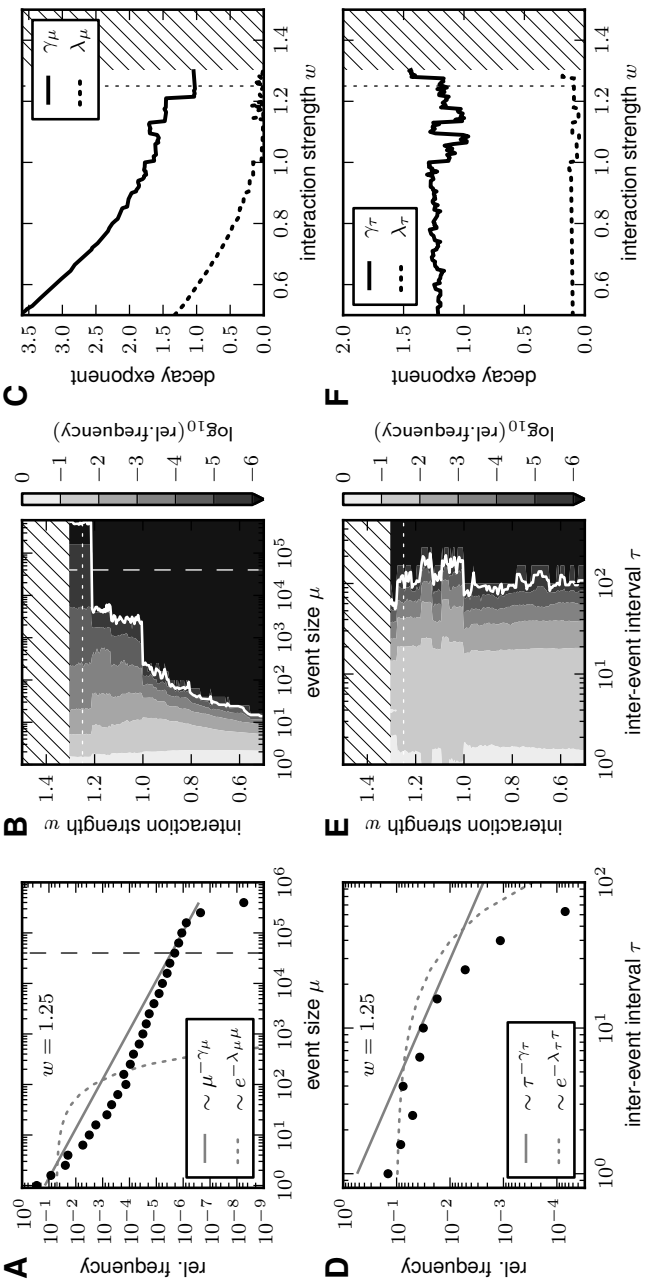

Figure 6.9: Size (top row) and inter-event interval distributions (bottom row) in the calving model. A,D: Distributions (log-log scale) of iceberg sizes μ (A) and inter-event intervals τ (D) for calving susceptibility $w = 1.25$. Simulation results (symbols), best-fit power-law (solid lines) and exponential distributions (dashed lines). B,E: Dependence of size and interval distributions (log-log scale) on interaction strenght w. White curves mark maximum size and inter-event intervals. C,F: Dependence of decay exponents of best-fit power-law (solid lines; γ_μ, γ_τ) and exponential distributions (dotted lines; λ_μ, λ_τ). Glacier width $W = 400$, glacier height $H = 100$. Vertical dashed lines in A and B indicate system size $WH = 40000$. Dotted horizontal and vertical lines in B and C, respectively, mark interaction strength used in A and D. Hatched areas in B,C,E,F correspond to regions with ongoing, self-sustained calving.

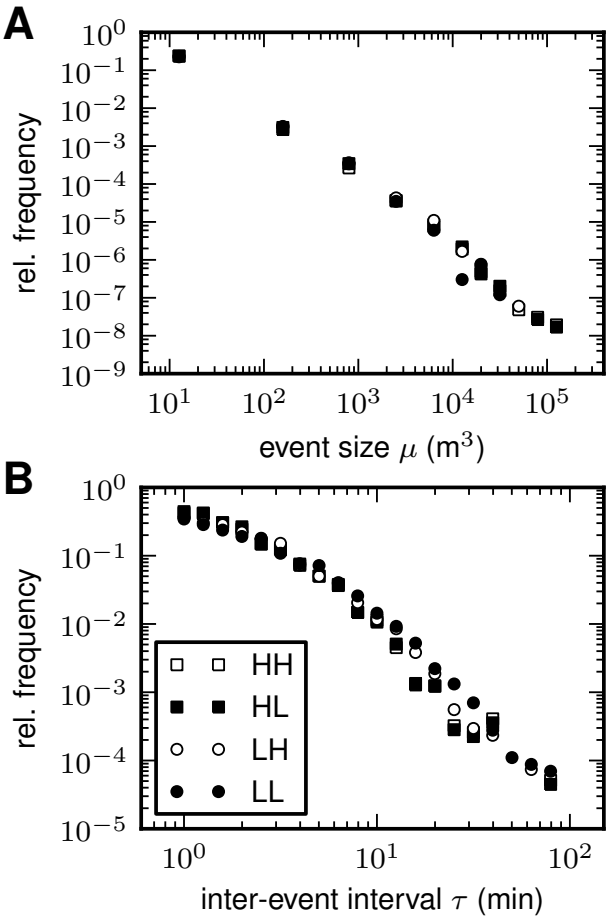

Figure 6.10: Distributions of iceberg sizes μ (A) and inter-event intervals τ (B) for four different combinations of air-temperature and tide ranges (Kronebreen, 2009; log-log scaling): high temperature – high tide (HH), high temperature – low tide (HL), low temperature – high tide (LH), low temperature – low tide (LL). Low/High air-temperature interval: −0.8–4.2/4.2–8.8 °C, Low/High tide-level interval: 14–92/92–178 cm.

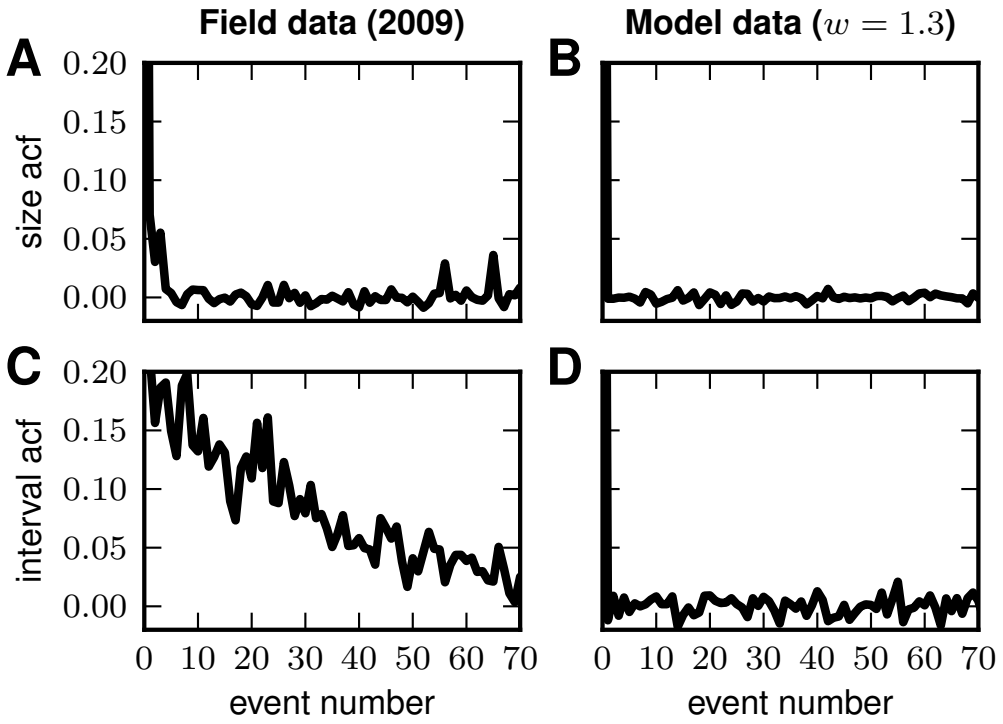

Figure 6.11: Auto-correlation function (acf) for sizes (A, B) and inter-event intervals (C,D) in the field (A,C) and model (B,D) data.

6.3.3 Predictability

Auto-correlation of inter-event intervals can inform about the predictability of the system. The higher the auto-correlation, the more predictable the sizes/timing of calving events. Fig. 6.11 shows the auto-correlation for sizes (Fig. 6.11 A and B) and inter-event intervals (Fig. 6.11 C and D). There is a small auto-correlation in the size and a small long-lasting inter-event interval correlation in the field data (Fig. 6.11 A and C). Oppositely there is no correlation in the model data for both the sizes and inter-event intervals. To explain this discrepancy between field and model data, we propose that the correlation in the field data arises from non-stationarities (see the long-scale cyclic changes in the average size and inter-event intervals on Fig. 6.6). Those non-stationarities can reflect external parameters such as storm periods or low visibility that would impact the observation quality cyclically, or from a more complex glacier dynamics inherently generated. It is clear that the simple model is perfectly stationary since there is no varying external parameters and since the perturbations are regular. To make the model more real it could be extended by adding non-stationary inputs, e.g. non-stationary perturbation rate, or other components, e.g. first and second order controls (see Tab. 6.1). In any case the correlations in the field data are very small, indicating a poor predictability of iceberg calving.

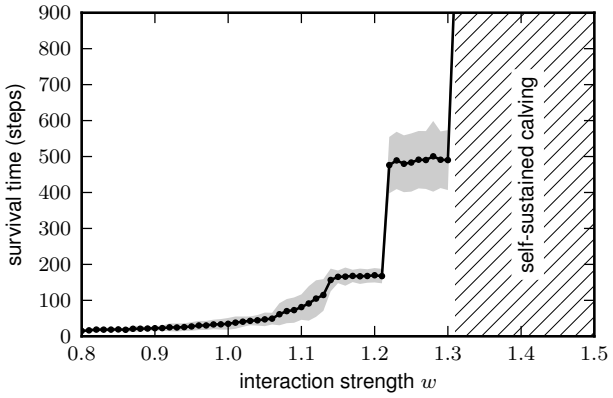

Figure 6.12: Survival time of calving activity after random stress initialization (with 1% of the cells being superthreshold, $z_{xy} > 1$, at time $t = 0$) as function of calving susceptibility w. Mean survival time (black circles) and mean±2 Standard Deviations (gray band) for 100 random glacier initializations. Glacier width $W = 400$, height $H = 100$.

6.3.4 Self-sustained calving

In the model results, we observe that above a critical calving susceptibility w, the glacier front becomes unstable and does not stop calving after an initial perturbation with infinite survival times (see Fig. 6.9 B, C, E and F, and Fig. 6.12). We interpret this model behavior as a possible description of rapid tidewater glaciers retreats (e.g. [88, 16, 68]). It means that, by increasing the calving susceptibility, we can initiate ongoing calving activity.

Concretely this simple model gives predictions that bring new understanding of the process of iceberg calving:

(i) The transition from a stable calving glacier with a rather constant front position to a calving glacier undergoing a rapid retreat is critical (abrupt).

(ii) The power law exponent of the size distribution of icebergs predicts how close a glacier is to this critical point. The distribution of icebergs sizes can be used as a prediction tool for a glacier fast retreat.

6.4 Discussion and conclusions

We showed that the calving-event sizes and inter-event intervals distributions for both field and model data are very similar: very broad and long-tailed. More precisely the size distributions are well fit by power laws and the inter-event intervals are better fit by exponentials. The shape of those distributions seems to be a prominent characteristic of iceberg calving, always emerging, even under stationary conditions. Large events, like small events, belong to the same size distribution and, as such, reflect the natural variability of the glacier system. This hypothesis is supported by the recent work of [85] where they found that the size distributions of iceberg calving events based on seismic measurement are well fit by power-laws.

Our findings about the dynamics of iceberg calving can be related to a theory that aims at explaining how complex processes work: Self Organized Criticality. In this theory, complex

systems tend to reach a critical state: a state that requires the least energy for the system but which is barely stable. The critical state acts as attractor for the dynamics. Once in this state, the combination of dynamical minimal stability and spatial interaction leads to unpredictable responses to perturbations characterized by the absence of spatial and temporal scale. This is expressed mathematically as power laws in the distributions of sizes. In nature, a variety of systems displays similar distributions of events sizes: for example earthquakes [7, 35], the luminosity of stars [6], sandpiles [6], landscape formation [32], life evolution [24], forest fires [20], subglacial water pressure pulses [50], dislocation avalanches in ice [97], and sea ice fracturing [93]. Another similarity with SOC systems is that the model used for sandpile dynamics is very close to the one we build for iceberg calving, suggesting similar dynamic behaviors. However, one prediction of our model that was not discussed by [8] and [9] is that there is a critical transition into self-sustained activity. The fact that the predictions of our model agree with the field data shows that the model manages to capture the essence of the process of iceberg calving.

Distributions of event-size described by a power laws gives indications about the dynamics of calving processes, in particular, the exponent of the power-law distributions might be an indicator about the glacier stability and potential rapid retreat. The distributions of calving-event sizes thus provide an indication of how close a glacier is to rapid retreat. In the same way as [12], we found what might be a critical stability number that indicates how stable a glacier is. In [12], the stability criterion depends on various geometric and dynamics near-terminus parameters. In our case, the diagnostic is based only on the distributions of individual event-sizes: in practice it means that a glacier more and more unstable and close to rapid retreat will produce less small icebergs and more huge and catastrophic icebergs. However, single large calving events, or average sizes, are not informative alone, the entire range of sizes must be observed. It is also interesting to note that the distributions of inter-event intervals do not depend on the glacier stability. We also showed that iceberg calving is hardly predictable.

Several points of this study can be subject to discussion, especially concerning the data collection and the construction of the model.

Direct observations made by humans is one of the most practical techniques to observe calving event on an individual scale, however it is hard to reproduce exactly the same results. Visual observations by different observers are somewhat subjective, they might become tired, distracted, or in different attentive states. Each new observer needs to adjust her- or himself to the scale 1-20. To minimize a too large error due to subjectivity we performed test periods where we confronted all of the observers size estimates (See in Methods). To further work with our hypothesis, more observations of event-sizes are needed, especially in different environments and for glaciers in different dynamical states, for example a glacier advancing, one stable and one retreating. To test our stability criterion we would need to monitor the same glacier year after year, for a few continuous days of observations. However, long-term continuous observations or observations in cold months are difficult. Automatic monitoring, e.g. seismic monitoring could help here even though seismic monitoring can detect only the largest events. But since power-laws are scale-free, one would need to investigate only one part of the size ranges, for example only the largest events. We suggest that any method

that can provide an estimation for the volume of the individual iceberg calving event might be suited to provide data to test our hypothesis. We also showed that even persons without glaciological training can collect valuable data of calving events.

The model we build is simplified. One of the main simplifications is that we model the stress at the glacier front in two spatial dimensions, whereas in reality, stress can propagate in three dimensions. Here, stress is considered as a scalar while it should be a tensor. Another simplification is related to the stress increment in the glacier cells. In our model, it is a jump while in reality it should be smoother. Another point is the stress decay: it is likely that stress slowly dissipates in the absence of perturbations, i.e. decays to zero. We assume that the time-constant is much larger than the time between perturbations and therefore can be approximated as being infinite (no decay). The model perturbation is another simplification, it is stochastic and the probability to perturb one part of the glacier is the same everywhere on the front, which would be different in reality and closer to the vertical velocity pattern at the front. The interaction kernel, or how one calving cell will influence its neighbors, is restricted to only nearest-neighbor interactions. We checked different types of interaction kernels (e.g. symmetric kernels) without observing any qualitative changes in the resulting distributions. Anyway such information about the propagation of stress in response to calving is still limited. Finally, we model only the subaerial part of the glacier front, thus we do not model submarine calving events which amount for about 13% of the total ice loss at the front. We assume that most of the submarine glacier face is lost through melting, as suggested by [67] where they found that 57% of the total ice loss at the terminus of LeConte Glacier was due to submarine melting. One way to account for the submarine dynamics would be to assess different values of calving susceptibilitys for the subaerial and the submarine parts. The resulting size distribution would be a mix of two power laws and would not change our conclusions.

Another problem inherent to the study of calving events in the way to define what is one event. It is relatively easy in the model where we consider a single event is trigger by only one perturbation. It is not so straightforward in the field and it is sometimes difficult to differentiate between single large events and a collection of small events.

To conclude we suggest that the distributions of calving-event sizes and inter-event intervals reflect the stability of the glacier and how close it is to a critical transition point. Observations of rapid glacier retreats can be explained by supercritical self-sustained calving and the transition to rapid retreat is abrupt. Even under stationary conditions, the same dynamical system can generate both small and large events. Climate does not have a direct impact on calving but might, through glacier melting, warmer ocean temperature and internal glacier processes, impact the calving susceptibility and change the distributions of calving-event sizes, with more large events. The occurrence of catastrophic calving events has to be expected for no specific reason, as part of the natural inherent variability of the glacier s internal dynamics.

6.5 Acknowledgements

We wish to thank Cecilia Marie Futsæther for the initiation of very fruitful discussions about SOC and complex systems We acknowledge support by the Research Council of Norway (IPY-GLACIODYN [project 176076], eVITA [eNEURO], Notur, and a "Institutt Basert strategisk Program" granted to the Department of Mathematical Sciences and Technology at the Norwegian University of Life Sciences) and the Svalbard Science Forum. We thank Cecilie Rolstad-Denby, Nial Peters, Allan Buras, Bas Altena and Karin Amby for their great work in the field, as well as the "Young Explorers and Leaders" of the "British Schools Exploring Society Arctic Adventure" expedition in 2010 for providing iceberg-calving data for Sveabreen.

Summary and outlook

Chapter 7

Summary and outlook

7.1 Conclusions

Calving is a non linear process that can lead to rapid glacier retreat, thus accelerating the response of glaciers to climate change. We propose in this thesis that the size distribution of iceberg calving reflects the dynamical state of tidewater glaciers and can inform about their stability. The most important contributions are now listed below:

- Ground-based RADAR has strong potential for automatic detection, as well as seismic monitoring. We also want to stress that visual observations remain very practical for short-term observations. At least, some periods of visual observations, together with repeat time-lapse pictures, are extremely useful to calibrate/validate other techniques. Additionally, direct observations allow a narrative account of the calving activity at a tidewater glacier front, which proved to be an integral part of the interpretation of the data.

- Most of the ice at a calving front is lost through the biggest and most rare events. Changes at the front happen by sudden and rare calving events rather than regular calving activity. Calving is a non linear process and cannot be considered as constant through time.

- Seismic activity linked to glacier dynamics and calving is marked by a strong increase in autumn, while velocity is at its lowest. This suggests a very complicated and intricate relationship between calving and glacier speed. The spatial variation in calving activity at a calving front is best explained by the longitudinal stretching rates, manifested on the glacier surface as crevasse fields and caused by the glacier geometry.

- Rapid tidewater glacier retreats can be explained by self-sustained calving, an ongoing calving activity state reached in our model when the calving susceptibility parameter exceeds a critical value. Concretely, it means that, if the calving susceptibility of a glacier is increased (e.g. higher air temperature, deeper water depth), the range of iceberg size will increase until it reaches a critical point beyond which calving activity becomes ongoing, leading to rapid glacier retreat. According to our model, the transition between a stable glacier and one in a retreat phase is abrupt.

- Even under stationary conditions, our model manages to reproduce the event-size and inter-event interval distributions of the observed calving events in the field. It means that (i) this simple model that only focuses on the impact of calving on the front stability, captures the essence of the calving process and that (ii) even under stationary conditions, calving events of all sizes happen, the range of sizes reflecting the inherent variability of the glacier s internal dynamics. We propose that catastrophic events might happen and should be expected to happen for no specific reasons, even under constant climate for example.

- Studying the size distribution of individual calving events is meaningful: the size distribution depends on the glacier stability state. One prediction of our model is that the size distribution of the icebergs of a glacier becoming more unstable will change: the proportion of large calving events will increase.

- We propose a stability number for tidewater glaciers – the exponent of the power law distribution of the iceberg sizes – which gives a measure of how close a glacier is to rapid retreat.

7.2 Future work

- No perfect monitoring method exists for the calving activity. Most of the work in this thesis is based on direct visual observations, and, as discussed in Paper 4, this technique presents numerous problems. To further work with the hypothesis that the distribution of iceberg sizes reveals the stability of the glacier, we would need to observe more glaciers, in different environments and for several years.

- Our calving model could be connected to previous calving models. Our model focusses only on one aspect of calving: the interplay between calving and front destabilization. External parameters like water depth, air temperature, etc., are treated as constant external perturbations, which is not the case in reality. Previous models parameterize calving based on those parameters [106, 114, 115, 82] or through glacier dynamics like [14, 73, 87]. The output of those models is an estimate of calving rate. Our model could be connected to those existing models by replacing the output *calving rate* by our model parameter *calving susceptibility*. Such a "multi-level" model could make predictions of the entire distribution of iceberg sizes and inter-event times, even though more work is needed to understand how to adjust the *calving susceptibility* as a function of *calving rate*.

- Our model alone has the potential to make predictions of calving activity. If one knows the dimensions of a glacier and has calving-event size distribution data to calibrate the model by adjusting the *calving susceptibility* such as the size and interval distributions look similar, one could predict current calving activity. By increasing the *calving susceptibility* according to different climate scenarios, one could potentially make calving activity predictions for the future. To achieve that, more work should be done on the relation between external parameters and our model parameter *calving susceptibility*.

Chapter 8

Bibliography

Bibliography

[1] Allen, R.V., 1978. Automatic earthquake recognition and timing from single traces. B. *Seismol. Soc. Am.*, **8** (5), 1521–1532.

[2] Amundson, J.M., Truffer, M., Lthi, M.P., Fahnestock, M.,West, M. and Motyka. R.J., 2008. Glacier, fjord, and seismic response to recent large calving events, Jakobshavn Isbrae, Greenland. *Geophys. Res. Lett.*, **35** (22).

[3] Amundson, J.M., Fahnestock, M., Truffer, M., Brown, J., Luthi, M.P., Motyka, R.J., 2010. Ice mlane dynamics and implications for terminus stability, Jakobshavn Isbrae, Greenland. *J. Geophys. Res.*, **115**, F01005.

[4] Amundson, J.M. and Truffer, M. 2010. A unifying framework for iceberg-calving models. *J. Glac.*, **56**, 199, 822–830.

[5] Anandakrishnan, S. and Bentley, C.R., 1993. Micro-earthquakes beneath Ice Streams Band C, West Antarctica: observations and implications. *J. Glaciol.*, **39** (133), 455–462.

[6] Bak, P. 1996. *How nature works: The Science of Self-Organized Criticality*. Springer, Copernicus, New York, Springer.

[7] Bak, P., Christensen, K., Danon, L., and Scanlon, T. 2002. Unified scaling law for earthquakes. *Phys. Rev. Lett.*, **88**.

[8] Bak, P., Tang, C., and Wiesenfeld, K. 1987. Self-organized criticality - An explanation of 1/f noise. *Phys. Rev. Lett.*, **59**, 381–384.

[9] Bak, P., Tang, C., and Weisenfeld, K. 1988. Self-organized criticality. *Phys. Rev. A*, **38**, 364–374.

[10] Bardainne, T.,Gaillot, T., Dubos-Salle, N., Blanco, J., and Snchal, G., 2006. Characterization of seismic waveforms and classification of seismic events using chirplet atomic decomposition. Example from the Lacq gas field (Western Pyrenees, France). *Geophys. J. Int.*, **166** (47), 699–718.

[11] Benn, D.I., Evans, D.J.A., 1998. *Glaciers and Glaciations*. London, Hodder Edition.

[12] Bassis, J.N. 2010. The statistical physics of iceberg calving and the emergence of universal calving laws. *J. Glac.*, **57**, 57, 3–16.

[13] Benn, D.I., Warren, C.R., and Mottram, R.H. 2007 (a). Calving processes and the dynamics of calving glaciers. *Earth-Sci. Rev.*, **82**, 143–179.

[14] Benn, D.I., Hulton, N.R.J., and Mottram, R.H. 2007 (b). Calving laws , sliding laws and the stability of tidewater glaciers. *A. Glac.*, **46**, 123–130.

[15] Blankenship, D.D.,Anandakrishnan, S., Kempf, J.L., and Bentley, C.R., 1987. Microearthquakes under and alongside Ice Stream B, Antarctica, detected by a new passive seismic array. *Ann. Glaciol.*, **9**, 30–34.

[16] Briner J.P., Bini A.C., Anderson R.S. 2009. Rapid early Holocene retreat of a Laurentide outlet glacier through an Arctic fjord. *Nat. Geosci.*, **2** (7), 496–499.

[17] Brown, C.S., Meier, M.F., Post, A. 1982. Calving speed of Alaska tidewater glaciers, with application to Columbia Glacier. *U.S. Geol. Surv. Prof. Pap.*, 1258-C.

[18] Chapuis, A., Rolstad, C., and Norland, R. 2010. Interpretation of amplitude data from a ground-based radar in combination with terrestrial photogrammetry and visual observations for calving monitoring of Kronebreen, Svalbard. *Ann. Glaciol.*, **51**, 34–40.

[19] Chapuis, A. and Tetzlaff, T., in prep. What do the distributions of calving-event sizes and intervals say about the stability of tidewater glaciers?

[20] Clar, S., Drossel, B., Schenk, K., and Schwab, F. 1999. Self-organized criticality in forest-fire models. *Physica A*, **266**, 153–159.

[21] Clarke, G.K.C., 1987. Fast glacier flow - ice streams, surging , and tidewater glaciers. *J. Geoph. Res-Solid Earth and Planet*, **92**, 8835–8841.

[22] Clauset, A., Shalizi, C.R., and Newman, M.E.J. 2009. Power-Law Distributions in Empirical Data. *Siam Rev.*, **51**, 661–703.

[23] Davies, D.L. and Bouldin, D.W., 1979. A cluster separation measure. *IEEE Trans. Pattern Anal. and Mach. Intell.*, **1** (2), 224–227.

[24] de Boer, J., Jackson, A.D., and Wettig, T. 1995. Criticality in simple models of evolution. *Phys. Rev. E*, **51**, 1059–1074.

[25] Deichmann, N., Ansorge, J., Scherbaum, F., Aschwanden, A., Bernardi, F., and Gudmundsson, G.H., 2000. Evidence for deep icequakes in an Alpine glacier. *Ann. Glaciol.*, **31** (1), 85–90.

[26] Dowla, F.U., Taylor, S.R., and Anderson, R.W., 1990. Seismic discrimination with artificial neural networks: Preliminary results with regional spectral data. *B. Seismol. Soc. Am.*, **80** (5), 1346–1373.

[27] Ekstrom, G., Nettles, M., and Abers, G.A., 2003. Glacial earthquakes. *Science*, **302** (5645), 622–624.

[28] Esposito, A.M., Giudicepietro, F., DAuria, L., Scarpetta, S., Martini, M.G., Coltelli, M., and Marinaro, M., 2008. Unsupervised neural analysis of very-long-period events at Stromboli volcano using the self-organizing maps. *B. Seismol. Soc. Am.*, **98** (5), 2449–2459.

[29] Falkner K.K., Melling, H., Munchow, A.M., and others, 2011. Context for the recent massive Petermann glacier calving event. *EOS*, **92**, (14), 117–118.

[30] Fischer, H. P. and Powell, R. D., 1998. A simple model for the influence of push-morainal banks on the calving and stability of glacial tidewater termini. *J. Glac.*, **44**, 31–41.

[31] Gould, S.J., 1989. *Wonderful Life*. W.W. Norton and Co., 347 pp.

[32] Guzzetti, F., Malamud, B.D., Turcotte, D.L., and Reichenbach, P. 2002. Power-law correlations of landslide areas in central Italy. *Earth Planet. Sc. Lett.*, **195**, 169–183.

[33] Haeberli, W. and Beniston, M., 1998. Climate change and its impact on glaciers and permafrost in the Alps. *Ambio*, **27** (4), 258–265.

[34] Hagen, J. O., Melvold, K., Pinglot, F. and Dowdeswell, J. A., 2003. On the net mass balance of the glaciers and ice caps in Svalbard, Norwegian Arctic. *Arctic, Antarctic, and Alpine Research*, **35**, 264–270.

[35] Hainzl, S. 2003. Self-organization of earthquake swarms. *J. Geod.*, **35**, 157–172.

[36] Hanson, B. and Hooke LeB., R. 2000. Buckling rate and overhand development at a calving face. *J. Glac.*, **49**, 167, 577–586.

[37] Herz, A.V.M., Hopfield, J.J. 1995. Earthquake Cycles and Neural Reverberations: Collective Oscillations in Systems with Pulse-Coupled Threshold Elements, *PRL* **75(6)**, 1222–1225.

[38] Howat, I.M., Joughin, I., and Scambos, T., 2007. Rapid changes in ice discharge from greenland outlet glaciers. *Science*, **315** (5818), 1559–1561.

[39] Howat, I.M., Joughin, I., Tulaczyk, S., and Gogineni, S. 2005. Rapid retreat and acceleration of Helheim glacier, east Greenland. *Geophys. Res. Lett.*, **32**, L22502.

[40] Hughes, T. 1986. The Jakobshavns Effect. *Geophys. Res. Lett.*, **13**, 46–48.

[41] Hughes, T., 1989. Calving ice walls. *A. Glac.*, **12**, 74–80.

[42] Hughes, T., and Nakagawa, M., 1989. Bending shear: the rate-controlling mechanism for calving ice walls. *J. Glac.*, **35** (120), 260–266.

[43] IPCC, 2001. *Climate Change 2001: The Scientific Basis*. Contribution of Working Group I to the Third Assessment Report of the Intergovernmental Panel on Climate Change, Cambridge University Press, Cambridge, United Kingdom and New York, NY, USA, 881 pp.

[44] IPCC, 2007. *Climate Change 2007 - The Physical Science Basis*. Contribution of Working Group I to the Fourth Assessment Report of the Intergovernmental Panel on Climate Change (ISBN 978 0521 88009-1 Hardback: 978 0521 70596-7 Paperback).

[45] Jacobs, S. S., Helmer, H. H., Doake, C. S. M., Jenkins, A. and Frolich, R. M., 1992. Melting of Ice Shelves and the Mass Balance of Antarctica. Journal of Glaciology, 38, 375-387.

[46] Jensen, H.J., 2002. Mathematics and painting. *Interdisciplinary Science Review*, **27** (1), 45–49.

[47] Joswig, M., 1990. Pattern recognition for earthquake detection. *B. Seismol. Soc. Am.*, **80** (1), 170–186.

[48] Joughin, I., Abdalati, W., and Fahnestock, M., 2004. Large fluctuations in speed on greenlands jakobshavn isbrae glacier. *Nature*, **432** (7017), 608–610.

[49] Joughin, I., Howat, I., Alley, R.B.,Ekstrm, G., Fahnestock, M., Moon, T., Nettles, M.,Truffer, M., and Tsai, V.C., 2008. Ice-front variation and tidewater behavior on helheim and kangerdlugssuaq glaciers, greenland. *J. Geophys. Res.*, **113** :F01004.

[50] Kavanaugh, J.L. 2009. Exploring glacier dynamics with subglacial water pressure pulses: Evidence for self-organized criticality? *J. Geophys. Res-Earth*, **114**.

[51] Kehrl, L.M., Hawley, R.L., Powell, R.D., Brigham-Grette, J., 2011. Glacimarine sedimentation processes at Kronebreen and Kongsvegen Glaciers, Svalbard. *J. Glac.*, **57** (205), 841–847.

[52] Kohler, A., Ohrnberger, M., andScherbaum, F., 2009. Unsupervised feature selection and general pattern discovery using Self-Organizing Maps for gaining insights into the nature of seismic wavefields. *Comput. Geosci.*, **35** (9), 1757–1767.

[53] Kohler, A., Ohrnberger, M., and Scherbaum, F., 2010. Unsupervised pattern recognition in continuous seismic wavefield records using Self-Organizing Maps. *Geophys. J. Int.*, **182**, 1619–1630.

[54] Kohonen, T., 2001. *Self-Organizing Maps*, volume30 of Springer Series in Information Sciences. Springer, third extended edition.

[55] Kirkbride, M.P. and Warren, C.R., 1999. Tasman glacier, new zealand: 20th-century thinning and predicted calving retreat. *Global Planet. Change*, **22** (1-4), 11–28.

[56] Krabill, W., Hanna, E., Huybrechts, P., Abdalati, W., Cappelen, J., Csatho, B., Frederick, E., Manizade, S., Martin, C., Sonntag, J., Swift, R., Thomas, R. and Yungel, J., 2004. Greenland Ice Sheet: Increased coastal thinning. *Geophys. Res. Lett.*, **31**.

[57] Krimmel, R.M. and Rasmussen, L.A., 1986. Using sequential photography to estimate ice velocity at the terminus of Columbia Glacier, Alaska. *Ann. Glac.*, **8**, 117–123.

[58] Kuhn, M., 1980. *Climate and glaciers*. IAHS Publication 131, 3–20.

[59] Langley, K., Lacroix, P., Hamran, S.-E. and Brandt, O., 2009. Sources of backscatter at 5.3 GHz from a superimposed ice and firn area revealed by multi-frequency GPR and cores. *J. Glac.*, **55** (190), 373–383.

[60] Lapicque L. 1907. Recherches quantitatives sur l excitation electrique des nerfs traitee comme une polarization. *J. Physiol. Pathol. Gen.*, **9**, 620–635.

[61] Lefauconnier, B., 1987. Fluctuations glaciaires dans le Kongsfjord, Baie du Roi, 79N, Spitsbergen, analyses et consquences. (PhD thesis, Universit de Grenoble.)

[62] Mann, D.H., 1986. Reliability of a fjord glaciers fluctuations for paleoclimatic reconstructions. *Quat. Res.*, textbf25 (1), 10–24.

[63] Maurer, W.J. , Dowla, F.U., and Jarpe, S.P., 1992. Seismic event interpretation using self-organizing neural networks. *Proc. SPIE Int. Soc. Opt. Eng.*, **1709**, 950–958.

[64] Meier, M. F. and Post, A., 1987. Fast Tidewater Glaciers. *J. Geoph. Res.-Solid Earth Planets*, **92**, 9051–9058.

[65] Milankovitch, M., 1941. *Canon of insolation and the Ice Age problem.* With introduction and bibliographical essay by Nolika Pantic. Alven Global, 636 pp.

[66] Motyka, R.J., ONeel, S., Connor, C.L., and Echelmeyer, K.A., 2003. Twentieth century thinning of mendenhall glacier, alaska, and its relationship to climate, lake calving, and glacier run-off. *Global Planet. Change*, **35** (1-2), 93–112.

[67] Motyka, R.J., Hunter, L., Echelmeyer, K.A., Connor, C. 2003. Submarine melting at the terminus of a temperate tidewater glacier, LeConte Glacier, Alaska, U.S.A.. *A. Glac.*, **36**, 57–65.

[68] Motyka, R.J., Truffer, M., Fahnestock, M., Mortensen, J., Rysgaard, S., Howat, I. 2011. Submarine melting of the 1985 Jakobshavn Isbr floating tongue and the triggering of the current retreat. *J. Geophys. Res-Earth*, **116**.

[69] Musil, M. and Plesinger, A., 1996. Discrimination between local microearthquakes and quarry blasts by multi-layer perceptrons and Kohonen maps. *B. Seismol. Soc. Am.*, **86** (4):1077–1090.

[70] Nettles, M. and Ekstrom, G., 2010. Glacial earthquakes in Greenland and Antarctica. *Annu. Rev. Earth Pl. Sc.*, **38**, 467–491.

[71] Nettles, M., Larsen, T.B., Elsegui, P., Hamilton, G.S., Stearns, L.A., Ahlstrøm, A.P., Davis, J.L., Andersen, M.L., deJuan, J., Khan, S., Stenseng, L., Ekstrom, G., and Forsberg, R., 2008. Step-wise changes in glacier flow speed coincide with calving and glacial earthquakes at Helheim Glacier, Greenland. *Geophys. Res. Lett.*, **35** (24), L24503.

[72] Nick, F.M., Vieli, A., Howat, I., and Joughin, I. 2009. Large-scale changes in Greenland outlet glacier dynamics triggered at the terminus. *Nat. Geosci.*, **2**, 110–114.

[73] Nick, F.M., van der Veen, C.J., Vieli, A., Benn, D.I.. 2010. A physically-based calving model applied to marine outlet glaciers and implications for the glacier dynamics. *J. Glac.*, **56**, 199, 781–794.

[74] Norland, R., 2001. Multipath scattering from complex targets. *IEE Proc. Radar Sonar Navig.*, **148** (6), 343–347.

[75] Norland, R., 2006. Differential interferometric radar for mountain rock slide monitoring. In: I.G.a.R.S. Symposium (Editor). Piscataway, NJ. Institute of Electrical and Eletronics Engineers, Denver, CO., pp. 3293-3296.

[76] Norland, R., 2007. Improving interferometric radar measurement accuracy using local meteorological data. In: I.G.a.R.S. Symposium (Editor). Piscataway, NJ. Institute of Electrical and Eletronics Engineers, pp. 4521-4524.

[77] Nuth, C., Moholdt, G., Kohler, J., Hagen, J.O., Kaab, A., 2010. Svalbard glacier elevation changes and contribution to sea level rise. *J. Geophys. Res*, **115**, F01008.

[78] Nuth, C., Schuler, T.V., Kohler, J., Altena, B., Hagen, J.O., in press. Estimating the long term calving flux of Kronebreen, Svalbard, from geodetic elevation changes and mass balance modelling. *J. Glac.*.

[79] Nye, J.F., 1960. The response of glaciers and ice-sheets to seasonal and climatic changes. *Proc. of the Royal Society of London series A-mathematical and physical sciences*, textbf256 (1287), 559-584

[80] Oerlemans, J., 2001. *Glaciers and climate change*. Swets and Zeitlinger BV, Lisse.

[81] Oerlemans, J., 2005. Extracting a climate signal from 169 glacier records. *Science*, **308**, 675–677.

[82] Oerlemans, J., Jania, J., Kolondra, L. 2011. Application of a minimal glacier model to Hansbreen, Svalbard. *The Cryosphere*, **5**, 1–11.

[83] O Neel, S., Pfeffer, W.T., Krimmel, R. and Meier, M., 2005. Evolving force balance at Columbia Glacier, Alaska, during its rapid retreat. *J. Geophys. Res-Earth Surf.*, **110** (F3).

[84] O Neel, S., Echelmeyer, K.A., and Motyka, R. 2003: Short-term variations in calving of a tidewater glacier: LeConte Glacier, Alaska, USA. *J. Glaciol.*, **49**, 587–598.

[85] O Neel, S., Larcen, C.F., Rupert, N., Hansen, R. 2010. Iceberg calving as a primary source of regional-scale glacier-generated seismicity in the St. Elias Mountains, Alaska. *J. Geophys. Res-Earth.*, **115**.

[86] O Neel, S., Marshall, H.P., McNamara, D.E., and Pfeffer, W.T. 2007. Seismic detection and analysis of icequakes at Columbia Glacier, Alaska. *J. Geophys. Res.*, **112**.

[87] Otero, J., Navarro, F.J., Martin, C., Cuadrado, M.L., Corcuera, M.I. 2010. A three-dimensional calving model: numerical experiments on Johnsons Glacier, Livingston Island, Antarctica. *J. Glac.*, **56**, 196, 200–214 .

[88] Pfeffer, W.T. 2007. A simple mechanism for irreversible tidewater glacier retreat. *J. Geophys. Res-Earth.*, **112** (F3).

[89] Plesinger, A.,Ruzek, B., and Bouskova, A., 2000. Statistical interpretation of WEBNET seismograms by artificial neural nets. *Stud. Geophys. Geod.*, **44** (2), 25–271.

[90] Post, A., 1975. Preliminary hydrography and historic terminal changes of Columbia glacier, Alaska. *USGS Hydrologic investigations Atlas*, HA559.

[91] Post, A. and Motyka, R.J., 1995. Taku and Leconte glaciers, Alaska - calving speed control of late-Holocene asynchronous advances and retreats. *Phys. Geog.*, **16**, (1), 59–82.

[92] Qamar, A. 1988. Calving Icebergs - a Source of Low-Frequency Seismic Signals from Columbia Glacier, Alaska. *J. Geophys. Res-Solid*, **93**, 6615–6623.

[93] Rampal, P., Weiss, J., Marsan, D., Lindsay, R., and Stern, H. 2008. Scaling properties of sea ice deformation from buoy dispersion analysis. *J. Geophys. Res-Oceans*, **113**.

[94] Reeh, N. 1968. On the calving of ice from floating glaciers and ice shelves. *J. Glac.*, **7**, 50, 215–232.

[95] Rees, W.G., Dowdeswell, J.A. and Diament, A.D., 1995. Analysis of ERS-1 synthetic aperture radar data from Nordaustlandet, Svalbard. *Int. J. Remote Sens.*, **16**(5), 905–924.

[96] Richardson, J.P., Waite, G.P., FitzGerald, K.A., and Pennington, W.D., 2010. Characteristics of seismic and acoustic signals produced by calving, Bering Glacier, Alaska. *Geophys. Res. Lett.*, **37** (3), L03503.

[97] Richeton, T., Weiss, J., and Louchet, F. 2005. Dislocation avalanches: Role of temperature, grain size and strain hardening. *Acta Mater.*, **53**, 4463–4471.

[98] Ritchie, J.B., Lingle, C.S., Motyka, R.J., Truffer, M. 2008: Seasonal fluctuations in the advance of a tidewater glacier and potential causes: Hubbard Glacier, Alaska, USA. *J. Glaciol.*, **54** (186), 401–411.

[99] Rocha, L.M., 1999. Complex systems modeling: using metaphors from nature in simulation and scietific models. *BITS: Computer and Communications News*. Computing, information, and communications division. Los Alamos National Laboratory.

[100] Rolstad, C., and Norland, R. 2009a. Ground based interferometric radar for velocity measurements of the calving front of Kronebreen, Svalbard. *Ann. Glaciol.*, **50**, 47–54.

[101] Rolstad, C., Chapuis, A. and Norland, R., 2009b. Electromagnetic interference in ground based interferometric radar data from Kronebreen (Svalbard) calving front due to multipath scattering and tidal cycles. *J. Glac.*, **55**, 193, 943–945.

[102] Stevens, S.S. 1957. On the psychological law. *Psychol. Rev.*, **64**, 153–181.

[103] Stuart, G., Murray, T., Brisbourne, A., Styles, P., and Toon, S., 2005. Seismic emissions from a surging glacier: Bakaninbreen, Svalbard. *Ann. Glaciol.*, **42** (1),151–157.

[104] Tarvainen, M., 1999. Recognizing explosion sites with a self-organizing network for unsupervised learning. *Phys. Earth Planet. Inter.*, **113** (1-4), 143–154.

[105] Tuckwell H.C. 1988. *Introduction to Theoretical Neurobiology*, Volume 1. Cambridge. Cambridge University Press.

[106] van Der Veen, C.J. 1996. Tidewater calving. *J. Glac.*, **141**, 375–385.

[107] van Der Veen, C.J. 1997. Calving glaciers: report of a workshop. *BPRC Report No.15 Byrd Polar Research Center*, The Ohio State University, Columbus, Ohio, 194 pp.

[108] van der Veen, C.J., Mosley-Thompson, E., Gow, A.J., and Mark, B.G., 1999. Accumulation at South Pole: Comparison of two 900/year records. *J. Geoph. Res-Atm*, **104**, 31067–31076.

[109] Vanwormer, D. andBerg, E., 1973. Seismic evidence for glacier motion. *J. Glaciol.*, **12**, 259–265.

[110] Velicogna I. and Wahr, J., 2005. Greenland mass balance from GRACE. *Geoph. Res-Lett*, **32**, L18505.

[111] Venteris, E.R., Whillans, I.M., and Vander Veen, C.J., 1997. Effect of extension rate on terminus position, Columbia Glacier, Alaska, USA. *Ann. Glaciol.*, **24**, 49–53.

[112] Vesanto, J. and Alhoniemi, E., 2000a. Clustering of the self-organizing map. *IEEE Trans. Neural Networks*, **11** (3), 586–600.

[113] Vesanto, J.,Himberg, J.,Alhoniemi, E., and Parhankangas, J., 2000b. *SOM toolbox for Matlab*. Technical report, Helsinki University of Technology, 2000.

[114] Vieli, A.,Funk, M., Blatter, H. 2001. Flow dynamics of tidewater glaciers: a numerical modelling approach. *J. Glac.*, **47**, 159, 595–606.

[115] Vieli, A., Jania, J., Kolondra, L. 2002. The retreat of a tidewater glacier: observations and model calculations on Hansbreen, Spitsbergen. *J. Glac.*, **48**, 163, 592–600.

[116] Wald, A. and Wolfowitz, J., 1940. On a test whether two samples are from the same population. *Ann. Math. Statist.*, **11** (2), 147–162.

[117] Warren C.R., Glasser N.F., Harrison, S., Winchester V., Kerr A.R:, Rivera, A. 1995. Characteristics of tide-water calving at Glaciar San-Rafael, Chile. *J. Glaciol.*, **41**, 273–289.

[118] Washburn, H.B., Jr. 1936a. The Harvard-Dartmouth Alaskan expeditions 1933-1934. *Geogr. J.*, **87**, 481–495.

[119] Washburn, B., 1936b. Exploring yukons glacial stronghold. *National Geographic Magazine*, 69(6), 715–748.

[120] WGMS, 2008. Global glacier changes: facts and figures. Genf.

[121] Weaver, C.S., and Malone, S.D., 1979. Seismic evidence for discrete glacier motion at the rock-ice interface. *J. Glaciol.*, **23** (89), 171–184.

[122] Wessel, P. and Smith, W.H.F., 1998. New, improved version of GMT released. *EOS Trans. Amer. Geophys. Un*, **79** (47), 579–579.

[123] Wolf, L.W. and Davies, J.N., 1986. Glacier-generated earthquakes from Prince William Sound, Alaska. *B. Seismol. Soc. Am.*, **76** (2), 367–379.